CONFORMATIONAL PROPERTIES OF LINEAR POLYMERS AT A POROUS INTERFACE:

A MONTE CARLO SIMULATION STUDY

PROEFSCHRIFT

ter verkrijging van
de graad van doctor aan de Universiteit Twente,
op gezag van de rector magnificus,
prof. dr. F.A. van Vught,
volgens besluit van het College voor Promoties
in het openbaar te verdedigen
op vrijdag 5 september 2003 om 13:15 uur

door

Gerard Frank Hermsen
geboren op 14 december 1972
te Venray

Dit proefschrift is goedgekeurd door de promotor prof. dr.-ing. M. Wessling en de assistant promotor dr. ir. N.F.A. van der Vegt

ISBN: 90-365-1958-6

Printed by PrintPartners Ipskamp, Enschede

CONTENTS

CHAPTER

ONE

Introduction

1.1 General Introduction

1.1.1 Scope of the Thesis

In this thesis Configurational Bias Monte Carlo simulations are used to study single homopolymer chains at the interface between a bulk solvent and a porous wall. The conformations of polymers that have partially penetrated a narrow pore at the interface are compared to their conformations in the bulk solvent and their completely confined conformation. Moreover, the change of accompanying properties such as the chain conformational entropy and free energies of adsorption are studied as function of their location compared to the position of the interface. Effects of adsorption on the outer surface and the pore walls on the polymer conformation are investigated, as is the influence of the solvent quality, to characterise the conformation of partially confined polymers.

1.1.2 An Introduction to Ultrafiltration and Polymer Deformation

In electrophoresis and chromatographic applications, linear polymers deform under influence of an imposed force field and obstacles in their solution. In experiments with zeolites, deformation of very small polymers and oligomers is reported to be common. Although ultrafiltration involves filtration of much larger particles, typically proteins and other colloidal particles having diameters of a few nanometres, one can expect polymer deformation in ultrafiltration when intramolecular interactions of the large polymers are weak. In membrane literature such events are not frequently mentioned although Baker and Strathmann[7] and Beerlage et al.[8,9] pointed out that these phenomena are quite likely for linear polymers. This has implications for Molecular Weight Cut-Off (MWCO) measurements, a popular membrane characterisation method. Pore sizes of ultrafiltration membranes are characterised by the molecular weight of a reference material, typically linear macromolecules like polyethylene glycol (PEG) or polydextran of various weights, where these reference solutes adopt a globular conformation. Already pointed out by Baker and Strathmann

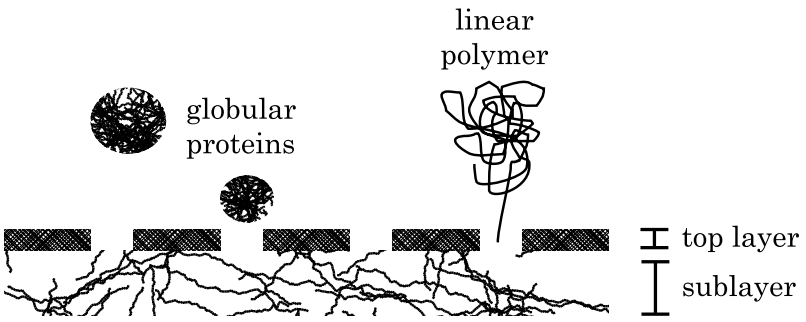

Figure 1.1: *Ultrafiltration experiment with globular and linear macromolecules.*

in 1970[7] there is a possible different behaviour of these linear polymers in MWCO measurements: linear polymers, slightly larger than the pore size, expected to be rejected by the membrane, permeated through the membrane instead by changing their shape, or conformation.

During MWCO measurements the solute-membrane interactions are assumed to play no role so that the polymer globule is able to enter the pore. The solute weight is varied to measure the solute fraction that permeates the membrane. The MWCO of a membrane is defined as the solute molecular weight at which 90% is rejected. Much depends on the type of solute to be filtrated, the membrane material and the solvent. The way the solute interacts with the membrane greatly influences the outcome of the MWCO measurements.

A nice example, which illustrates the above stated problem in ultrafiltration is published by Baker.[6] Table 1.1 shows rejection data of typical solutes filtrated in an ultrafiltration

	globular protein		**linear polymer**
Solute	*Pepsin*	*Cytochrome c*	*Polydextran*
MW (kDa)	35	13	100
Rejection (%)	90	70	0

Table 1.1: *The rejection of globular proteins can differ substantially from the rejection of linear polymers of similar molecular weights.*[6]

experiment as shown in figure 1.1. On the left side are two globular proteins (Pepsin and a lighter protein, Cytochrome c) being rejected for 90% and 70%, respectively. A linear polymer like polydextran is about nine times heavier than Cytochrome c, but is not rejected at all. Apparently the linear polymer is able to deform itself at the membrane interface in order to penetrate the pore and permeate across the membrane, while the dense globular proteins are packed in such a way that deformation results in an increase in free energy, too large to overcome in order to enter the pore.

1.1.3 Outline of the Thesis

In this thesis I will try to answer mainly three questions about conformational changes of homopolymers at the entry of a narrow pore: first, how does a flexible linear polymer change its conformation in the transition from a bulk solvent to a pore. Second, what is the influence of surface adsorption phenomena on this conformational change. Third, what is the role of solvent quality.

Introduction In the remainder of this chapter some important concepts of ultrafiltration and of polymer physics used throughout this thesis are introduced and explained.

Simulation Methods In this chapter Monte Carlo simulation is briefly explained with a focus on the Configurational Bias algorithm, the method used throughout the thesis. It is an algorithm for equilibrium simulations meaning that only static information can be obtained, not dynamical information. The polymers are modelled on a lattice using the Bond Fluctuation model, which is explained next, after which the simulation system and some important quantities are explained.

Monte Carlo simulations of partially confined flexible polymers The conformational change of a flexible polymer is studied in this chapter for various degrees of penetration in a cylindrical pore. The polymer is dissolved in a good solvent and the walls of the membrane and the pore are repulsive or weakly attractive. It turns out that for pore

radii smaller than the polymer radius of gyration the polymer partly deforms adopting an asymmetric conformation being 'over-stretched' along the pore axis.

Monte Carlo simulations of polymer adsorption at the entrance of cylindrical pores in flat adsorbing surfaces When a strong segment-wall interaction (above the critical adsorption energy) is introduced, the polymer conformations change completely. The polymer adopts differently deformed conformations adsorbed onto the membrane interface, maximising the number of wall contacts, at various distances from the interface.

Polymer intrusion in narrow pores on adsorbing and non-adsorbing surfaces: a Monte Carlo study When the solvent quality is worsened to Θ-conditions or below Θ-conditions the polymer conformations are more tightly packed in the bulk solvent. Decreasing degrees of penetration cause the polymer to swell after which it adopts a stretched conformation inside the pore. This effect is overshadowed by adsorption to the outer surface and inner pore walls when strongly attractive polymer-wall interactions are introduced.

Evaluation and recommendations The most important conclusions drawn in the different chapters are discussed here and some recommendations for future work are proposed.

Noteworthy, the simulation method gives only static polymer conformations, not conformations as a result of dynamics e.g. shear. This does not render the results obtained useless for practical situations, but the results are equilibrium polymer conformations that will also be dominant in a dynamic situation. As will be shown, the quantities derived from these conformations give usefull information about bottlenecks for diffusion, e.g. partition coefficients and energy barriers. Also we get an idea how polymers have to deform in order to diffuse from bulk solvent to bulk pore.

1.2 Retention Experiments and Flow Induced Deformation

The outcome of retention experiments depends strongly on adsorption characteristics of the solute, solvent quality, and concentration of the solute. High concentrations can cause concentration polarisation and solute clustering while strong surface adsorption causes fouling. The solvent quality can be a crucial factor determining the shape of polymeric solutes: the solute particles can be dense spheres or they can adopt a conformation of a loose deformable coil. In the ideal situation of dense spheres caused by a relatively poor solvent or very strong intramolecular forces, like they occur in proteins, membrane permeation can be modelled by a sieving mechanism. Then the retention of the solute is related to the solute concentration in the feed and permeate for non adsorbing spheres and non-adsorbing inner pore surfaces. $R = (c_{feed} - c_{permeate})/c_{feed} = (\lambda(2-\lambda))^2$. Also the region for degree of confinement (solute size divided by the pore size) is restricted.[36] The model only applies for pores larger than the solute spheres when diffusion is the dominant driving force and expansions of the model were made to account for the case where convection is dominant.[61,67]

In a bulk solvent, the polymer adopts a coil like conformation when there are no external forces acting on the polymer. When a large force is imposed on the polymer coil, the coil deforms and adopts a more stretched conformation.[30] In ultrafiltration experiments solvent flow may cause such strong forces and initiate 'flow induced deformation'. Suppose we have a dilute polymer solution, where the polymer has a radius of gyration slightly larger than the radius of a pore. At low transmembrane pressures shear forces acting on the coil are also low. The polymer will not enter the pore and retain its original coil conformation.[29] At high pressures this shear can become so large that it exceeds the 'critical shear'. At this coil-stretch transition point the polymer starts to unroll itself and enters a small pore.[8] This situation can be related to a critical flow.[10]

The coil-to-stretch transition was calculated by de Gennes to be very sharp.[29] This would mean that at the critical shear rate (or flow rate), the retention of a membrane for flexible polymers would immediately drop to zero. Experimentally this is not seen, because of distributions in pore size.[70] Also for membranes with a uniform pore distribution a gradual transition was found.[1] Another type of model also predicted a more gradual transition.[54] Deformation caused by shear flow was proven experimentally by several authors on dilute polystyrene solutions, where polystyrene oriented or stretched in the direction of the imposed flow.[58,62,69,71] Studies on shear induced deformation of polymer aggregates and microcapsules gave similar results.[53,79,106] These microcapsules have their enclosing membrane also rotate around themselves.[79,106]

1.3 Polymers in Confining Geometries

1.3.1 Polymers in Good Solvents

As pointed out above, the shape of the polymer (or conformation) can be a crucial factor in separation processes based on size exclusion. The polymer conformation depends greatly on the environment it resides in. Intermolecular interactions and interactions with various geometries, e.g. pore walls or surfaces, affect the polymer conformation depending on the strength of this particular interaction potential.

The conformation of polymers in solution has been extensively studied and characterised by scaling laws as function of e.g. chain length and concentration.[30] Single chains in an ideal solvent adopt a coil-like structure and the size of the coil scales as $\langle R^2 \rangle \sim Na^2$, where R is the end-to-end distance, N the number of segments (or monomer units), and a the size of the segment. In a good solvent this relation becomes $\langle R^2 \rangle \sim N^{1.2}a^2$ Increasing the concentration results in a gradual decrease of the coil size (in a good solvent in the semidilute regime) and is predicted with the power law $\langle R^2 \rangle \sim c^{-0.5}$, where c is the polymer concentration.[30]

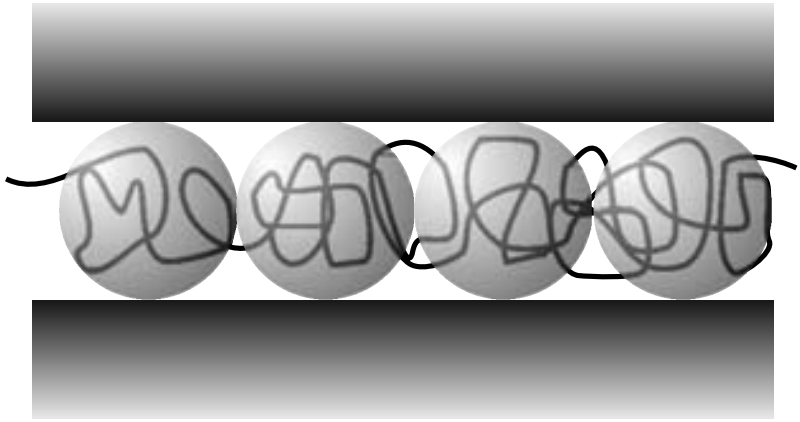

Figure 1.2: *A confined polymer subdivided into a sequence of 'blobs'.*

1.3.2 Confined Polymers

Determining the conformation of confined polymers is more complex due to various geometrical, often asymmetric, restrictions of the polymer segments. A confined flexible polymer dissolved in a good solvent can be pictured as a sequence of 'blobs' where the blobs have a diameter equal to the pore diameter (Fig. 1.2). Inside each blob the chain conformation is not perturbed by the presence of the wall. The total confinement energy scales linearly with the number of blobs in the confinement.[27,44]

In equilibrium such a flexible polymer chain in contact with a porous interface will diffuse into a cylindrical pore without much difficulty as long as the polymer radius of gyration R_g is smaller than the pore radius. The confinement energy is then in the order of $kT(R_g/D)^{5/3}$.[30] In strong confinements (a narrow cylinder as in Figure 1.2) the increase of confinement energy equals $TN(a/D)^{5/3}$, where D is the pore diameter.[30] Although this seems like a large energy barrier to overcome, application of an additional driving force can provide the extra energy making it possible for large flexible linear polymers to enter a small pore as shown above.

The degree of confinement, λ, is expressed as the size of the polymer coil divided by the size of the confinement, i.e. the pore, as $\lambda = R_g/R_{pore}$. When λ is small the confinement

is large compared to the polymer dimensions and when λ is large the confinement is small compared to the polymer dimensions.

The deformation of polymers as a result of confining geometries can be divided into four regimes depending on the degree of confinement λ. Van Vliet et. al.[104] defined these regimes for a flexible chain confined in a slit (Fig 1.3). The results are easily translated to cylindrical pores. If we define $\delta = L/N^{\nu(3)}$ with L the distance between the plates, N the chain length, and $\nu(3)$ the Flory exponent for three dimensions, then the regimes are:

regime IV ($\delta \geq 2.5$) The average conformation of the polymer coil resembles that of an unconfined polymer. The polymer is not influenced by the walls.

regime III ($1.5 \leq \delta \leq 2.5$) The polymer coils are oriented with their main principle axis to the plates (in case of a cylindrical pore the coils are aligned to the pore axis). The average shape does still largely resemble the unconfined coil conformation. *

Regime II ($1 \leq \delta \leq 1.5$) The polymer chain is squeezed in the direction of all three principal axes.

Regime I ($\delta \leq 1$) The smallest principle axis of the polymer coil is squeezed towards its minimum, meaning that in a slit the coil adopts a 2-dimensional 'pan-cake'-structure and in a cylindrical pore the coil is completely stretched (one-dimensional).

Partitioning of polymer coils depends greatly on the degree of confinement; the confinement energy increases with increasing degrees of confinement λ. The partition coefficient K, defined as the polymer concentration in the pore divided by the concentration in the bulk solvent region, decreases as $K = \exp(-F_{conf}/kT)$, where F_{conf} is the increase of the chain conformational free energy. Teraoka[102] reviewed the behaviour of various polymer architectures confined in various geometries where only excluded volume (repulsive)

*An important fact to note here is that a polymer in bulk solvent is *not* spherical but has a slightly ellipsoid conformation[72]

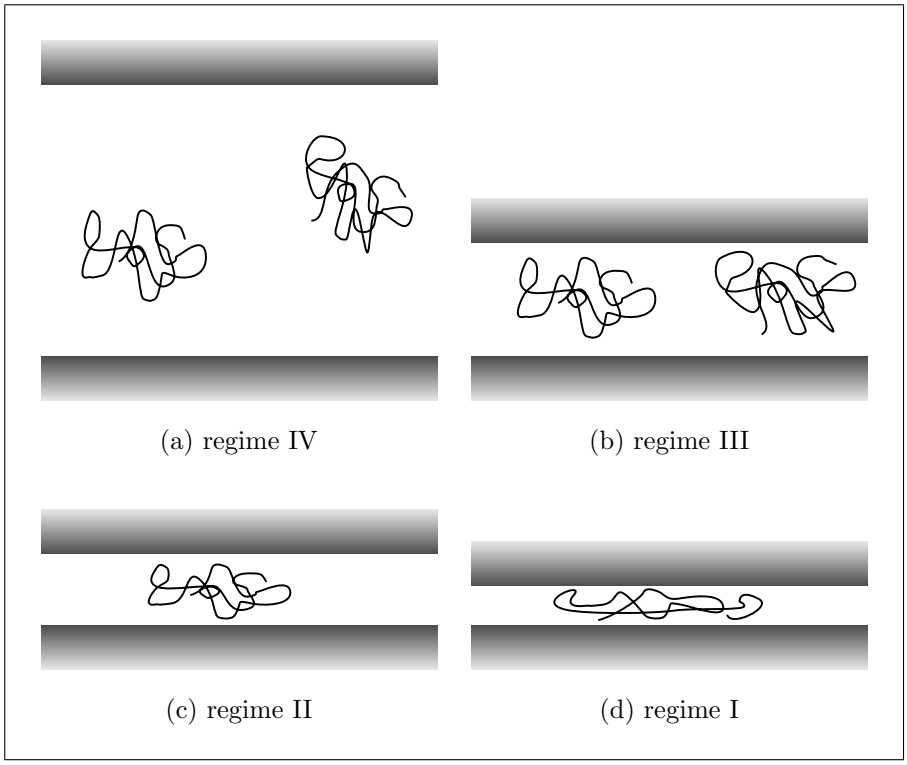

Figure 1.3: *The regimes of confinement for polymers in confinement.*

polymer-wall interactions were involved; the space occupied by the geometries material is not accessible to the polymer segments as is the space occupied by other polymer segments. Theoretical models of partitioning of confined polymers deal predominantly with infinitely dilute solutions or flexible macromolecules having only excluded volume interactions with their geometries walls[17,18] and with themselves.[27] Also other polymer architectures, e.g. random networks, have been investigated.[40]

Partition coefficients depend not only on the degree of confinement λ, but also on the polymer chain length and concentration.[12,28,41,42] At small degrees of confinement ($\lambda << 1$) the partition coefficient K equals approximately unity. Increasing λ results in lower K values due to an entropy penalty caused by decreasing degrees of freedom of the confined polymer conformations. Large degrees of confinement ($\lambda > 1$) result in very small K values.[17,18,28]

The effect of concentration was also taken into account in theoretical studies[41,42] and confirmed by Monte Carlo simulations[12] where an increase of concentration results in higher values of the partition coefficient K for given degrees of confinement; polymer chains in good solvents contract with increasing concentration because of the screening of intramolecular interactions.[33]

In a system of small chains confined in small pores the partition coefficient is smaller than in a system of large chains in large pores with equal degree of confinement λ. This implies that the longer, more flexible polymer chains are likely to enter a pore more easily.[28]

1.3.3 Variation of Solvent Quality

When the solvent quality decreases the solvent is expelled from the coil interior and, the polymer collapses into a tight globule. This has implications for situations where porous interfaces are involved. When the pores in the interface are large, i.e. small degrees of confinement ($\lambda \ll 1$), confinement energies and consequently the partition coefficient, are not really affected by the worsening of the solvent quality.[25] At large degrees of confinement however ($\lambda \gtrapprox 1$), the confinement energy increases towards very large values resulting in negligible K values already before λ equals unity.[13]

In very good solvents a polymer behaves as a self avoiding walk . Due to favourable monomer-solvent interactions the coil swells to larger dimensions, a process that can be modelled just as well by assuming effective repulsion between monomers, which is accounted for by modelling chain conformations as self avoiding walks. On the other hand, monomers in polymer chains dissolved in a Θ-solvent are arranged as a random walk. In this case, the solvent quality is such that solvent-monomer attractive interactions (that swell the solvent chain) exactly balance against monomer-monomer attractions (that contract the chain). The resulting coil conformation can then be modelled by a random walk in which monomer excluded volume (repulsive) interactions are absent and monomer units, on average, do not experience each others presence.

In good solvents the partition coefficient depends largely on polymer concentration. When polymers are dissolved in a Θ-solution this concentration dependence does not hold anymore: at low concentrations in Θ-solutions the partition coefficient is approximately equal the partition coefficient of athermal chains (chains in a good solvent) for the same chain dimensions. At high concentrations, however, below the overlap concentration, the partition coefficient in the Θ-solvent is independent of the concentration.[24,26] Above the overlap concentration the partition coefficient increases towards unity for Θ-chains. This increase of the partition coefficient occurred at much higher concentrations for athermal chains[26] because of clusters forming in the bulk solvent, caused by unfavourable polymer-solvent interactions, and by screening of intra-molecular interactions.[13,26]

1.3.4 Adsorption Effects of Polymers

Polymer Adsorption on Flat Walls

Before going on to the effects of surface adsorption on polymer properties in pores, some important quantities characterising adsorption effects are introduced in view of polymer adsorption on flat walls. The polymer types dealt with are generally homopolymers of various chain lengths.

The conformation of polymers adsorbed onto a wall depends predominantly on the adsorption potential between the monomer units and the wall. At low interaction strengths, the polymers do not lay flat on the wall, but they exist as a sequence of loops, trains and tails (Fig. 1.4). The trains are fractions of successive monomers adsorbed on the surface. The loops are series of non-adsorbed monomers in the chain connecting the trains. The tails are only in contact with the surface with one end connected to a train, the other end free in the solvent.[32,80,83,84]

A very important quantity to describe the extent of adsorption is the critical adsorption energy ϵ_{cr}. At this point the effect of conformational entropy loss near the wall is

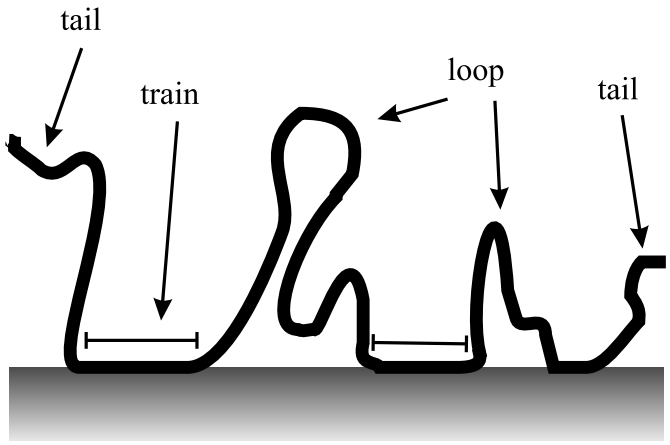

Figure 1.4: *The monomers of polymers adsorbed on a flat wall are arranged in sequences of adsorbed 'trains', 'loops' connecting the trains, and 'tails' at the ends of the chains.*

exactly compensated by the attractive energy of the monomers with the wall[32] and is a function of surface topology. Also the conformation of an adsorbed polymer changes from 3 dimensional to a quasi 2-dimensional conformation at this critical adsorption point.[34] At adsorption energies lower than the critical adsorption energy one speaks of weak adsorption and at adsorption energies higher than the critical adsorption energy one speaks of strong adsorption.

Weakly adsorbed polymer chains are only loosely adsorbed maintaining a coil-like conformation at the surface where only a few monomers are adsorbed on the surface (trains) connected by large loops. Generally also 'tails' take up a large part of the chain.[84] Strongly adsorbed chains lay relatively flat on the surface having very small loops and large trains.[32,84] The influence of tails is then negligible.[84]

The influence of solvent quality can be considerable, because when the solvent quality drops, also favourable intramolecular monomer interactions start to compete with monomer-wall interactions. In Θ-solvents, when the bulk concentration is not infinitely dilute, a larger part of the surface is covered by the polymer compared to adsorbed poly-

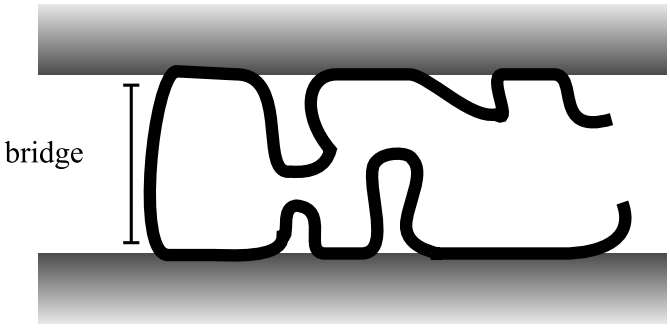

Figure 1.5: *Adsorbed polymers confined in narrow pores or slits are able to form 'bridges' between opposing walls.*

mers in athermal (very good) solvents, because polymers attract each other in other than good solvents.[83] An increasing concentration also accounts for a smaller fraction per polymer chain able to be adsorbed.[83] Increasing the chain length causes a similar effect.

Polymer Adsorption in Confinements

When polymers adsorb on the surface of confinements the situation becomes more complicated; a polymer chain is now able to adsorb to more than one surface. This has important implications for polymer permeation and many industrial applications that involve oligomer and polymer permeation, e.g. chromatography, membrane filtration and diffusion in zeolites, rely heavily on the possibility of polymers to adsorb on the porous material. A polymer chain confined between two flat plates, i.e. a slit like pore, can adsorb on both plates where the polymer parts adsorbed on one plate are connected to the parts adsorbed on the other plate by 'bridges' (Fig. 1.5).[32,83] Increasing the polymer-wall interaction strength, ϵ_{pw}, results in a decrease of the average number of bridges and also a decrease of the number of monomers inside the bridges.[32]

Also loops, trains, and tails are present in polymers adsorbed in confinements, like on flat walls. The introduction of a small attractive interaction potential has little effect on

the confined polymer conformation, compared to the situation with repulsive walls.[23,24] At the critical adsorption point and above, this situation changes drastically in a similar way as with adsorbed polymers at and above the critical adsorption energy on flat walls. The polymers are largely adsorbed to the confined walls as with flat walls,[23] where the polymer conformation is largely dependent on the geometry of the confinement e.g. slit, cylinder, cubicle pore, or a random network of fibres. Adsorbed parts on one side of the confinement are connected with bridges to the parts on the other side. Above the critical adsorption point the adsorbed conformations are very stable and an increase of polymer concentration only decreases the entropy penalty making the conformations even more stable.[24] Polymer dynamics are largely dependent on the polymer conformation inside the pore.[76]

Also an increase in the interaction strength results in increasing partition coefficients where the partition coefficient K rises towards values greater than unity around the critical adsorption point.[23,24,43,44] K is equal to unity at ϵ_{cr} for ideal polymer chains (polymers dissolved in a Θ-solution) but is slightly smaller for self avoiding walks (polymer chains in a good solvent) depending on the chain length N and λ.[43] Solvent quality has also a large effect on the critical adsorption strength: ϵ_{cr} decreases with increasing solvent quality.[83]

The nature of the interaction potential being long ranged or short ranged is also a matter of importance. Lin et al.[57] found that a weak potential over a long distance had a larger effect on polymer adsorption than a strong short ranged potential. Particularly for polyelectrolytes long ranged potentials come into play due to the long-range nature of the Coulombic forces. The partitioning is governed by steric and electrostatic polymer-pore interactions depending on the ionic strength in the solvent surrounding the polymer.[73]

An interesting analogy can be drawn with critical chromatography. Confined polymers are able to migrate with the same speed inside the porous network as inside the bulk at the point where adorption compensates for the entropic penalty of being confined in the network.[23] At that point also the concentration of polymer segments at the pore wall is

equal to that in the middle of the pore.[37] For ideal polymer chains this compensation point is equal to the critical adsorption point but for realistic polymers this is not true.[43]

There are many similarities between the diffusion of completely confined polymers through membrane material and chromatography and electrophoresis of polymers, but this is only marginally related to the topic of this thesis. The interested reader is referred to an excellent review of chromatography and electrophoresis theory and polymer dynamics written by Viovy.[105]

1.3.5 Polymer Flowers and Escape Transitions

The subject described in this section, polymer flowers and escape transitions of end-grafted polymers, are not investigated in this thesis but have some similarities with the subject of study. The remainder of this chapter deals with some peculiar properties of end-grafted polymers at the interface between two regions e.g. in transition from a bulk solvent region to a pore interior. An example of such a transition is the stretching of grafted DNA molecules after which the relaxation process of the molecules was followed in time (Fig. 1.6).[77] The DNA molecule's free end recoiled rapidly, after which a slower relaxation of the rest of the molecule followed. The rapidly recoiled free end of the molecule resembled a compact coil and the rest of the molecule still remained stretched. Imposing a strong flow on a relaxed grafted DNA molecule showed the molecule unrolling itself assuming transition conformations similar to the recoiling conformations.[78] Brochard-Wyart[15] proposed a 'stem and flower' model for those situations and later simulations were consistent with this model.[90,91]

Another situation in which these 'flower' conformations can be expected is when a polymer resides at the interface between two different environments, one more favourable for the polymer than the other. Such a situation occurs when a polymer is confined between two plates where the space separating the plates (the degree of confinement) can be varied

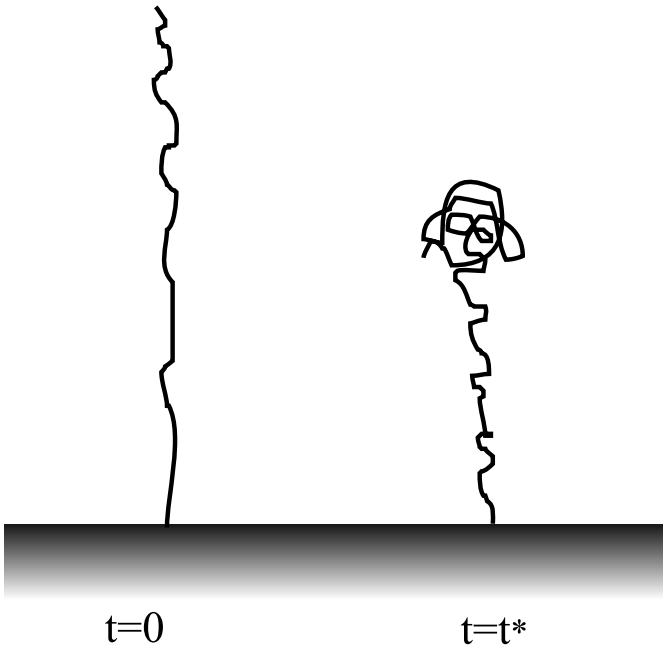

Figure 1.6: *The relaxation behaviour of stretched DNA molecules. At $t = 0$ the end grafted DNA molecule is completely stretched. When one end of the molecule is allowed to relax that end recoils into a coil whereas the relaxation of the lower part of the molecule near the graft point is much slower.*

and the length of the plates is slightly larger than the radius of gyration of the polymer (Fig. 1.7).

The polymer is grafted at the middle of the plate and the monomers are repelled by the surface. Such an end-grafted polymer is generally referred to as a 'mushroom'. When this mushroom is compressed it looses entropy and deforms. At a certain degree of confinement the polymer stretches out to the solvent outside the confinement so that only a small part of the polymer 'feels' the unfavourable confinement while the rest resides in a coil in the more favourable environment. The coil is then only connected to the grafting point by a stretched, small part of the polymer chain. This transition from the squeezed polymer conformation to a partially deformed polymer having one stretched part in the confinement and one part outside is known as the 'escape transition'[65,66,98,99] and can be proven by

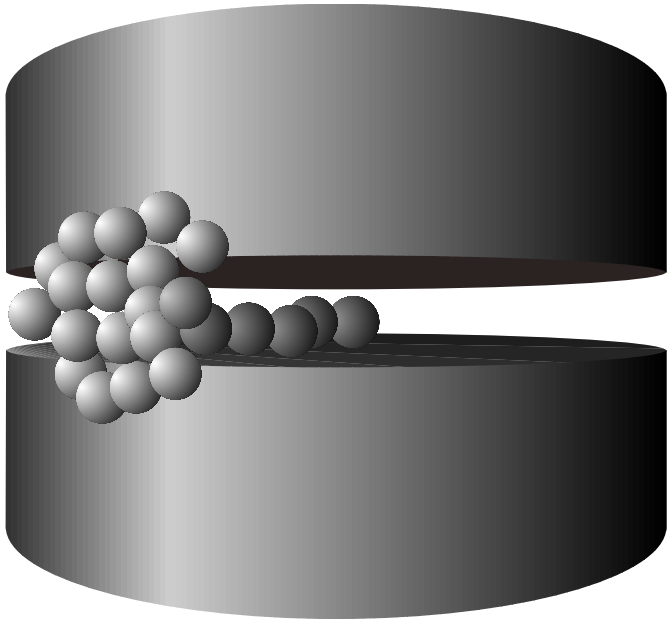

Figure 1.7: *A grafted polymer confined between two finite plates escapes from its confinement.*

AFM studies.[52] This picture changes when a polymer grafted on a repulsive cylinder is pushed towards a large flat wall having strong adsoptive interactions, above the critical adsorption energy, with the polymer. There is no sharp 'escape transition' to be found in the free energy plot as function of the degree of confinement.[55] The polymer conformation is for all degrees of confinement a 2D conformation adsorbed on the wall, also outside the confinement.

Such an escape transition is also found in situations where a grafted polymer chain resides in an unfavourable environment near an interface with a more favourable region by means of a potential step, e.g. an interface between a good and a poor solvent for the polymer (Fig. 1.8). Two regions are defined by a step-wise external potential creating a favourable and an unfavourable region for the polymer chain to reside in.[56,95] The end-grafted polymer again resembles a flower where part of the polymer resided in the unfavourable region and part of it in the favourable region. In the favourable region the

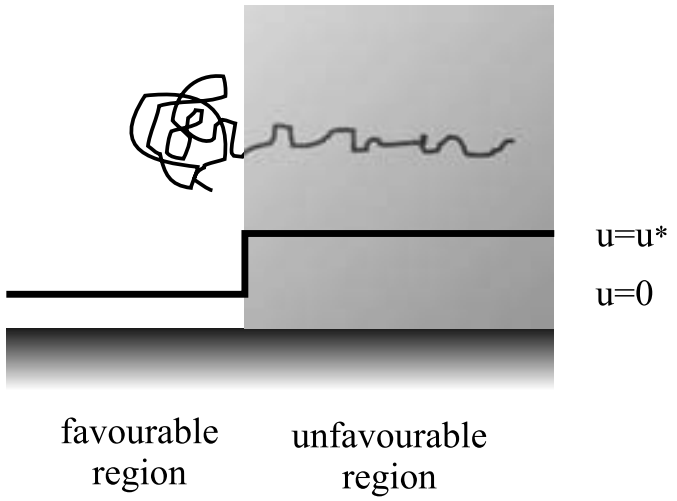

Figure 1.8: *A grafted polymer in a high (unfavourable) potential region escapes partly to the lower potential region similar to the escape transition from a confined polymer between two plates.*

chain adopts a coil-like structure resembling the 'crown' of a flower. This crown is connected to the graft point inside the unfavourable region by a stretched 'stem' (Fig 1.8). The escape from the high potential region and from the confinement was proven to be essentially the same.[89]

Experimentally such transition conformations are reported for systems where DNA molecules were analysed by means of entropic trapping.[46,47,103] Microsized (wide) compartments were separated by narrow slits. The trapped DNA molecules escape with a probability, which is determined by the ease at which a small part of the DNA molecule can enter this narrow slit. The longer molecules were able to escape much faster from these entropic traps than the smaller ones.

Such 'entropic trappings' are also present in zeolites where relatively large cages are connected by small cylindrical channels. During cage-to-cage diffusion the polymer head enters the channel and then stretches out while the 'body' remains in a coil conformation inside the cage.[60] The crossing of these molecules from cage to cage involves an entropic

barrier[88] and is closely related to the subject of our interests. Polymer and oligomer diffusion in zeolites depends largely on adsorption to specific sites in the channel for small molecules,[109,110] oligomers, and polymers[11,82] enhancing the viability of deformed polymer coils, even when the radius of gyration of the original unconfined coils is larger than for instance the radius of the cylindrical confinement; the excess free energy is decreased considerably due to these attractive interactions.[49,60]

Theoretical studies on infinitely thin membranes with small holes, the size of the hole was in the order of the monomer unit of the polymer chain, also showed the importance of adsorption effects: polymer translocation was much faster when the polymers could adsorb on the back side of the membrane compared to translocation through inert membranes. This was particularly clear at adsorption temperatures under the critical adsorption temperature (strong adsorption).[75] The curvature of the membrane also proved to be important for the polymer translocation.[68,74]

CHAPTER

TWO

Simulation Methods

2.1 Monte Carlo Simulations

To obtain information on conformational behaviour of partially confined polymers, Monte Carlo (MC) computer simulations were carried out. MC simulations heavily rely on a massive amount of random numbers which are used to impose small 'random events' on the system. These random events, or MC moves, may be monomer displacements, changes of dihedral angles within the chain, reptation moves, and so on. The move is accepted (or not) according to an acceptance rule that ensures that after many attempts the configurations sampled by this procedure obey the appropriate statistical distribution characterising the 'configurational space' of the system at equilibrium. The set of configurations obtained in the simulation is next used to obtain average quantities ('configurational space averages') like chain dimensions and confinement energies.

Clearly, the method provides static information only. This is due to the non-dynamic nature of the MC moves used to sample the systems configurational space. One may of course chose moves to closely resemble the natural dynamics of the system, but often this leads to a very slow sampling of configurational space. For example, if a polymer close to the entry of a narrow pore ($R_{pore} < R_g$) samples its conformational space by allowing small monomer displacement moves (mimicking Brownian motion) only, it probably never fully explores the pore interior during the course of the simulation. To speed up the sampling, moves involving the removal of a chain and its reintroduction at a random new point may for example be used. We then just take the chain from the bulk solution and put it inside a narrow pore and forget about how long the chain might have stayed in front of the pore entrance or how quickly it diffuses inside the narrow pore. The method to take away chains somewhere and reintroduce them somewhere else will be discussed below (section 2.3). First, however, the general principle of the MC method is introduced.

2.1.1 The Metropolis Method

The Metropolis method[39,63] provides us with a recipe to perform a random walk through configurational space, in such a way that the probability to visit a given configuration i (a set of coordinates $\vec{X}_i = \{\vec{r}_1, \vec{r}_2, \ldots, \vec{r}_N\}$) is proportional to the Boltzmann weight ρ_i of that configuration. In order to make such a random walk, MC moves are required some of which were briefly mentioned above. An important condition is that, if we prepare an ensemble of systems in equilibrium, then after one Monte Carlo step this ensemble is still in equilibrium. This can be achieved by imposing the detailed balance condition:

$$\rho(\vec{X}_{old})P_{old\to new} = \rho(\vec{X}_{new})P_{new\to old} \tag{2.1}$$

Thus, the probability that the system leaves an old configuration $\vec{X}_{old}$ and arrives at the new configuration $\vec{X}_{new}$ must be equal to the probability of the reverse process. $\rho(\vec{X}_{old})$ ($\rho(\vec{X}_{new})$) is the probability of finding the system in configuration $\vec{X}_{old}$ ($\vec{X}_{new}$) and $P_{old\to new}$ ($P_{new\to old}$) is the probability of accepting a trial move from *old (new)* to *new (old)*. From eq. 2.1 it follows,

$$\frac{P_{old\to new}}{P_{new\to old}} = \frac{\rho(\vec{X}_{new})}{\rho(\vec{X}_{old})} = e^{-\beta(U_{new}-U_{old})} \tag{2.2}$$

where in the last step the Boltzmann weights were substituted. In eq. 2.2, U_{new} is the energy of the new configuration, U_{old} the energy of the old configuration, and $\beta = 1/k_bT$ where k_b is the Boltzmann constant and T the absolute temperature.

A choice of $P_{old\to new}$ that satisfies the above condition is

$$P_{old\to new} = \min\left(1, e^{-\beta\langle U_{new}-U_{old}\rangle}\right) \tag{2.3}$$

which is known as the Metropolis acceptance criterion.

In practice this criterion is used as follows:

- A trial move is performed and $\Delta U = U_{new} - U_{old}$ is calculated
- If $\Delta U < 0$ the trial move is accepted
- If $\Delta U > 0$ a random number $\mathcal{R}$ is drawn. If $\mathcal{R} < \exp(-\beta \Delta U)$ the move is accepted, it is rejected otherwise.

2.1.2 Self Avoiding Walk

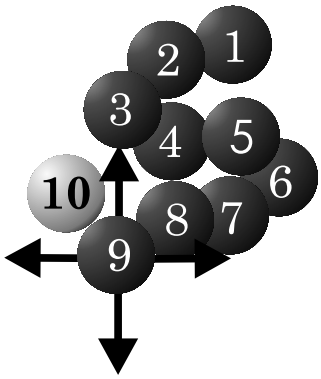

Figure 2.1: *A polymer chain growing by a Self Avoiding Walk.*

Based on the Metropolis algorithm above one could try to sample the conformational space of a polymer by performing a random walk on a lattice in which conformations are generated ('grown') by performing trial moves in which new segments are placed in a random direction on the lattice one after the other. At the end of the walk the trial step is accepted or rejected according to eq. 2.3. Of course, only conformations that do not violate excluded volume restrictions are accepted. These conformations are called self-avoiding walks, an example of which is shown in Fig. 2.1. If the monomers have, in addition to their excluded volume interactions, attractive interactions as well such a method would allow studying the effects of solvent quality on chain conformational behaviour. One could also think of performing such a walk inside a narrow pore to study confinement effects.

In practice, this will not work. The majority of those trial conformations will violate excluded volume restrictions and hence be rejected causing the procedure to become infeasible, in particular, when long polymer chains are studied in dense media (like melts) or confining geometries. A way to avoid generating overwhelming numbers of trial conformations that all go down the drain is to 'look ahead' when introducing a new repeat

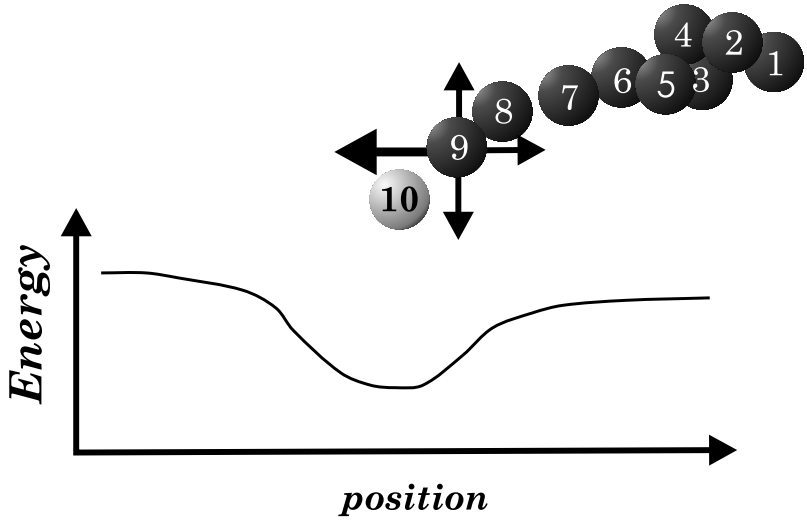

Figure 2.2: *Growth of a polymer chain using the Configurational Bias Monte Carlo algorithm. Chain conformations are generated by 'growing' a chain, one segment after the other, with a bias toward low energies.*

unit and choose the direction which is energetically most favourable. In that way we bias the chain to adopt low energy conformations, which of course leads to a non-Boltzmann distributed set of configurations. One can correct for the introduced bias by assigning to each chain a conformational dependent weight factor W. This was first done by Rosenbluth and Rosenbluth[81] and led to the Configurational Bias Monte Carlo method that will be discussed below.

2.1.3 Configurational Bias Monte Carlo

Configurational Bias Monte Carlo (CBMC) is an algorithm that generates chain conformations with a particular bias towards energetically favourable ones.[38,39,48,94] The algorithm is set up such that the correct (Boltzmann) distribution of chain conformations is recovered in the Monte Carlo sequence. CBMC can successfully be applied in systems where topological constraints play a dominant role.[96,97]

The CBMC method is based on attempts to remove an *old* chain conformation (denote above by $\vec{X}_{old}$) from the system and replace it by a *new* one. The success probability of such

attempts depends on the statistical weights of the new and the old conformations which are determined in two steps. First, the new conformation is generated by introducing repeat units one after the other (a 'growing' algorithm) in such a way that the direction of each newly grown monomer is biased towards directions of low energy (Fig. 2.2). The growth of a chain starts with the insertion of the first monomer at a randomly chosen starting point on the simulation lattice. The energy change resulting from this insertion is $u_1(new)$ and $w_1(new) = \mathcal{N} \exp(-\beta U_1(new))$ is the Rosenbluth weight of the first monomer. Here $\mathcal{N}$ is the number of possible directions on the lattice. Thus, for successive segments there are always $\mathcal{N}$ possible directions and the energy of segment i with direction j is denoted by $u_i(j)$. After the first monomer has been placed, all others follow and each new monomer i can choose from $\mathcal{N}$ possible directions of which one is chosen with a probability

$$p_i(new) = \frac{e^{-\beta u_i(new)}}{w_i(new)} \tag{2.4}$$

where $w_i(new)$ is defined as

$$w_i(new) = \sum_{j=1}^{\mathcal{N}} e^{-\beta u_i(j)} \tag{2.5}$$

The interaction energy $u_i(j)$ includes all interactions of monomer i with other molecules in the system and with monomers 1 through $i-1$. Note that this energy includes the interactions between monomer i and the pore surface as well. It does, however, not include interactions with monomers $i+1$ to M (the last monomer). In this way, once the entire chain is grown, its energy is given by $U(new) = \sum_{i=1}^{M} u_i(new)$. If the entire chain has been grown, one determines the Rosenbluth factor (the statistical weight) of the new configuration:

$$W(new) = \prod_{i=1}^{M} w_i(new) \tag{2.6}$$

Similarly, to determine the Rosenbluth factor of the old chain, one proceeds by first selecting one of the chains in the system at random. The energy of the first monomer of this old chain is $u_1(old)$ and $w_1(old) = \mathcal{N}\exp(-\beta u_1(old))$. The Rosenbluth factor of the remainder of the chain is next calculated by evaluating the energy $u_i(o)$ of monomer i at its actual position and the energies it would have had if it were located at any of the remaining $\mathcal{N}-1$ neighbouring sites. These energies are used to compute:

$$w_1(old) = \mathcal{N}e^{(-\beta u_1(old))} + \sum_{j=2}^{\mathcal{N}} e^{(-\beta u_i(j))} \tag{2.7}$$

Once the entire chain has been 'retraced', the Rosenbluth factor is determined as:

$$W(old) = \prod_{i=1}^{M} w_i(old) \tag{2.8}$$

Finally, the trial move from $old \rightarrow new$ is accepted with a probability given by:

$$acc(old \rightarrow new) = min\left[1, \frac{W(new)}{W(old)}\right] \tag{2.9}$$

It is easily shown[39] that this acceptance criterion satisfies the detailed balance condition (eq. 2.1).

2.1.4 Rosenbluth sampling

The use of the Metropolis method as the sampling method to obtain the quantities that characterise the polymer conformations seems to be the logical choice. However, in a system with two regions, where in one region the polymer growth results in more probable chain conformations, the conformations in the region with low probability chains is not sampled properly due to the acceptance criterium of the Metropolis method (equation 2.9), which is likely to reject such chains. This leads to poor convergence in the high energy region.

This poor convergence can be avoided by using Rosenbluth sampling instead of the Metropolis method.[39] Then every trial conformation is accepted and the quantities calculated from these conformations are taken into account for averaging with a weighting factor, the Rosenbluth factor W. The Rosenbluth average of the quantity $\mathcal{A}$ to be measured is then calculated as follows:

$$\langle \mathcal{A} \rangle_{\mathcal{R}} = \frac{\sum_{n=1}^{N} W(n)\mathcal{A}(n)}{\sum_{n=1}^{N} W(n)} \tag{2.10}$$

where N is the number chains generated. Unfinished, failed growth attempts, are accompanied with a weighting factor $W = 0$, so that the unfinished chains do not contribute to the average result other than decreasing the probability, i.e. increasing the excess chemical potential, of the chain (see page 42). It is trivial to show that $\mathcal{A}_{\mathcal{R}}$ is equal to the canonical average of $\mathcal{A}$.

2.2 Bond Fluctuation Model

In many cases of Monte Carlo simulations of polymers cubic lattice models are used. The position of a neighbour polymer segment can only be at the six lattice sites neighbouring the previous segment in 3 dimensional space. Linear polymers of only a few segments long tend to look rather artificial on such a lattice. Throughout this thesis a polymer length of 50 segments is used and also in this case the polymer shape will have such characteristics. It will be very undesirable to base statistical information of polymer conformations on such models. In order to obtain more realistic conformations of this small polymer the Bond Fluctuation model will be used.[16]

The polymer segments are modelled as cubes taking up eight lattice points. The centre of the cube is used as connection point of the bonds. The Bond Fluctuation model uses flexible bonds between the segments that can vary in length and direction. The bonds between the segments have a length such that another segment is not able to cross the bond

when excluded volume conditions are used. This also means that two segments can take up 108 different configurations on a 3 dimensional lattice so the bonds fluctuate between a length of 2 and $\sqrt{10}$ making it effectively an off-lattice case. When combining Bond Fluctuation with Configurational Bias Monte Carlo, it becomes very CPU-time intensive to sample all possible directions in order to decide where a new polymer segment must be placed. In order to save CPU time only 50 directions randomly chosen from the set of 108 possible directions are sampled. *

It is also possible to simulate dynamic properties of polymer systems using this model resulting in Rouse behaviour in case of polymer melts.[16] The model is ergodic which makes simulating dense polymer systems also possible. As already mentioned before throughout this thesis only self avoiding walks of single chains are considered.

Interaction of the segments with other segments or foreign geometries other than excluded volume is also possible by assigning an interaction energy with the other object to the cubic polymer segment. The eight lattice points occupied by the segment all interact with objects on neighbouring lattice points. When for instance a segment is in contact with a flat wall four lattice points will interact with this wall. The total interaction energy is the sum of these four individual interaction energies. Inter-segment interaction defines the quality of the solvent: in a good solvent these are absent and only excluded volume restrictions are relevant. In a poor solvent monomer-monomer interactions are strong. A more detailed description can be found on page 40.

An important property of our system is critical adsorption energy of the polymers on the wall material. At this monomer-wall interaction energy the confornational entropy loss

*The $\mathcal{N}$ in equation 2.5 and 2.7 on page 34 was stated to be the number of trial directions being sampled for the Rosenbluth factor w_i normally taken to be the coordinate number of the lattice, or the number of grow-directions. Because only 50 randomly chosen directions of the possible 108 are sampled, $\mathcal{N}$ must be taken 50.

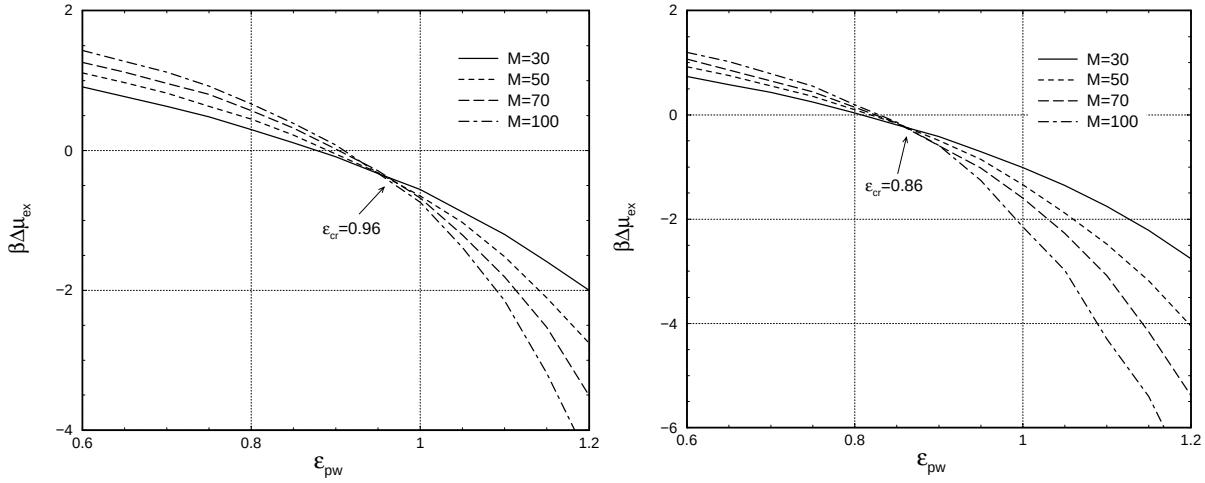

(a)

(b)

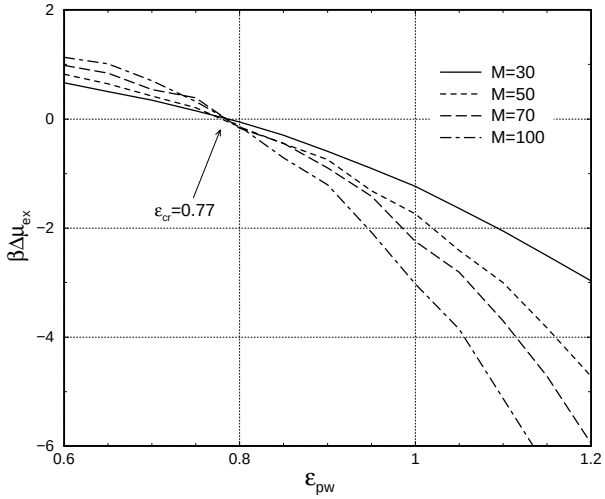

(c)

Figure 2.3: *Reduced chemical potential, $\beta\Delta\mu_{ex}$, at attractive surfaces of varying monomer-wall energies ϵ_{pw}, relative to the chemical potential in the bulk solvent. The intersection points provide the critical adsorption points ϵ_{cr} for a) athermal solvents ($\epsilon_{pp} = 0.0kT$), b) Θ-solvents ($\epsilon_{pp} = 0.2577kT$) and c) poor solvents ($\epsilon_{pp} = 0.30kT$). Below ϵ_{cr}, longer chains are more strongly repelled by the surface, above ϵ_{cr} longer chains are more strongly attracted.*

due to the presence of the impenetrable wall is exactly compensated by the energy gained due to monomer adsorption. Then, the adsorbed polymers will change their 3 dimensional coil conformation to a 2 dimensional 'pancake' conformation covering as much of the surface as possible. In this thesis the critical adsorption point of our system has been determined using the method of Gong and Wang.[43] These authors used end-grafted polymers (random walks and self-avoiding walks) to calculate the polymer's average excess chemical potential of the polymers and plotted this as a function of the monomer-wall interaction potential for various chain lengths. The critical adsorption energy was then identified with the energy where the graphs of the different chain lengths intersect. The latter definition is used in liquid chromatography of macromolecules. In liquid chromatography at the critical adsorption point (LCCAP), polymer adsorption on the column material does not depend on chain length resulting in elution times becoming independent of the polymer chain length too. The critical point in LCCAP, however, not necessarily coincides with the definition given above that requires the free energy change of adsorption to be zero. Theoretically, both definitions are equal for random walk chains.[43] Gong and Wang showed that when excluded volume effects are introduced the critical adsorption point (as defined from LCCAP) is found at monomer-wall contact energies where chain adsorption has already started and the free energy change of adsorption is negative. Despite this fact, the definition from LCCAP is used in this thesis to locate the critical adsorption energy. We modified Gong and Wang?s method by releasing the surface anchoring constraint and only take adsorbed polymers into account for computing the polymer excess chemical potential. Polymer lengths of 30, 50, 70, 100 monomers have been used. Figure 2.3 a, b and c show reduced chemical potential differences between polymers contacting the surface and polymers in a bulk solvent presented versus the monomer-wall contact energy for good solvent, a Θ-solvent and a poor solvent ($\epsilon_{pp} = 0.30kT$) condition respectively. The critical adsorption point in a good solvent is situated at $\epsilon_{cr} = 0.96kT$. In Θ-solvent and in the poor solvent the critical adsorption points are $\epsilon_{cr} = 0.86kT$ and $\epsilon_{cr} = 0.75kT$ respectively.

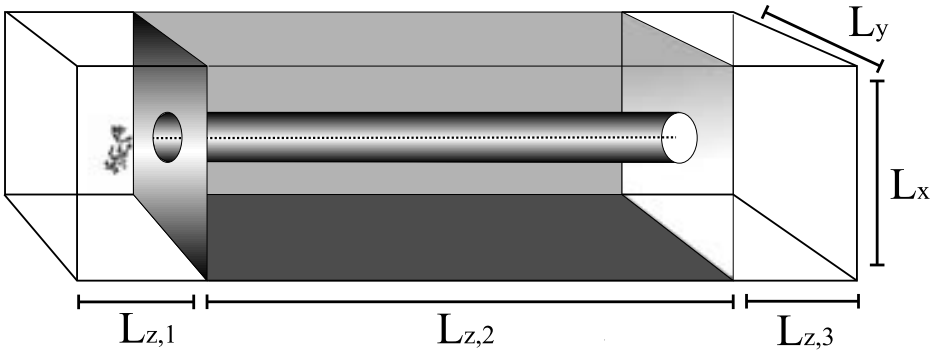

Figure 2.4: *simulation box used in all chapters*

2.3 System Properties

The simulation box is set up by putting a wall with a single straight pore in the middle of the box. The length of the cylindrical pore is large enough for the polymer to stretch completely without finding both ends at opposite pore mouths (Figure 2.4). All polymers are 50 repeat units long unless noted otherwise.

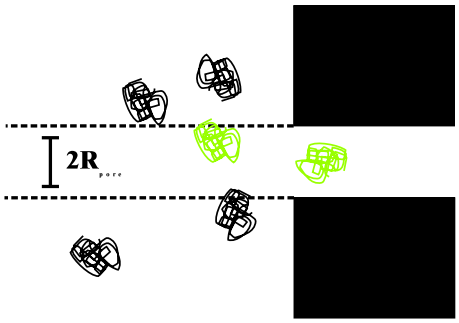

Figure 2.5: *Polymer chains start to grow at a starting points taken at random in the free space in the simulation box. Only chains with their centre of mass in the continuation of the pore are taken into account for averaging.*

The total monomer-monomer interaction energy of a polymer chain is equal to the amount of lattice points taken up by the monomer cube in contact with lattice points taken up by another monomer cube times the monomer-monomer interaction potential ϵ_{pp}. The total interaction energy of a polymer with the wall is equal to the amount of monomer-wall contacts times the interaction potential ϵ_{pw}. This differs from the calculation of the total intramolecular energy because of the following: the membrane, including the cylindrical pore, is modelled on a lattice. As a result strongly curved geometries e.g. narrow cylindri-

cal pores, become very irregular having a very rough, chequered inner surface. A monomer in contact with a flat wall would have four contacts with the wall, highly irregular surfaces can give rise to more than 4 contacts creating artefacts in the monomer-wall interaction energy in narrow cylindrical pores. In this system pore radii smaller than 5 lattice points cannot be used for quantitative analyses.

The radius of the pore is based on the radius of gyration of the polymer R_g by using a pore size relative to the radius of gyration, namely λ. This degree of confinement λ is defined as: $\lambda = R_g/R_p$. Under athermal conditions in the bulk solution the radius of gyration of the polymer coil R_g is equal to 11.3 grid points. In a Θ-solvent the R_g becomes 8.7. The intramolecular interaction potential ϵ_{pp} is equal to -0.2577 at Θ-conditions. Below the Θ-temperature at $\epsilon_{pp} = -0.30$, the radius of gyration equals 7.5. We chose this particular value of ϵ_{pp} because at a degree of confinement λ=1.5 the used pore radius becomes 5 lattice points. This is the minimal pore radius to be used when adsorption effects are to be studied.

The dimensions of the simulation box are $L_{z,1} = L_{z,3} = 90$ grid points, $L_{z,2} = 201$ and $L_x = L_y = 82$ grid points. The MC simulations are performed as follows: the polymer chain starts to grow at a random location in the free space (not taken up by the membrane material). 100 million growth attempts take place and only polymers with their centre of mass within the cylinder, with a radius equal to the pore radius in the continuation of the pore (see Fig. 2.5), are taken into account for averaging to avoid that membrane porosity can influence the results. Also minimum image conventions are used in all three directions. The pore entry is defined as $z = 0$, so that negative z-values refer to positions inside the pore and positive z-values refer to positions outside the pore. The pore radius R_p is varied such that $\lambda = R_g/R_p$ normally varies between $\lambda = 1.5$ and $\lambda = 0.5$.

2.4 Important Quantities

2.4.1 Free Energy of Chain Molecules

Accompanied with conformational changes, the increase of the (excess) chemical potential of a chain (with respect to the chemical potential in the bulk solvent) as a function of its centre of mass position (along the pore axis) contains important information on pore penetration and polymer partitioning. This quantity is obtained from the probability to successfully insert a particle in the system. The chains are inserted using again the CBMC algorithm.[39] Every segment i has a chance to go into $\mathcal{N}$ directions and the direction with the highest Boltzmann factor is favoured over the other directions. The sum of the Boltzmann factors of all possible directions gives the Rosenbluth weight w_i of the ith segment:

$$w_i = \sum_{j}^{\mathcal{N}} e^{-\beta u_i(j)} \tag{2.11}$$

where $u_i(j)$ is again the energy of trial direction j of the ith segment. Then the accompanying excess chemical potential becomes:

$$\beta\mu_{ex} = -\ln\left(\prod_{i=1}^{M}\frac{w_i}{\mathcal{N}}\right) = -\ln\langle W\rangle \tag{2.12}$$

where the average Rosenbluth factor $\langle W\rangle$ is obtained by averaging over all growth attempts.

The free energy is calculated as a function of the chain centre of mass position along the pore axis. A histogram at the appropriate entry (the bin value representing the centre of mass z-component) is updated with the chain Rosenbluth factor W.

The centre of mass of incomplete chains resulting from failed growth attempts was calculated using only the successfully grown monomers in the chain. In a case of unsuccessful

growth, the growth usually breaks off between the 30th and the last monomer so the calculated centre of mass for incomplete polymer chains will be close to a fully grown chain. Around 10% of the growth of polymers in small confinements ($\lambda = 1.6$) is unsuccessful. Almost all growth attempts in the bulk are successful.

2.4.2 Conformation Related Quantities

The deformation of polymers entering narrow pores can be characterised by defining an asphericity that quantifies how much the average coil shape deviates from a perfect spherical one. The asphericity is obtained from the radius of gyration tensor $S_{ij} = \frac{1}{50}\sum_{m=1}^{50}(r_{m,i} - r_i^{cm})(r_{m,j} - r_j^{cm})$, which is calculated for each generated chain conformation and next diagonalised. Here $r_{m,i}$ is the position of monomer m on the cartesian axis i and r_i^{cm} is the centre of mass position of the polymer on cartesian axis i. The three eigenvalues obtained by this procedure provide information about the average shape of the polymer. We use these eigenvalues to define the asphericity A of the coil:[87]

$$A = 0.5\left(\frac{3V_1}{V_1 + V_2 + V_3} - 1\right) \tag{2.13}$$

where V_1 is the largest eigenvalue and V_3 is the smallest eigenvalue of matrix S. The asphericity A equals 0 when the polymer coil takes on the shape of a perfect sphere. An infinitely thin cylinder has an asphericity $A = 1$. In bulk (athermal) solution the polymer studied (chain length 50) has an asphericity $A_{bulk} = 0.61$.

When more detail of the polymer conformations is needed, it is useful to calculate the average components of the radius of gyration parallel and perpendicular to the pore axis:

$$\langle R^2_{g,parallel}\rangle = \left\langle \frac{1}{M}\sum_{m=1}^{M}(r_{m,z} - r_z^{cm})^2 \right\rangle \tag{2.14}$$

$$\langle R^2_{g,perpendicular}\rangle = \left\langle \frac{1}{M}\sum_{m=1}^{M}\frac{(r_{m,x} - r_x^{cm})^2 + (r_{m,y} - r_y^{cm})^2}{2} \right\rangle \tag{2.15}$$

Here $\langle R^2_{g,parallel} \rangle$ is the radius of gyration component parallel to the pore axis and $\langle R^2_{g,perpendicular} \rangle$ the radius of gyration component perpendicular to the pore axis. $r_{m,x}$, $r_{m,y}$ and $r_{m,z}$ are the monomer positions on the Cartesian axes x, y and z respectively and r_x^{cm}, r_y^{cm}, r_z^{cm} are centre of mass positions of the polymers on the Cartesian components and M is the number of repeat units in the polymer chain.

CHAPTER

THREE

Monte Carlo Simulations of Partially Confined Flexible Polymers

Abstract We have studied conformational properties of flexible polymers partially confined to narrow pores of different size using Configurational Biased Monte Carlo simulations under athermal conditions. The asphericity of the chain and its R_g components parallel and perpendicular to the pore axis have been studied as a function of its centre of mass position along the pore axis. Both the asphericity and the parallel R_g component pass through a maximum well before all segments are located inside the pore. Rather than deforming gradually, we find that at intermediate penetration degrees, where the centre of mass is within distances of approximately one radius of gyration away from the pore entry, the chain adopts an asymmetric conformation, where the part inside the pore stretches out along the pore axis while the remaining part outside the pore is coil-like. When the centre of mass is located further inside the pore, this strong chain extension along the the pore axis diminishes and the average conformation becomes that of a deformed coil. At $\lambda \geq 1.0$, polymers located at the pore entry explore the pore predominantly with one of its end groups. Introduction of weakly attractive monomer-wall interactions does not affect these observations significantly.

Published as: G.F.Hermsen, B.A. de Geeter, N.F.A. van der Vegt and M. Wessling "Monte Carlo simulations of partially confined flexible polymers" *Macromolecules 35* (2002), 5267

3.1 Introduction

The shape of flexible polymers depends for a large extent on their environment viz. polymer concentration, the presence of other components, solvent quality and spatial confinements. Especially the shape of confined polymers and oligomers is a field of great interest, due to its significance in e.g. liquid chromatography, gel electrophoresis, oil recovery and membrane based separation processes.

Several computer simulation studies on confined polymers have been reported in the literature. Milchev et. al.[64] performed simulations on polymer chains confined in straight tubes and compared their results with existing scaling arguments. Cifra and Bleha[21,22] used Self Avoiding Walk Monte Carlo simulations in a slit like pore to find out the relation between the conformational behaviour of confined chains and polymer concentration at theta and athermal conditions. Varying the slit width, the coils adopted pancake-like conformations at small widths. Adsorption effects of polymer segments with the wall were not taken into account. The end-to-end-distance became greater with smaller slit widths. Later studies also took attractive polymer-wall interactions[23] and chain flexibility[24] into account and these findings confirm an analytical theory derived for a theoretical polymer chain between two repulsive plates by Shiokawa.[92,93] Also the shape of small end-grafted polymer chains, for which scaling arguments do not really apply, was studied for various degrees of confinement.[4] Even the shape of confined polyelectrolytes has been studied.[73]

Some molecular dynamics studies take polymer wall attractions into account: Zhang[111] studied linear decane films in carbon tubes with Lennard-Jones type segment-wall interactions and found that the chains aligned to the walls when close to the walls. Earlier Boyd et. al.[14] already studied effects of polymer shape of confined oligomers on partitioning. Aoyagi et. al.[3] performed molecular simulations on melts of coarse grained chains and found that polymers near the walls are deformed by attraction and the presence of other molecules and studied also the relaxation times of the chains in confinements for strong

attractive segment-wall interactions. Brownian dynamics simulations of hydrocarbons in (biological) membranes were carried out to cover greater time intervals.[35] These studies were all for fully confined polymers.

Escape transitions of end-grafted polymer chains from a confinement of two opposing walls of a piston are found[65,66] for various chain lengths. When varying the width of the confinement between the walls they found a relation for the escape width as function of polymer length and piston radius. These polymers burst out at a certain width after which the radius of gyration increases considerably. This transition is sharper for increasing chain lengths. A study of polymers confined inside a sphere escaping through a small hole to a bulk phase has also been done.[68,74,100] Here a free energy barrier is found in the transition from confinement to bulk.

Conformations of end-grafted polymers have been studied close to an interface modelled by a step-wise external potential. The authors found a transition of a coil-like to a flower-like conformation: a stretched stem of segments and, in the region of lower monomer potential, a coil-like crown containing the remaining segments.[56,95] Such flower conformations are very similar to some of the possible conformations found in this chapter for very small pores.

Although a lot is known about conformational behaviour of confined polymers, the intermediate conformations adopted by a polymer entering a pore from the bulk solution is still a rather unexplored yet important field. For example, entropic trapping of DNA molecules in microsized (wide) regions separated by nanofluidic (narrow) channels (smaller than the DNA radius of gyration) has been reported as a mean to separate long DNA molecules[46,47] in a practically integrated DNA analysis system. The trapped DNA molecules escape with a probability which is determined by the ease at which a small part of the DNA molecule can enter the narrow channel.

In this chapter we show that chain conformations of partially confined flexible polymers are very much different from the ones adopted at full confinement. It is the purpose of this chapter to find out how a polymer conformation exactly changes at different polymer centre of mass positions in cylindrical pores of various size during the diffusion process. Monte Carlo simulations are used to sample the conformational space of a flexible polymer model under good solvent conditions.

3.2 Simulation Details

A discrete Configurational Bias Monte Carlo (CBMC)[39] method is used to carry out the simulations, combined with the Bond Fluctuation method[16] to model the polymers. All simulated polymers are 50 monomers (M) long, each monomer taking up 8 grid points (a box) on a 3D simulation grid. Apart from their excluded volume interactions, no additional thermal interactions between monomers are taken into account, hence the simulations are performed under good solvent conditions. The interaction of one polymer segment with the (pore)wall is the summed interaction potential of the four grid points that are in direct contact with the wall and equals in total $0.0kT$ (no attraction) and $0.8kT$ (weak attraction). Note that $\epsilon_{cr} = 0.96kT$ is the critical adsorption energy of our model (chapter 2).

Because the bond-fluctuation model allows for the CBMC algorithm to let each segment explore 108 directions, making it effectively an off-lattice case, the procedure is very time consuming. For this reason all conformations are grown by choosing each new monomer growth direction from a set of 50 directions randomly selected from the complete list of 108 possibilities.

The simulation box is set up by putting a wall with a single straight pore in the middle of the box. The length of the cylindrical pore is large enough for the polymer to stretch completely without finding both ends at opposite pore mouths (Figure 3.1). The radius of the pore is based on the radius of gyration, R_g, of the polymer under athermal conditions

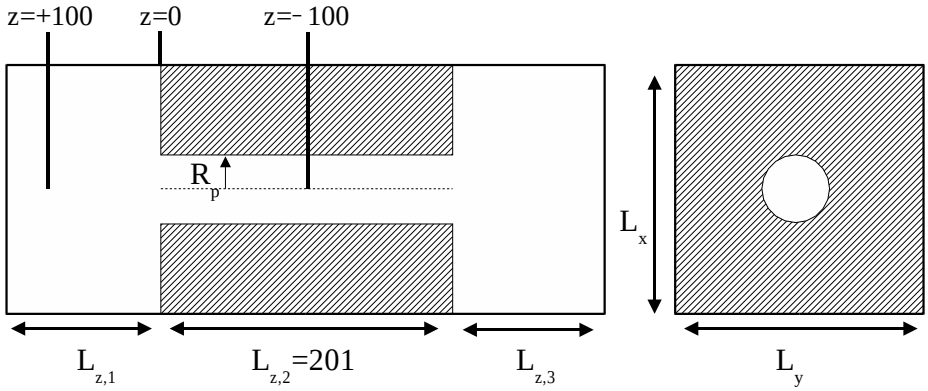

Figure 3.1: *Geometrical details of the simulation box.*

in the bulk solution, where the R_g is 11.3 grid points big. The dimensions of the simulation box are $L_{z,1} = L_{z,3} = 90$ grid points, $L_{z,2} = 201$ and $L_x = L_y = 82$ grid points. Periodic boundaries are used in all three directions. The MC simulations are performed as follows: 85 million chain growth attempts are performed starting from a random position of the first monomer in the free space between $z = +100$ and -100 grid points away from the surface. We use Rosenbluth sampling to obtain the conformation related quantities. Every successfully grown chain is used for averaging with an accompanying Rosenbluth weight according to:[39]

$$\langle \mathcal{A} \rangle_{\mathcal{R}} = \frac{\sum_{n=1}^{N} W(n)\mathcal{A}(n)}{\sum_{n=1}^{N} W(n)} \tag{3.1}$$

with $\mathcal{A}(n)$ and $w(n)$ the measured quantity and its accompanying Rosenbluth weight respectively and, $\langle \mathcal{A} \rangle_{\mathcal{R}}$ the Rosenbluth average of quantity $\mathcal{A}$. We computed the z-component of the centre of mass position of each generated conformation and updated a histogram at the appropriate entry (the bin value representing the centre of mass z-component) with quantity $\mathcal{A}(n)$ and the chain Rosenbluth factor W. The conformations grown at $z = +100$ do not experience the wall and resemble unconfined polymers in a good solvent. The conformations grown at $z = -100$ are fully confined by the pore geometry. The pore radius R_p is varied such that $\lambda = R_g/R_p$ varies between $\lambda = 2.1$ and $\lambda = 0.33$.

Accompanied with conformational changes, the increase of the (excess) free energy of a chain (with respect to its bulk solvent value) as a function of its centre of mass position (along the pore axis) may serve to define the transition region between bulk solution and bulk confinement. This quantity may be obtained from the probability to successfully insert a particle in the system, which in the Rosenbluth sampling scheme equates to the average Rosenbluth factor $\langle W \rangle$ obtained by averaging over all growth attempts. The excess chemical potential is obtained from $\beta\mu_{ex} = -ln\langle W \rangle$.[39]

The centre of mass of incomplete chains resulting from failed growth attempts (where a term $W = 0$ is contributing to the average Rosenbluth factor) was calculated using only the successfully grown monomers in the chain. In a case of unsuccessful growth, the growth usually breaks off between the 30^{th} and the last monomer so the calculated centre of mass for incomplete polymer chains will be close to a fully grown chain. Around 10% of the growth of polymers in small confinements ($\lambda = 1.6$) is unsuccessful. Almost all growth attempts in the bulk are successful.

3.3 Results

3.3.1 Conformational Changes and Conformation Excess Chemical Potential of Partly Confined Polymers

Figure 3.2 shows a series of snapshots of chain conformations with different centre of mass positions $CM(z)$, at a degree of confinement $\lambda = R_g/R_p = 1.6$. In the bulk solution (Fig. 3.2a) and the bulk part of the pore (Fig. 3.2f) the chain assumes a coiled conformation. At intermediate degrees of penetration (Fig. 3.2b-e) the chain conformations look different: at a centre of mass position along the pore axis of 5 grid points outside the pore, just in front of the interface, there are mainly two types of conformations to be found. One type, (Fig. 3.2b) , has a large part outside the pore in a coil like conformation and is already starting to penetrate the pore. The chain stays away from the interface as much as possible. Another

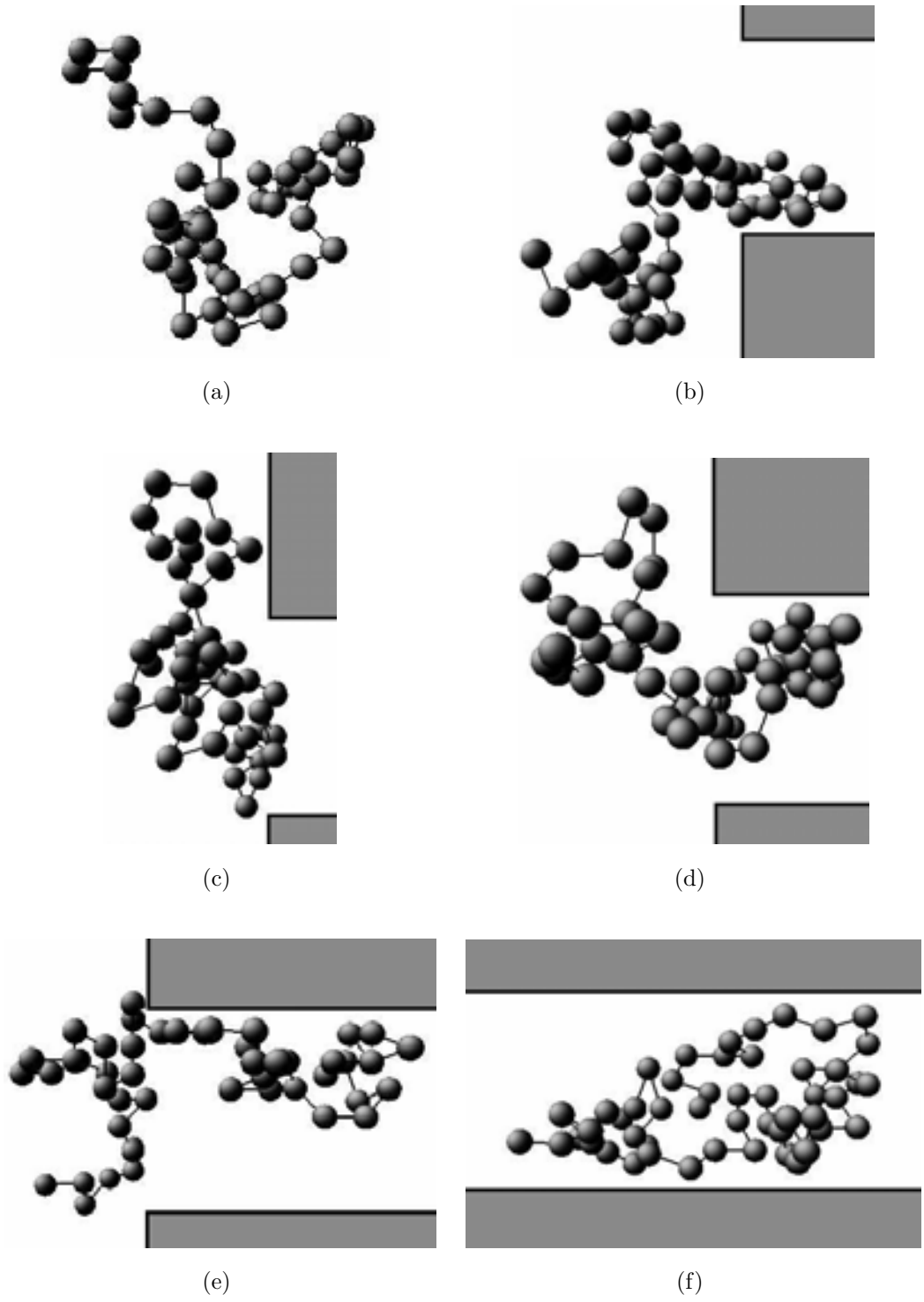

Figure 3.2: *Snapshots of polymer conformations under good solvent conditions, degree of confinement* $\lambda = 1.6$ *and repulsive walls at various centre of mass positions along the pore axis: (a) bulk solvent, (b) and (c) with a centre of mass inside the solvent, 5 grid points away from the interface, (d) at a centre of mass position of 0, at the interface, (e) at a centre of mass position inside the pore, 5 grid points away from the interface and (f) in the bulk pore.*

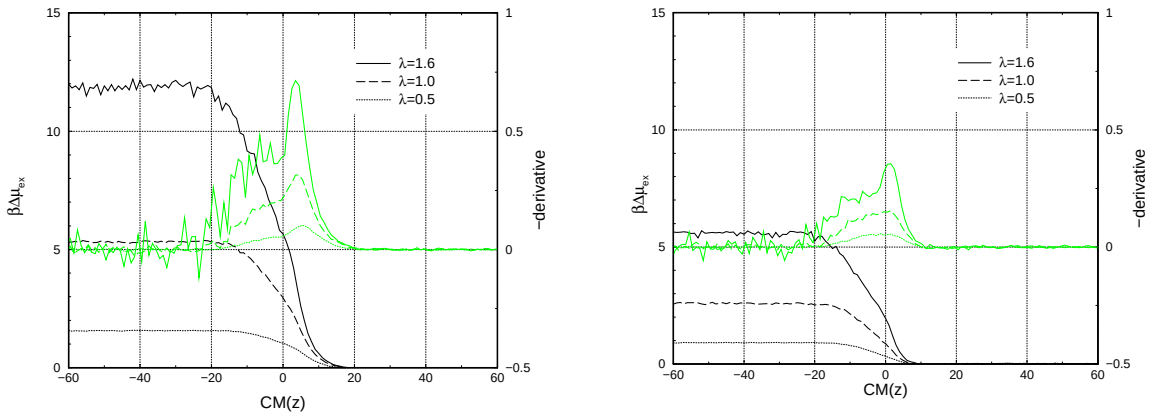

Figure 3.3: *Excess chemical potential, $\beta\Delta\mu_{ex}$, of the average polymer conformation and the its derivative with respect to z ($\partial\beta\Delta\mu_{ex}/\partial z$) as a function of the polymer centre of mass for $\lambda = 1.6$, 1.0 and, 0.5 with different monomer-wall interactions (a) $\epsilon_{pw} = 0.0kT$ and (b) $\epsilon_{pw} = 0.8kT$. Negative $CM(z)$ values indicate that the polymer centre of mass is inside the pore and at positive CM(z) values the polymer centre of mass is inside the bulk solvent. The interface is located at CM(z)=0.*

dominant type of conformation at the same centre of mass position is conformation (Fig. 3.2c). The polymer chain is for the larger part outside the pore and remains coil-like, although the position of the individual monomers is restricted by the presence of the wall resulting in conformations where the main principle axis is oriented perpendicular to the pore axis. When the centre of mass is positioned exactly on the interface (Fig. 3.2d), the polymer penetrated the pore even further. Although the conformation as a whole is somewhat stretched, both parts of the polymer, inside and outside the pore, retain their coil-like shape. At a centre of mass position of 5 grid points inside the pore (Fig. 3.2e) the polymer is already for the larger part confined and resides in a stretched conformation oriented parallel to the pore axis.

Figure 3.3 shows the conformational excess chemical potential (excess free energy) and its derivative, the force needed to diffuse into the pore, along the axial pore direction as

a function of the chain centre of mass position. Fig. 3.3a shows these quantities in case there are no attractive monomer-wall interactions, while in Fig. 3.3b a weak interaction of $0.8kT$ was applied. This weak attraction lowers the excess chemical potential substantially, whereas it affects the strong conformational transition discussed above only a little (see below). Also its derivative is decreased significantly at $\epsilon_{pw} = 0.8kT$. Starting from the bulk solution in Fig. 3.3a the excess chemical potential starts to increase at distances of approximately 18 grid points (about 1.6 times the radius of gyration of the polymer chain in solution) away from the interfaces with pore dimensions $\lambda = 1.0$ and 1.6. For $\lambda = 0.5$ the increase starts at a slightly smaller distance. The excess chemical potential profile turns from convex into concave just in front of the pore entry, which is likely due to the fact that at this close proximity parts of the chain enter the pore. The excess chemical potential increases monotonically until it reaches a constant value at approximately $z = -10$ ($\lambda = 0.5$), $z = -15$ ($\lambda = 1.0$), and $z = -20$ ($\lambda = 1.6$). The extension of the transition region between the two values of constant excess chemical potential increases with the value of λ. The force needed for diffusion shows that a clear diffusion barrier lies in front of the pore, approximately 5 grid points in front of the interface, for all investigated pore sizes, coinciding with conformations (b) and (c) in Figure 3.2.

If a weak monomer-wall interaction of $0.8kT$ is introduced (Fig. 3.3b) the extension of the transition region reduces. Starting from the bulk solution, the excess chemical potential profiles start to rise only at a distance of about 10 grid points away from the surface. Apparently here, the energy gained in the event of monomer adsorption onto the wall avoids the excess chemical potential from incrementing up to this small distance. The excess chemical potential reaches a constant value inside the pore at distances slightly closer to the interface for all three values of λ presented here. Furthermore, not only the force for diffusion is substantially reduced, as already mentioned, but also the diffusion barrier is shifted to a position closer to the interface, just outside the pore.

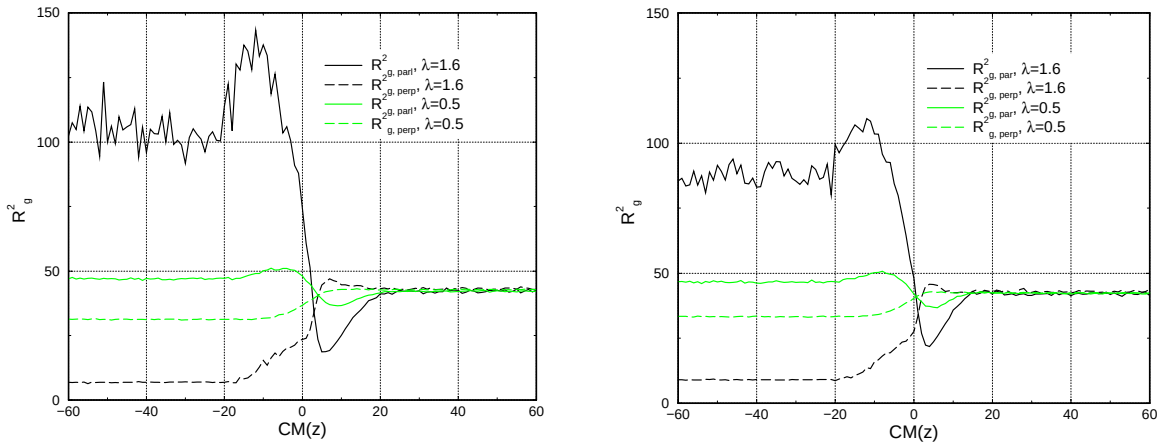

(a) (b)

Figure 3.4: $\langle R^2_{g,parallel} \rangle$ *and* $\langle R^2_{g,perpendicular} \rangle$ *as a function of the centre of mass z-position for* $\lambda = 1.6$ *and* $\lambda = 0.5$ *at monomer-wall interactions* ϵ_{pw} *of (a)* $0.0kT$ *and (b)* $0.8kT$*. Again negative CM(z) values indicate that the polymer centre of mass is inside the pore and positive values indicate that the polymer centre of mass is inside the bulk solvent.*

3.3.2 Conformational Properties

To quantify conformational change as a function of polymer position relative to the position of the interface, one may determine the change of the radius of gyration parallel $\langle R^2_{g,parallel} \rangle$ and perpendicular $\langle R^2_{g,perpendicular} \rangle$ to the pore axis as a function of the polymer centre of mass z-position, $CM(z)$. Figure 3.4a shows this for $\epsilon_{pw} = 0.0kT$ for $\lambda = R_g/R_p = 1.6$ and 0.5. Going from positive $CM(z)$ values (inside de bulk solvent) towards negative $CM(z)$ values (inside the pore) at $\lambda = 1.6$, one can see that $\langle R^2_{g,parallel} \rangle$ starts to decrease at approximately 20 grid points ($2R_g$) away from the interface, having a minimum at 6 grid points ($\frac{1}{2}R_g$)away from the interface of 19. At that same $CM(z)$ $\langle R^2_{g,perpendicular} \rangle$ has a small maximum of 46, about 4 units larger than the bulk value. Snapshots (b) and (c) of Figure 3.2 coincide with this $CM(z)$ position.

Decreasing $CM(z)$ further, one observes a sharp increase of the parallel R_g component while the perpendicular component sharply decreases. The slope of both plots becomes less

steep after passing the interface. The perpendicular oriented conformations as in Figure 3.2c are replaced by conformations which have penetrated the pore for a large part as in Figure 3.2d. The small number of monomers just outside the pore can no longer readily stretch or orient in the direction perpendicular to the pore axis and the confinement forces the part of the polymer inside the pore to orient into the direction parallel to the pore axis. At this large degree of confinement, $\lambda = 1.6$, this part of the polymer chain is also slightly squeezed. The decrease of the slopes after the polymer centre of mass has entered the pore is probably induced by the fact that due to a lesser amount of monomers outside the pore, the average radius of the coil there has reached the same order of magnitude as the pore radius which causes the R_g components to change at a slower rate.

At approximately 10 grid points inside the pore (one R_g from the interface) the polymer experiences a strong maximum in $\langle R^2_{g,parallel} \rangle$ of 140, after which the parallel component levels off to a constant value of 100. After being stretched up to the maximum, the chain relaxes again to a coil-like shape inside the confinement, oriented parallel to the pore axis and slightly squeezed. Also at $\lambda = 0.5$ ($R_g = \frac{1}{2} R_{pore}$) one observes again a minimum in $\langle R^2_{g,parallel} \rangle$ in front of the interface and a maximum inside the pore, but the deformation is minimal.

Figure 3.4b shows the same quantities now influenced by a weakly attractive monomer-wall interaction of $\epsilon_{pw} = 0.8kT$, below the critical adsorption energy. Immediately a few differences compared to the case of repulsive walls attract the attention: firstly the minimum in front of the interface is less deep than at repulsive monomer-wall interactions and this minimum, as is the maximum in the perpendicular component, is shifted to a position closer to the interface. The maximum inside the pore for the parallel component is 110, significantly lower than at $\epsilon_{pw} = 0.0kT$ and also its constant value when the polymer is completely confined is lower, 85, while the perpendicular component has decreased to 9, higher than at $\epsilon_{pw} = 0.0kT$. A preliminary conclusion is here, although at weakly attractive energies the same phenomena can be observed as for repulsive walls, an attractive

interaction between the monomers and the wall results in less deformation at the interface, due to the fact that the attractive energy partly compensates the entropy loss near the interface and inside the pore.

To account for the chain deformation in a single quantity we invoke the 'chain asphericity' in the remainder of this chapter. The asphericity is obtained from the radius of gyration tensor $S_{ij} = \frac{1}{50}\sum_{n=1}^{50}(r_{n,i} - r_i^{cm})(r_{n,j} - r_j^{cm})$, which is calculated for each generated chain conformation and next diagonalised. The three eigenvalues obtained by this procedure provide information about the average shape of the polymer. We use these eigenvalues to define the asphericity A of the coil:[87]

$$A = 0.5\left(\frac{3V_1}{V_1 + V_2 + V_3} - 1\right) \tag{3.2}$$

where V_1 is the largest eigenvalue and V_3 is the smallest eigenvalue of matrix S. The asphericity A equals 0 when the polymer coil takes on the shape of a perfect sphere. An infinitely thin cylinder has an asphericity $A = 1$. In bulk (athermal) solution the polymer studied (chain length 50) has an asphericity $A_{bulk} = 0.61$.

Figures 3.5a and b present the chain asphericities as a function of the chain centre of mass position along the pore axis for $\epsilon_{pw} = 0.0kT$ and $\epsilon_{pw} = 0.8kT$, respectively. Again, the interface is located at $z = 0$. Going from bulk solvent to bulk pore, for $\lambda = 1.6$, the asphericity starts to decrease at approximately $CM(z) = 20$ grid points ($2R_g$) away from the interface inside the bulk solvent to a value of $A = 0.58$, and reaches a minimum at approximately $z = +3$, just in front of the pore. After this it increases towards a maximum of approximately $A = 0.84$ at 15 grid points inside the pore caused by a stretching of the part of the chains inside the pore. In the end, inside the pore, the asphericity decreases again to a constant value of approximately 0.75. With a pore size $\lambda = 1.0$, this maximum inside the pore shifts to a position closer to the interface and the minimum shifts to a

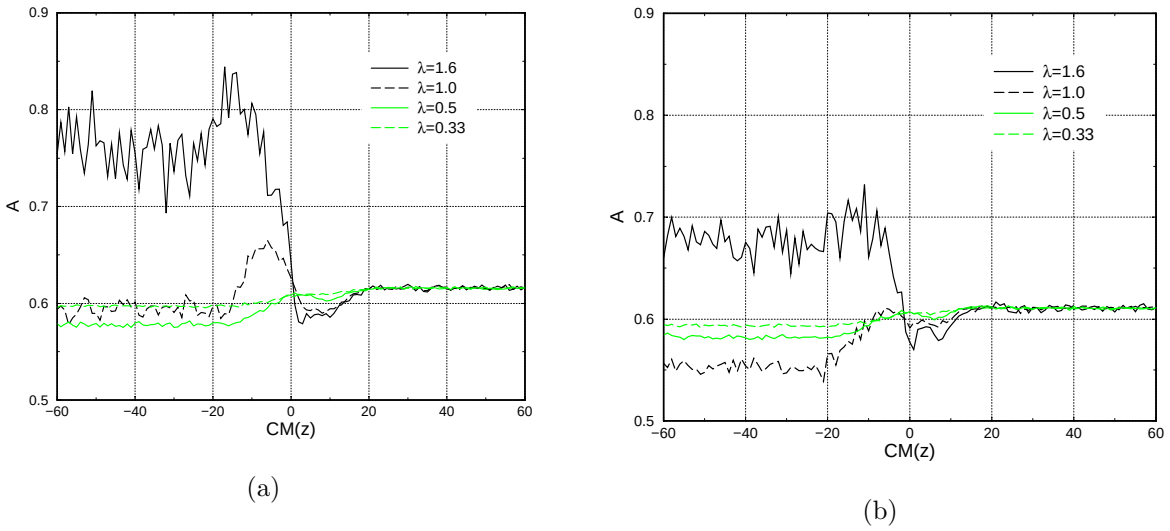

Figure 3.5: *Asphericity versus centre of mass position for* $\lambda = 1.6$, 1.0, 0.5 *and* 0.33 *at (a)* $\epsilon_{pw} = 0.0kT$ *and (b)* $\epsilon_{pw} = 0.8kT$. *In small pores* ($\lambda \geq 1$) *at both monomer-wall interaction potentials clear deformations of the polymer chains are found at the transition from bulk solvent to bulk pore (decreasing* $CM(z)$*).*

position further inside the solvent. At $\lambda = 0.51$ and $\lambda = 0.33$ no maximum occurs. The asphericity has a shallow minimum in front of the pore after which it starts to drop and levels off to a smaller value inside the pore (Fig. 3.5a). Noteworthy, when the polymer is completely confined at $\lambda \geq 1$, the asphericity decreases below its value in the bulk solution. The minimum in front of the pore has vanished at $\lambda = 0.33$ and the value for A inside the pore has taken a value almost equal to that of A inside the bulk solvent. These smaller values of A inside the pore compared to A inside the bulk solvent are probably caused by the fact that a certain number of chain conformations that run into the direction of the pore wall are reflected once they approach, i.e. less orientation entropy, rendering the average conformation somewhat more spherical compared to the conformation in the bulk solution. This effect is strongest with $\lambda = 0.51$ (Fig. 3.5a) and diminishes again if the pore radius is made larger ($\lambda = 0.33$). The conformational properties of completely confined chains is discussed in more detail in ref. 104. With $\lambda = 1.0$ and, more obvious, $\lambda = 1.6$ a much stronger confinement causes the monomer units to preferentially succeed along the

pore axis (see Fig. 3.6, below) and the asphericity never drops below the value in bulk solution.

If a weak monomer-wall interaction is introduced (Fig. 3.5b) the situation changes; in this case the curve for $\lambda = 1.0$ drops below that of $\lambda = 0.33$ once the chain centre of mass position proceeds beyond $z = -10$ to smaller z-values. This effect is likely caused by a competition between confinement, which promotes extension of the chain in the z-direction, and adsorption effects, which promote extension in the directions perpendicular to the z-axis. Another effect which shows up at this monomer-wall potential is a secondary maximum appearing at 5 grid points in front of the interface for small pores ($\lambda \geq 1$). This is caused by polymers in front of the interface having some of the monomers adsorbed on the outer surface. This then results in conformations slightly stretched into the direction perpendicular to the pore axis making the average conformation at that point more aspherical. Not surprisingly this effect becomes more pronounced at larger degrees of confinement i.e. smaller pores.

3.3.3 Monomer Density and Average Monomer Position Along the Pore Axis

Figures 3.6a and b show the monomer density profiles along the z-direction for three values of λ. The curves apply to those conformations that have $CM(z) = 0$. The density curves are normalised in such a way that the integral under one curve is equal to the chain length $M = 50$. Again the interface is located at $z = 0$. In the absence of monomer-wall attraction (Fig. 3.6a), the monomer density profile for $\lambda = 0.51$ follows a Gaussian distribution indicating that this pore is big enough to not significantly affect the distribution of monomers inside the coil. With $\lambda = 1.0$ a maximum appears just outside the pore and a plateau value occurs just inside. The polymer part outside the pore resides in a coil conformation while the part inside the pore is forced in a more stretched or squeezed conformation. An anal-

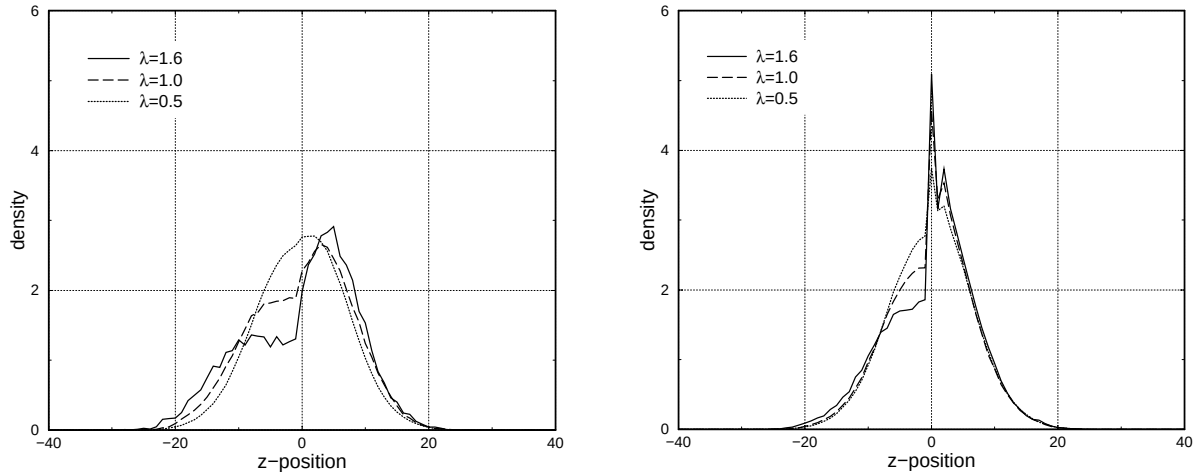

Figure 3.6: *Monomer density distribution for chain conformations having* $CM(z) = 0$ *for* $\lambda = 1.6$, 1.0 *and* 0.5 *at (a)* $\epsilon_{pw} = 0.0kT$ *and (b)* $\epsilon_{pw} = 0.8kT$. *The curves are normalised in such a way that the integral under one curve equals 50*

ogy exists with 'flower' conformations mentioned earlier: the coil like 'crown' of the flower is outside the pore and the stretched 'stem' of the flower coincides with the part outside the pore although, at this λ-value, this 'stem' is rather diffuse. If λ increases to 1.6, the plateau value drops below 1.5 monomer per lattice position but is still significantly larger than unity, a perfect 'stem', and extends to regions further inside the pore. The magnitude of the maximum just outside the pore does not significantly change. Fig. 3.6b shows the density profiles for the same values of λ, but now with a weak attractive monomer-wall attraction of $0.8kT$. Clearly, at the bulk solution side of the interface, strong adsorption peaks can be identified. Inside the pore ($\lambda = 1.0$ and $\lambda = 1.6$), the density plateau's are still present but extend less far, which indicates that the extension of the stem gets smaller due to monomer adsorption onto the pore wall. Also, the area under the density curves at $z < 0$ is smaller at $\epsilon_{pw} = 0.8kT$ marking a smaller amount of monomers inside the pore at attractive monomer-wall interactions at equal $CM(z)$ values.

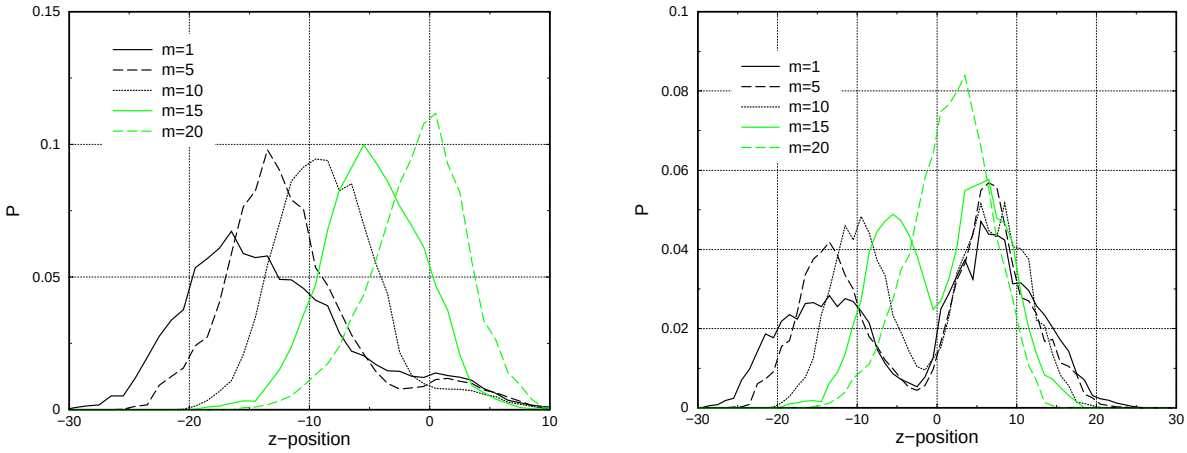

(a) (b)

Figure 3.7: *The probability to find successive monomers at a z-position when the polymer centre of mass equals* 0 *at* $\lambda = 1.6$. *When the polymer head* ($m = 1$)*is defined as the terminal monomer with the lowest z-position the peaks of the probability curves shift in positive z-direction with increasing monomer index m (a). When the polymer head and tail are indistinguishable the probability to find* 'one' *end of the polymer on a z-position is presented in (b). The monomer-wall interaction* ϵ_{pw} *equals* $0.0kT$.

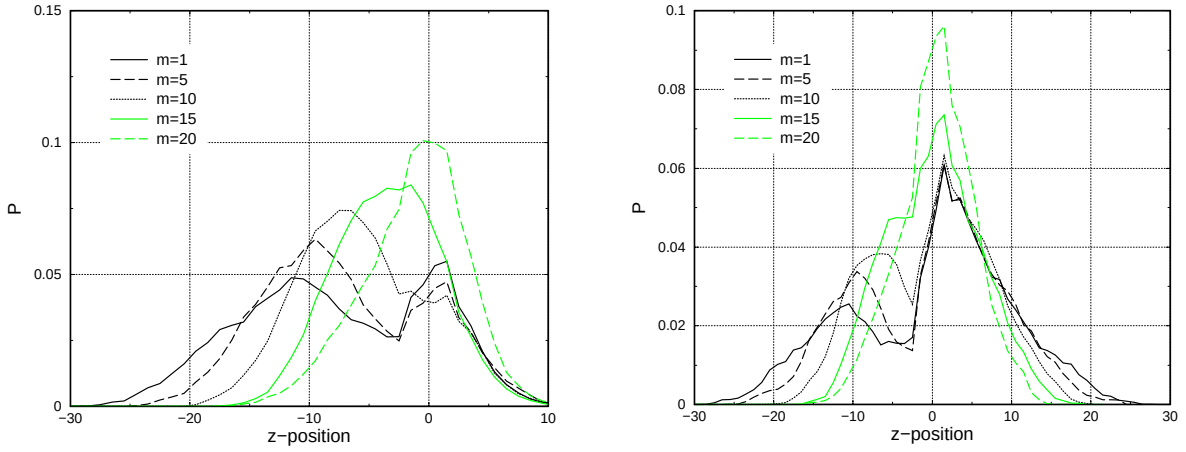

(a) (b)

Figure 3.8: *The same quantities as in Figure 3.7 are presented here for an attractive monomer-wall interaction potential of* $\epsilon_{pw} = 0.8kT$.

At this point the average z-position of the successive monomers along the chain can clarify the polymer conformation during permeation to a greater extent. Figure 3.7a shows distributions of the z-position of monomer 1, 5, 10, 15 and 20 given that the polymer centre of mass is located at the interface ($CM(z) = 0$), at $\lambda = 1.6$ and the 'head' of the polymer, monomer $m = 1$, is defined as the chain end with the lowest z-position. One can see that the maxima of the probability curves shift in positive z-direction with an increasing monomer index. Also the 'fronts' of the curves are positioned in the same order. Apparently a large part of the polymers enters the pore with one end, the 'head', first. The curves also overlap to a great extent and the curve of the head of the polymer, $m = 1$, even has 7% outside the pore, indicating at least a large percentage of polymers does not enter the pore with its head first, but with monomers further inside the chain.

When the chain head and tail are treated indistinguishable, we obtain the 'unbiased' picture of Figure 3.7a as in Figure 3.7b. Here the curves have two peaks per monomer because now each index value m occurs twice. The same trend for the parts of the curves inside the pore can be observed here as in Figure 3.7a: the maxima of the curves at $z < 0$ shift to larger z-values with increasing m. Monomer $m = 1$, however, has a broader distribution probably because the terminal monomers have more degrees of freedom which makes it more possible for those monomers to explore also the space the way back to the interface. Outside the pore ($z > 0$) peak maxima overlap, except the curve for $m = 20$ which has only one peak just outside the pore with the larger part of the area under its curve also outside the pore. This clearly indicates that this monomer resides on average outside the confinement at this polymer centre of mass position and degree of confinement. Another phenomenon that attracts the attention is that the height of both maxima in all the curves (except for $m = 20$) is approximately the same. On average the one terminal monomer is inside the pore and the other end is outside the pore. This conclusion is supported by the fact that the peak positions inside the pore in Figure 3.7b coincide with the peak positions in Figure 3.7a and that the height is about half of that in Figure 3.7a. At higher λ values these effects become stronger: the polymer head enters the pore first with

increasing probability for increasing λ values and the probability curves of the successive monomers have less overlap with each other (not shown). Decreasing λ values cause this effect to diminish until the probabilities to find the successive monomers on a particular z-value become equal.

Introducing an attractive interaction potential of $\epsilon_{pw} = 0.8kT$ results in some changes of the curves. Although peaks of the successive monomers$m$ in Figure 3.8a again shift in positive z-direction with increasing m, the maxima are less sharp. The head ($m = 1$) as well as monomer 5 show a secondary peak just outside the pore with a height in the same order of magnitude as the peak inside the pore. Apparently the head has a larger preference to stay on the outer surface, induced by the attractive monomer-wall potential. In Figure 3.8b the unbiased probability to find a monomer m on a certain z-position is presented at $\epsilon_{pw} = 0.8kT$. The peak of monomer 1 outside the pore is almost 3 times higher than the peak inside the pore. In fact, the peaks outside the pore are larger for all monomers as is the area under the curves outside the pore ($z > 0$) compared to the area under the curves inside ($z < 0$). The difference in height between the two peaks becomes smaller, however, for increasing monomer index m. The terminal monomers are preferably outside the pore at this interaction potential and the amounts of monomers inside the pore are also smaller compared to the situation at $\epsilon_{pw} = 0.0kT$. Again, at $m = 20$ there exists only one peak and the larger part of the curve is outside the pore. Again a larger λ value reinforces these effects while a decreasing λ value cause these effects to diminish until the probabilities are equal.

3.4 Summary and Conclusions

Configurational Bias Monte Carlo (CBMC) simulations together with the Bond Fluctuation model have been used to study the confinement excess chemical potential and conformational properties of athermal flexible polymers upon entering cylindrical pores along the pore axis coordinate. Simulations were performed without attractive monomer-wall

interactions as well as with a weak interaction of $0.8kT$ per segment. For small pores ($\lambda \equiv R_g/R_{pore} \geq 1.0$, with R_g denoting the chain radius of gyration in bulk solution) the chain adopts an asymmetric conformation that is 'over-stretched' along the pore axis once it enters the pore while relaxing to a smaller asphericity once it is completely inside. The overstretched conformations are best characterised by a stretched, but rather thick, 'stem' inside the pore, and on top of it, just outside the pore, a 'crown' composed of the remaining segments. The chain end predominantly enters the pore first while the opposite end remains outside. The conformation turns into a (deformed) coil as soon as the chain centre of mass position extends as far as approximately $2R_g$ inside the pore. Monomer adsorption onto the pore wall and the outer surface (facing the bulk solution) interferes with the above picture to some extent. It causes the stem to become less extended and the crown to adsorb onto the surface. Also, due to this adsorption effect, the chain ends preferably stay outside the pore.

Several properties, such as solvent quality, chain length and chain flexibility have not been considered in this work, yet are likely to affect the conformational changes. These properties will be subject to chapter 4 and 5 and to future studies.

CHAPTER

FOUR

Monte Carlo Simulations of Polymer Adsorption at the Entrance of Cylindrical Pores in Flat Adsorbing Surfaces

The influence of surface interactions on the conformation of flexible polymers partially confined inside narrow cylindrical pores in a flat surface is studied above the critical adsorption energy in a good solvent. We use a Configurational Bias computational sampling method to calculate the adsorption free energy and the radius of gyration components parallel and perpendicular to the pore axis as function of the polymer centre of mass position at different degrees of confinement. We find strong free energy minima just in front of the pore entry for all degrees of confinement studied. At the location of the free energy minimum polymers are partially adsorbed inside the pore and on the outer solid surface and adopt 'drawing pin'-like conformations. A distinct maximum in the average loop length at the pore entry indicates that the polymer bridges the pore entry of small pores.

Submitted to *Soft Materials*

4.1 Introduction

The conformation of a flexible polymer in solution depends greatly on the nature of its environment. Changes in the solvent quality and polymer concentration, as well as spatial constraints imposed by confining geometries affect the average coil shape and size to a large extent.[30] In particular, the conformations of polymers and oligomers crossing the boundary between a bulk solvent and a porous medium deviate strongly from those adopted in either of the two bulk phases. Despite the importance of this subject in e.g. electrophoresis, chromatography, membrane ultrafiltration, and oligomer diffusion in zeolites, it has not been studied extensively[5,20,51] and many questions remain on phenomena occurring at the interface.

In previous work we performed Monte Carlo computer simulations of flexible polymer chains at the entry of narrow cylindrical pores.[49] At the interface, polymers, partially confined to pores smaller than the unperturbed (bulk) radius of gyration, assumed conformations neither alike fully confined nor alike unperturbed conformations. Instead, strongly asymmetric conformations with extended chain parts probing the pore entry were observed. When only excluded volume or weakly attractive interactions were present between polymer segments and the pore wall or the flat outer surface, the polymer was found to adopt an over-extended conformation parallel to the pore axis while penetrating the pore predominantly with its terminal repeat units. This process causes the chain asphericity to run through a maximum when the chain centre of mass has just entered the pore. When the chain centre of mass diffuses further inside, the asphericity relaxes to a smaller value. These features, which may provide insights in the dynamic process of pore intrusion, all occur at the expense of the chain's conformational entropy while not being compensated by a favourable energy of adsorption onto the pore wall. It is the purpose of this paper to examine how the above picture changes when conditions of strong adsorption are simulated.

A significant number of computational studies on polymer partitioning in confined geometries are documented in the literature.[12,13,23,24,26,28,43,44,57,73] Most studies dealt with polymer partitioning as a function of the degree of confinement and adsorption energy. Reports on cylindrical pores[28] and slit-like pores[23,24] showed that the partition coefficient in confinements increases with increasing adsorption potential and equals unity at the critical adsorption energy. Changes in polymer conformation as a function of the degree of confinement were reported for polymer chains between two flat walls.[104] The polymers changed from a 3D coil to a 2D pancake structure. Although polymer dynamics studies have been carried out on polymer translocation through a small hole in an infinitely thin membrane,[75] to the authors knowledge, the effects of chain adsorption on the intermediate conformations of polymers from a bulk solvent phase to a pore interior have not been reported.

In this paper we examine the influence of surface adsorption on the conformations of partially confined polymers by means of computer simulation of a lattice chain model. We focus on chain conformation properties under conditions of strong adsorption, i.e. adsorption at conditions below the critical adsorption temperature, and on changes of the adsorption energy, entropy and excess chemical potential (free energy) for various degrees of pore penetration. The calculation details are presented in section 2. In section 3 we present the results and. Conclusions are summarised in section 4.

4.2 Simulation Details

The Bond Fluctuation lattice model[16] was used together with a Configurational Bias sampling scheme[39] to sample the chain conformation space. All simulated polymers are 50 monomers (M) long, each monomer occupying 8 grid points (a box) on a 3D simulation grid. All conformations are self-avoiding walks, hence monomer-monomer interactions are repulsive mimicking good solvent conditions. When one or more of the grid points of the

monomer-box is in contact with the wall, the monomer experiences an interaction energy $\epsilon_{pw} = 0.0$, 0.8 or 1.2 (units kT). This differs from our previous work where the interaction energy was defined as the summed interaction energies of the four grid points in contact with the (flat) wall.[49]

Because the Bond-Fluctuation model allows for the Configurational Bias sampling algorithm to let each segment explore 108 directions, making it effectively an off-lattice case, the procedure is very time consuming. For this reason all conformations are generated by choosing each new monomer growth direction from a set of 50 directions randomly selected from the complete list of 108 possibilities. Configurational averages are obtained from the Rosenbluth average:[39]

$$\langle \mathcal{A} \rangle_{\mathcal{R}} = \frac{\sum_{n=1}^{N} W(n)\mathcal{A}(n)}{\sum_{n=1}^{N} W(n)} \tag{4.1}$$

in which $\mathcal{A}$ is the configurational quantity of interest and $W(n)$ denotes the Rosenbluth factor of chain conformation n.

The chemical potential of a single chain as a function of its centre of mass (CM) position along the z-coordinate is obtained from the chain Rosenbluth weight. In the configurational biased sampling algorithm, chains are inserted segment by segment. During the insertion of the ith segment, one has the choice of $\mathcal{N}$ possible directions and chooses the direction favouring the largest Boltzmann factor. The sum of Boltzmann factors of all possible directions during insertion of the ith segment is called the Rosenbluth factor w_i[39]

$$w_i = \frac{1}{\mathcal{N}} \sum_{j=1}^{\mathcal{N}} \exp\left(-\beta u_i(j)\right) \tag{4.2}$$

where $\beta = 1/k_b T$, k_b is the Boltzmann constant, T the temperature and $u_i(j)$ the energy associated with inserting the ith segment in the jth direction. The chemical potential μ of the inserted chain is calculated relative to the chemical potential of a nonreversing random

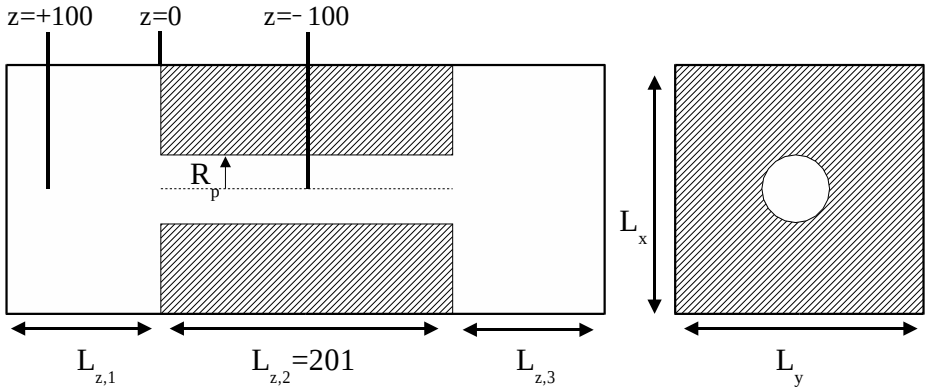

Figure 4.1: *The simulation box. Side view (left), top view (right).*

walk, μ_{id}, in which monomer overlap is allowed. The reduced excess chemical potential $\beta\mu_{ex} = \beta\mu - \beta\mu_{id}$ is calculated from[39]

$$\beta\mu_{ex} = -ln \left\langle \prod_{i=1}^{M} w_i \right\rangle = -ln\langle W \rangle \tag{4.3}$$

where M is the number of repeat units in the chain.

We calculated the excess chemical potential $\beta\Delta\mu_{ex}$ (relative to the chemical potential in the bulk solvent) as a function of the chain centre of mass position along the pore axis, $CM(z)$. Chain conformations are generated from random positions in the available space between 100 grid points inside the pore ($z = -100$) and 100 grid points outside ($z = +100$). The interface is located at $z = 0$ (Fig. 4.1). Typically 85 million conformations are generated during which histograms $\mathcal{A}(z_{CM}, n)$ and $W(z_{CM}, n)$ are updated (z_{CM} is the chain centre of mass z-position).

The simulation box is set up by putting a wall with a single straight pore along the z-direction in the middle of the box. The length of the cylindrical pore is large enough for the polymer to stretch out completely without finding both ends at opposite pore mouths. The dimensions of the simulation box are $L_{z,1} = L_{z,3} = 90$ grid points, $L_{z,2} = 201$ and $L_x = L_y = 82$ grid points (Fig. 4.1). The simulations are performed such as to

obtain average chain conformational properties as a function of the chain centre of mass z-coordinate, $CM(z)$. Periodic boundary conditions are applied in all three directions. The conformations located at $z = +100$ do not experience the wall and resemble unconfined polymers in a good solvent at infinite dilution. The conformations located at $z = -100$ are fully confined by the pore geometry. The pore radius R_p is varied such that the pore-to-coil size ratio λ, defined as $\lambda = R_p/R_g$, varies between $\lambda = 3.0$ and $\lambda = 0.5$. The polymer radius of gyration, R_g, under athermal conditions equals 11.3.

For $z > 0$, the x and y position coordinates of the first monomer od each newly generated chain is chosen within a radius of $2.5R_g$ around the pore axis. For all λ-values studied in this work, this radius exceeds R_p. Only fully grown chains that find their centres of mass within a radius R_p from the axis are considered in the statistical sampling of conformational averages. This choice is motivated by two reasons. First, we want to understand conformational properties of chains that have partially entered a pore while their remaining unconfined monomers should still have the opportunity to adsorb onto the outer surface facing the bulk solution. Thus, conformations of adsorbing chains not at all experiencing the pore must not be considered. Second, we hope to obtain some insights in the chain conformational free energy along a coordinate perpendicular to an adsorbing surface with a cylindrical pore in the centre. This chemical potential (as well as its energetic and entropic components discussed later on) may contain information on energetic or entropic barriers at the pore entry and thus should exclude contributions of adsorbed chains not experiencing this entry.

The centre of mass of incomplete chains resulting from failed growth attempts (where a term W=0 is contributing to the average Rosenbluth factor) was calculated using only the successfully grown monomers in the chain. In a case of unsuccessful growth, the growth usually breaks off between the 30th and the last monomer so the calculated centre of mass for incomplete polymer chains will be close to a fully grown chain. Around 10% of the growth of polymers in small confinements ($\lambda = 1.6$) is unsuccessful. Almost all growth attempts in the bulk solvent phase are successful.

4.3 Results

4.3.1 Critical Adsorption Energy

To identify the regimes of weak and strong adsorption we calculated the critical adsorption energy, ϵ_{cr}, using the method of Gong and Wang.[43] The method involves the calculation of the chemical potential $\beta\Delta\mu_{ex}$ of adsorbed chains relative to the value in the bulk solvent as a function of the monomer-wall adsorption energy, ϵ_{pw}, and the polymer chain length. The value of ϵ_{pw} where the chemical potentials for different chain lengths coincide corresponds to the critical adsorption energy.

This assignment is based on the argument that below the adsorption transition (small ϵ_{pw}) longer chains are more strongly repelled by the surface than shorter chains, whereas beyond the adsorption transition longer chains are more strongly attracted by the surface than shorter chains. At the critical adsorption point the entropic repulsion is exactly balanced by the energetic attraction and becomes independent of the chain length.[32] Although Gong and Wang used conformations terminally anchored to the surface to determine ϵ_{cr}, we used no such constraint and sampled polymer conformations above a flat surface taking only those into account for calculating $\beta\Delta\mu_{ex}$ if at least one of their repeat units is in contact with the surface. We used polymer chain lengths of 30, 50 70 and 100 repeat units. Fig. 4.2 shows $\beta\Delta\mu_{ex}$ as a function of ϵ_{pw} for the various chain lengths. The critical adsorption point is located at $\epsilon_{cr} = 0.96kT$. We note

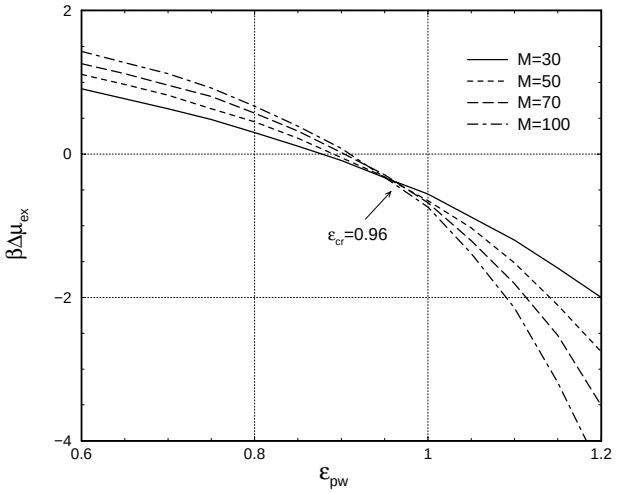

Figure 4.2: *Reduced chemical potential $\beta\Delta\mu_{ex}$ versus reduced polymer-wall interaction ϵ_{pw} for chains of lengths M in contact with a solid surface. The interception point gives the critical adsorption energy ϵ_{cr}.*

that theoretically one expects $\beta\Delta\mu_{cr} = 0$. We find $\beta\Delta\mu_{cr} = -0.40$ which compares to $\beta\Delta\mu_{cr} = -0.346$ reported by Gong and Wang (see also page 39).[43]

4.3.2 Excess Chemical Potential, Interaction Energy and Entropy Profiles

At $\epsilon_{pw} = 0.0kT$ changes in the chain's excess chemical potential are solely due to entropic effects. Figure 4.3a shows the change in the excess chemical potential for various pore sizes as function of the centre of mass position, as already found in previous work.[49] Negative centre of mass ($CM(z)$) values indicate that the polymer centre of mass is located inside the pore.

Following the polymer centre of mass from the bulk solvent towards the pore, the excess chemical potential $\beta\Delta\mu_{ex}$ increases due to loss of conformational entropy when the centre of mass is located in the vicinity of the interface. It increases further until its centre of mass is far inside the pore. The plateau value of $\beta\Delta\mu_{ex}$ inside the pore is reached at $CM(z)$-positions further inside when λ is larger. For $\lambda > 1$, $\beta\Delta\mu_{ex}$ does not increase as steeply inside the pore as outside the pore due to the asymmetric conformations present at the interface: the part of the polymer inside the pore is stretched, but the part outside the pore remains a coil-like conformation.[49,56,95] Introduction of weakly attractive interactions ($\epsilon_{pw} < \epsilon_{cr}$) of the monomers with the wall does not change this picture other than reducing the steep increase of $\beta\Delta\mu_{ex}$ by partly compensating the entropy cost with an energetic payback resulting in increasing partition coefficients.[49]

This picture changes completely when using monomer-wall interactions ϵ_{pw} above the critical adsorption energy ϵ_{cr}. Figure 4.3b shows the excess chemical potential profiles for several λ values as a function of the polymer $CM(z)$ at $\epsilon_{pw} = 1.2kT$ ($\epsilon_{cr} = 0.96kT$). The most striking difference with the profiles in Fig. 4.3a is the minimum just in front of the interface. Chains apparently prefer the interface over either the bulk solvent phase

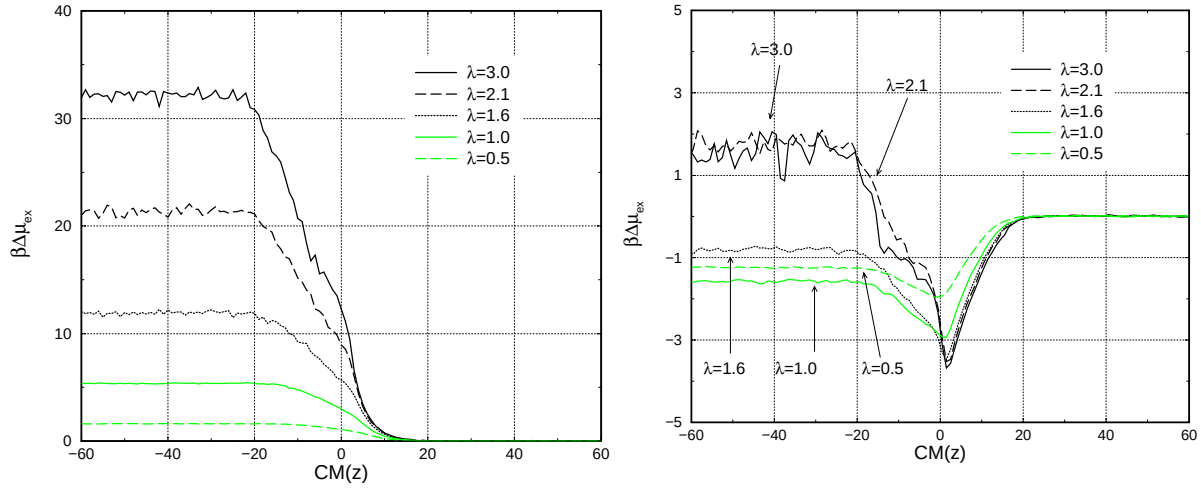

Figure 4.3: *Excess chemical potential profiles versus the chain centre of mass position along the pore axis, $CM(z)$, at $\epsilon_{pw} = 0.0kT$ (a) and $\epsilon_{pw} = 1.2kT$ (b) for various λ-values. Positive $CM(z)$ positions denote the bulk solvent region, negative values the pore region.*

or the pore interior. A similar kind of observation was made for the partitioning of liquid hexadecane molecules at the interface between the zeolite silicalite and liquid hexadecane.[51] The depth of the minimum is about $3.5kT$ relative to the solvent bulk value for all the λ values except for wide pores ($\lambda = 0.5$) where the minimum equals $2kT$. The smaller excess chemical potential drop for $\lambda = 0.5$ is caused by the large pore cross-sectional area that inhibits chain repeat units to have favourable energetic contacts with the flat surface facing the bulk solvent phase. It also explains why the excess chemical potential inside the pore is less negative for λ=0.5 than for $\lambda = 1.0$ also reported by Cifra and Bleha for this range of confinement degrees.[24]

As already stated the excess chemical potential profile at weakly attractive segment-wall energies ($\epsilon_{pw} < \epsilon_{cr}$) does not differ in shape from the situation where the segment-wall interaction is repulsive (Fig. 4.3a). When the excess chemical potential as function of the centre of mass position is decomposed into the energetic and entropic contributions as done

in Figure 4.4 for $\epsilon_{pw} = 0.8kT$ and $\lambda = 1.6$, one can see that at as far as 30 grid points (about 3 bulk radii of gyration) away from the interface the energy already decreases. Extended conformations must therefore occur, which have some of their monomers adsorbed. Interestingly, this energy is exactly compensated by a reduction of the conformational entropy, which causes this adsorption phenomenon to be non-visible in $\beta\Delta\mu_{ex}$. The excess chemical potential starts to deviate from the bulk solvent value at much smaller distances (about one radius of gyration) from the interface, where the dominant entropic contribution causes $\beta\Delta\mu_{ex}$ to rise. The entropy keeps on decreasing faster than the adsorption energy, causing the excess chemical potential rise gradually towards its constant value inside the pore. At 20 grid points (approximately $2R_g$ inside the pore) all three quantities reach a constant value.

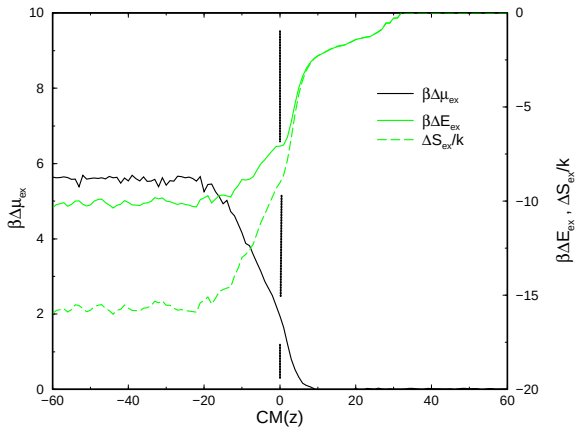

Figure 4.4: *Excess chemical potential (left scale), energy and entropy (right scale) as function of the polymer centre of mass ($CM(z)$) position for λ=1.6 at ϵ_{pw}=0.8kT.*

Figure 4.5a, b and c show the entropic and energetic contributions to the excess chemical potential profiles at $\epsilon_{pw} = 1.2kT$ for $\lambda = 2.1$, 1.6 and 0.5 respectively. Again we note that at about 2–3 bulk radii of gyration away from the interface the energy and entropy changes exactly compensate in the chemical potential. The minimum in $\beta\Delta\mu_{ex}$ at the pore entry cannot be attributed to either an extremum in the energetic or entropic component. Rather, it occurs because, upon approaching the pore entry from the bulk solvent, the adsorption energy drops faster than the entropy while the reverse applies when the polymer enters the pore. For $\lambda = 0.5$ and 1.6 at full confinement ($z < -20$) the adsorption energy outweighs the conformation entropy loss causing partition coefficients $K = e^{-\beta\Delta\mu_{ex}} > 1$.

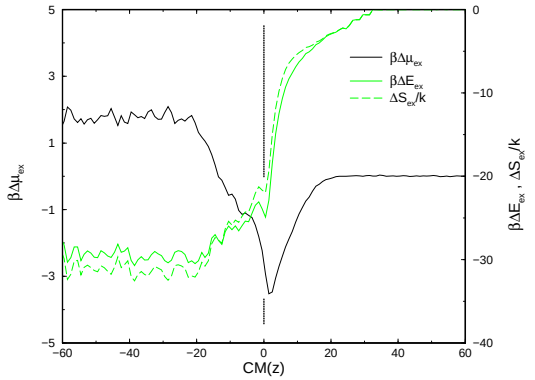

(a) $\lambda = 2.1$

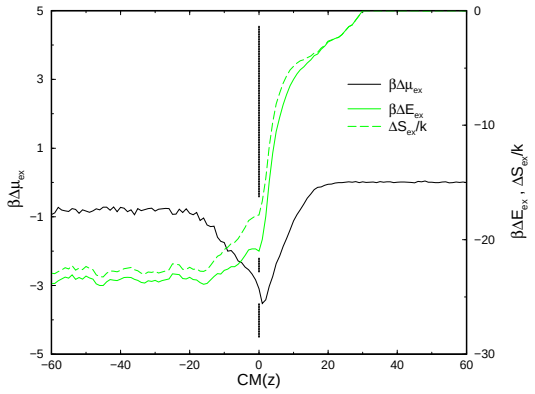

(b) $\lambda = 1.6$

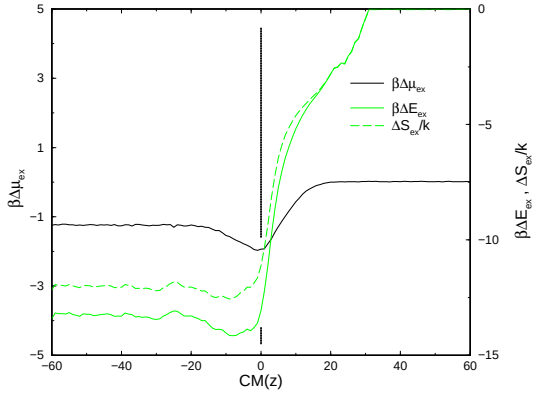

(c) $\lambda = 0.5$

Figure 4.5: *Excess chemical potential (left scale), energy and entropy (right scale) as function of the polymer centre of mass (CM) for (a)* $\lambda = 2.1$*, (b) 1.6 and (c) 0.5 at* ϵ_{pw}*=1.2kT.*

For $\lambda = 2.1$ (Fig. 4.5a) the entropy loss upon entering the pore is much stronger than the adsorption energy gain causing the curves of βE_{ex} and $\Delta S_{ex}/k$ to intersect at approximately $CM(z) = -12$. This causes a positive value of $\beta\Delta\mu_{ex}$ and consequently a partition coefficient smaller than unity. Large degrees of confinement result in a greater loss of conformational entropy whereas the number of adsorbed monomers, the adsorption energy, is limited by the number of monomers in the chain. It is therefore not surprising that at a certain degree of confinement the entropy will dominate over the adsorption energy. In this system (chain length $M = 50$) at $\epsilon_{pw} = 1.2kT$ this happens for values of λ somewhere between 1.6 and 2.1. This 'critical degree of confinement' depends on the chain length and will be larger for stronger attractive monomer-wall potentials. Although Cifra and Bleha concluded that the partition coefficient rises with increasing degrees of confinement above the critical adsorption energy, they did not report data for confinement degrees larger than 1.6.[24]

Figure 4.5c shows the same quantities for λ=0.5. Although the entropy, $\Delta S_{ex}/k$, inside the pore is much higher compared to the smaller pores i.e. -12.0 instead of -22.5 for λ =1.6, also the adsorption energy, $\beta\Delta E_{ex}$, has a less negative value (-13.0 instead of -23.5 for λ =1.6), because fewer monomers are near the pore wall to experience favourable monomer-wall contacts. Like for $\lambda > 0.5$ at $z > 0$, in the vicinity of the interface the value of $\beta\Delta\mu_{ex}$ decreases due to a faster drop of the adsorption energy compared to the entropy. However, inside the pore, the entropy loss is to a much larger extent compensated by a favourable energy causing the excess chemical potential barrier for entering the pore to get much smaller in comparison to the smaller pores (Fig. 4.5a and b).

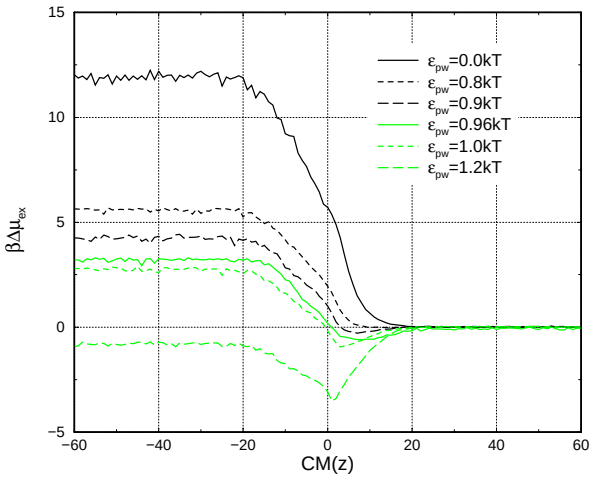

Figure 4.6: *Excess chemical potential versus the centre of mass position at λ=1.6 for various values of ϵ_{pw}. The minimum in front of the interface starts to develop at ϵ_{pw}=0.96kT.*

To illustrate how the excess chemical potential minimum develops just in front of the pore entry, Fig. 4.6 presents $\beta\Delta\mu_{ex}$ versus the centre of mass position at a degree of confinement λ=1.6 for various ϵ_{pw} values. As can be seen in Fig. 4.6 an increasing ϵ_{pw} reduces $\beta\Delta\mu_{ex}$ inside the pore. Upon approaching the critical adsorption energy ϵ_{cr} ($\epsilon_{pw} = 0.96kT$) the excess chemical potential profile starts to form a very shallow minimum at 10 grid points (approximately one bulk radius of gyration) away from the interface. A minimum located at 4 grid points away from the interface can eventually be found at $\epsilon_{pw} = 1.0kT$ and moves even closer to the interface for $\epsilon_{pw} = 1.2kT$ where the minimum becomes very strong.

We end this section by noting that at λ-values larger than 2.1 artefacts related to the underlying lattice appear in the excess chemical potential. Because all geometries including the cylindrical pore are modelled on a lattice, a scatter on the number of available adsorption sites as a function of the pore radius appears for $\lambda > 2.1$ due to irregularities of the cylinder. This causes artefacts in the energy inside the cylindrical pore. Conclusions for λ values greater than 2.1 should therefore be taken with caution.

4.3.3 Conformational Changes

The conformational properties of chains adsorbed above the critical adsorption point, ϵ_{cr}, are expected to deviate strongly from those observed below ϵ_{cr}. In previous work we used the chain asphericity to characterise the 3D conformation of non-adsorbing polymers.[49] The asphericity replaced the radius of gyration components (parallel and perpendicular to the pore axis) with a single quantity. Here we expect to see many conformational changes depending on the polymer position relative to the surface. The polymer radius of gyration components perpendicular and parallel to the pore axis provide greater detail of such conformational changes and are examined here. The R_g-components are calculated as follows:

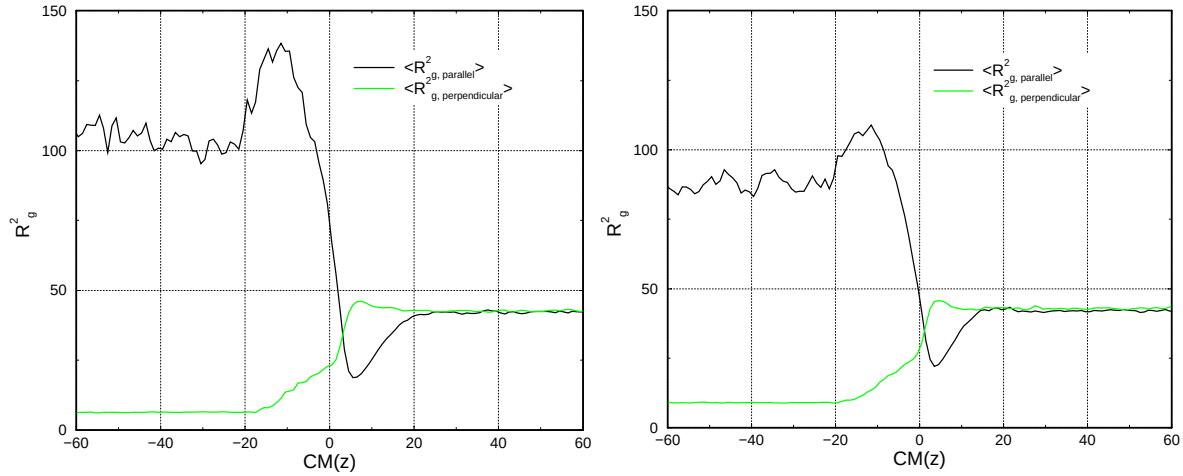

(a) (b)

Figure 4.7: *Radius of gyration components as function of the centre of mass (CM) position at (a) ϵ_{pw}=0kT (repulsive walls) and at (b) ϵ_{pw}=0.8kT (weakly attractive walls) for λ=1.6.*

$$\langle R^2_{g,parallel} \rangle = \left\langle \frac{1}{M} \sum_{i=1}^{M} (r_{z,i} - r_z^{cm})^2 \right\rangle \tag{4.4}$$

$$\langle R^2_{g,perpendicular} \rangle = \left\langle \frac{1}{M} \sum_{i=1}^{M} \frac{(r_{x,i} - r_x^{cm})^2 + (r_{y,i} - r_y^{cm})^2}{2} \right\rangle \tag{4.5}$$

where M is the number of repeat units.

Fig. 4.7a shows the $\langle R^2_{g,parallel} \rangle$ and $\langle R^2_{g,perpendicular} \rangle$ as function of the polymer centre of mass position for λ=1.6 at $\epsilon_{pw} = 0kT$. Approximately 24 grid points (2.5 bulk radii of gyration) away from the surface, the parallel component starts to decrease from its bulk solvent value of 43 while the perpendicular component increases slightly due to the repulsive nature of the interface. At a chain centre of mass position of 8 grid points in front of the interface the parallel component increases steeply. At this distance, most monomers still remain outside the pore, but few of them poke inside giving rise to a sudden increase of $< R_g^2 >$ at $z = -12$ after which the parallel 'over-extension' disappears and $< R_g^2 >$

assumes a value of approximately 100. At the same time $< R^2_{g,perpendicular} >$ reaches a value of 7.

Similar phenomena can be observed under conditions of weakly attractive interactions. For $\epsilon_{pw} = 0.8kT$, the R_g component perpendicular to the pore axis first increases slightly until 6 grid points in front of the surface. After that it gradually decreases towards a lower constant value approached at 21 grid points inside the pore (Fig. 4.7b). The parallel component first starts to decrease at 15 grid points away from the interface, towards a minimum at 4 grid points in front of the interface. The weak monomer-wall interactions cause a somewhat weaker chain deformation compared to what happens close to repulsive walls (Fig. 4.7a) under identical degrees of confinement.[49]

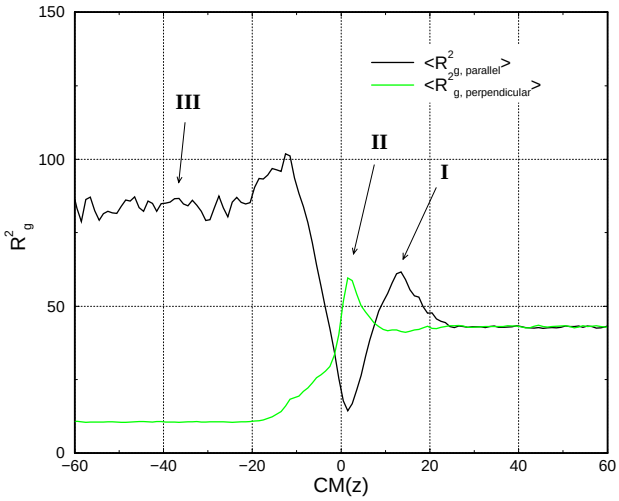

Figure 4.8: *Radius of gyration components as function of the centre of mass (CM) position at ϵ_{pw}=1.2kT (strongly attractive walls) and λ=1.6.*

The situation above the critical adsorption energy changes dramatically, as shown in Fig. 4.8 for ϵ_{pw}=1.2kT. Here two clear maxima for $\langle R^2_{g,parallel} \rangle$ inside the pore and outside the pore as well as a maximum in $\langle R^2_{g,perpendicular} \rangle$ on the interface attract the attention. These peaks and valleys will be explained based on the snapshots in Fig. 4.9. Following the polymer centre of mass from the bulk solvent towards the pore in Fig. 4.8, the $\langle R^2_{g,parallel} \rangle$ increases from its bluk solvent value of 43 starting at approximately 25 grid points away from the interface until it has reached a maximum of 61 at 14 grid points in front of the interface (situation I). The $\langle R^2_{g,perpendicular} \rangle$ has a shallow minimum of 41 at that point. This corresponds to polymer chains stretching out to the surface to come into contact with

the wall to experience the favourable monomer-wall interactions (see Fig. 4.9, situation I). As can be seen in Fig. 4.5b this leads to a reduction of the conformational entropy, however, the energy gain is sufficiently large to lower the conformational excess chemical potential relative to the value in bulk solution.

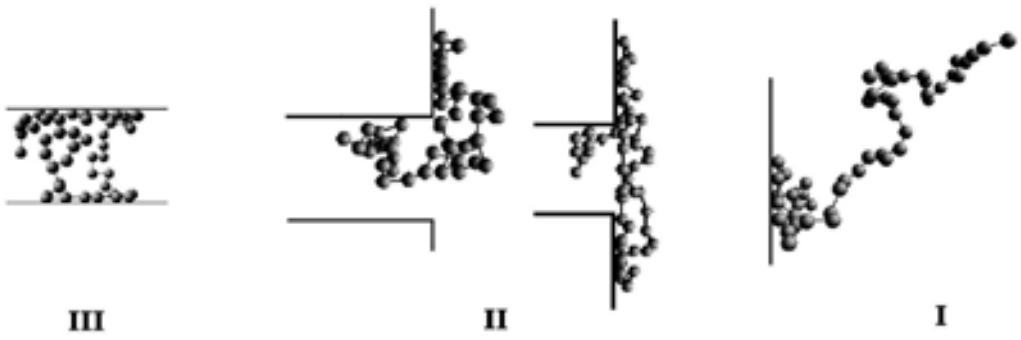

Figure 4.9: *Snapshots of partially confined polymers at various degrees of penetration at ϵ_{pw}=1.2kT and λ=1.6. The number corresponds to those shown in Figure 4.8.*

At positions closer to the interface, the $\langle R^2_{g,parallel} \rangle$ has a clear minimum just before the interface of only 14 and the $\langle R^2_{g,perpendicular} \rangle$ has a strong maximum of 59 (situation II). In this situation chains preferentially adsorb on the flat surface facing the bulk solution while a small part of the repeat units in front of the pore tends to adsorb onto the inner pore surface. Chain parts adsorbed on the surface outside the pore can expand in the x- and y directions in order to maximise the surface coverage causing the perpendicular part of R_g to increase and the parallel part to become smaller. The dominant polymer conformations found in situation II typically are partly adsorbed inside the pore and on the outer surface in 'hooked' structures or resemble 'drawing-pins' (Fig.4.9, situation II). Also conformations adsorbed on the outer surface encircling and bridging the pore entry, not penetrating the pore, are found in abundance. Note that at the $CM(z)$ position corresponding to situation II the minimum in the excess chemical potential (Fig. 4.5b) occurs. These conformations, therefore, dominate the polymer partitioning at infinite dilution.

At 12 grid points inside the pore there is a small maximum in $\langle R^2_{g,parallel} \rangle$ of 102 similar to the maximum at ϵ_{pw}=0kT and is also caused by part of the polymer chain being stretched inside the pore and part residing still outside the pore, but now adsorbed on the outer surface. Because of the adsorption features shown in Fig. 4.9 the polymer is no longer that much stretched in the direction parallel to the pore axis in comparison to its completely confined conformation, which starts at approximately 25 grid points inside the pore (situation III). The maximum in $\langle R^2_{g,parallel} \rangle$ is about 20 units higher compared to $\langle R^2_{g,parallel} \rangle$ at $z = -25$, in contrast with a difference of approximately 35 R^2_g units in the case of ϵ_{pw}=0kT.

Also smaller degrees of confinement, e.g. λ=0.5, show these very distinct maxima and minima. The maximum inside the pore for the parallel component of R^2_g, however, is almost vanished and also the maximum in $R^2_{g,parallel}$ in front of the interface is somewhat smaller and becomes even smaller for smaller degrees of confinement (not shown).

4.3.4 Loops and Trains

Data on loops and trains at interaction energies above the critical adsorption energy give some valuable information about conformations of adsorbed polymers in the interface region. In Figure 4.10a the loop and train length of adsorbed polymers is plotted as function of the centre of mass position for λ=1.6 and $\epsilon_{pw} = 1.2kT$. Figure 4.10b shows the number of loops and trains in the same situation.

In Figure 4.10a the first thing that attracts the attention is the maximum in the loop length ($\lambda = 1.6$) approximately 4 grid points away from the interface. The train length does not show such a maximum and increases gradually towards a constant value inside the pore. The peak in the loop length in front of the interface vanishes for $\lambda = 0.5$ and is replaced by a sharp kink to a plateau value at $CM(z)$ values of 0 and lower. The maximum in loop length at $\lambda = 1.6$ indicates that parts of the polymer chain at the interface bridge the pore entry. Bridging of the pore entry becomes less probable for increasing pore sizes.

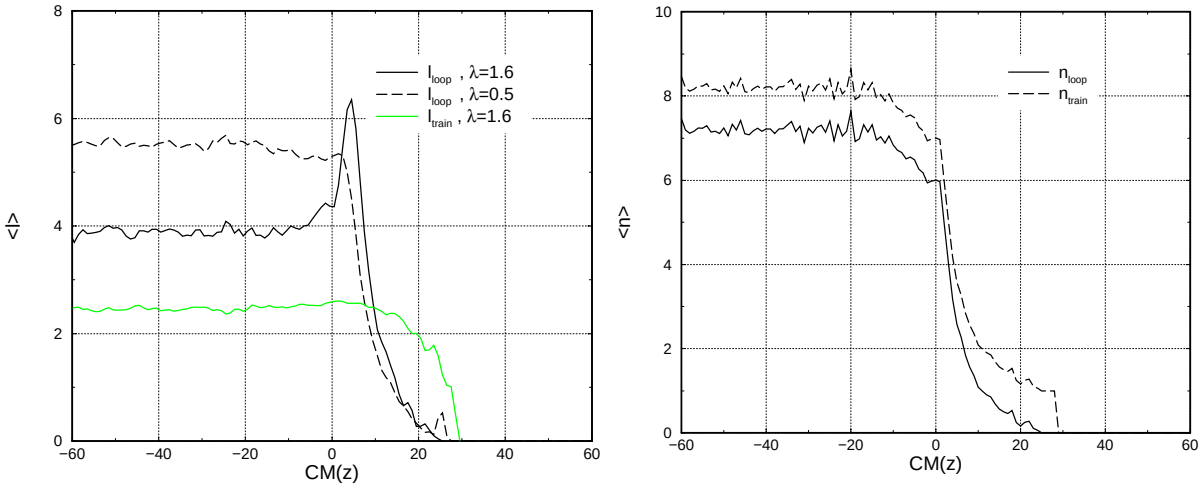

(a) (b)

Figure 4.10: *Loop and train lengths (a) and amount of loops and trains (b) of adsorbed polymers versus the chain centre of mass position at* $\epsilon_{pw} = 1.2kT$ *and* $\lambda = 1.6$.

Figure 4.10b shows a gradual increase of the number of trains and loops with decreasing centre of mass positions. At full confinement the number of loops and trains reach values slightly larger than 7 and 8, respectively. The train length (Fig. 4.10a) is already constant at the interface. The trains start to appear at 30 grid points away from the interface while the loops appear at approximately 25 grid points away. After that the number of loops n_{loop} equals $n_{train} - 1$. Larger degrees of confinement show similar effects.

4.4 Conclusions

Configurational Bias Monte Carlo simulations with the Bond Fluctuation model have been performed to study the adsorption free energy and conformational properties of flexible polymers near the entrance of cylindrical pores in a flat surface and at various degrees of pore penetration. The system studied in this work consists of a flat, adsorbing surface containing a pore of variable dimensions $0.5 \leq \lambda (= R_g/R_{pore}) \leq 3$ in contact with a good solvent containing a polymer with chain length $N = 50$ at infinite dilution.

Upon approaching the adsorption transition, excess chemical potential profiles computed as a function of the chain centre of mass position along the pore axis develop a minimum just in front of the pore entry at the bulk solvent side of the interface for all pore sizes examined in this work. The polymer favours this location near the interface over either the bulk solution where its conformational entropy is at a maximum or the pore interior, where its adsorption energy is at a minimum. The chain conformation at this point is best characterised as a "drawing-pin", which has most of its repeat units adsorbed on the outer surface and some on the inner pore surface. Train lengths examined as a function of the chain centre of mass position reveal no differences between adsorption onto the inner pore surface and the flat outer surface. The loop length as a function of the chain centre of mass position for small pore sizes ($\lambda = 1.6$) runs through a maximum just outside the pore indicating that the chain bridges the pore entry.

Above the critical adsorption transition, the excess chemical potential profiles start to decrease upon approaching the surface from the bulk solution at centre of mass distances approximately 2 bulk radii of gyration away from the surface. At this distance the radius of gyration component parallel to the pore axis increases considerably due to the attempt of the chain to bring as many as possible of its repeat units into contact with the surface. At distances smaller than one bulk radius of gyration away from the surface the parallel R_g component decreases while the perpendicular component increases as a consequence of the formation of 'drawing-pin' like conformations.

CHAPTER

FIVE

Polymer Intrusion into Narrow Pores at the Interface between a Poor Solvent and Adsorbing and Non-Adsorbing Surfaces: a Monte Carlo Simulation Study

We report thermodynamic and conformational properties of collapsed polymer globules in a poor solvent close to adsorbing and non-adsorbing surfaces containing a cylindrical pore that is either smaller or larger than the coil size in bulk solution. Configurational Bias Monte Carlo simulations at infinite dilution were used for this purpose. We find that above the critical adsorption transition changing from good solvent to poor solvent conditions causes an increase of the partition coefficient due to cooperative monomer adsorption on the pore wall. Below the adsorption transition, the reverse effect is observed. The radius of gyration components as well as conformational (free) energies and entropies as a function of the chain centre of mass (CM) position along the pore axis reveal strong anomalies in the vicinity of the pore entrance. Below the adsorption transition, the dense globule in a poor solvent swells and deforms when penetrating the pore and recollapses once it is fully confined. Above the adsorption transition in solvents above and below the Θ-point, minima occur in the free energy at chain CM positions just in front of the pore entry causing a barrier upon pore penetration. Upon approaching the small pore from the bulk poor solvent region, the chain conformational entropy and energy run through a maximum below and above the adsorption transition.

Submitted to *Polymer*

5.1 Introduction

When the solvent quality of polymer solutions decreases, polymeric coils collapse into tight globules. This feature has great implications on polymer separation methods where porous interfaces are employed. In liquid chromatography and gel permeation chromatography (GPC) the solvent quality influences the migration and conformations of the polymers inside the matrix. In ultrafiltration of polymer solutions solvent quality also influences the separation e.g. a tightly packed polymer slightly larger than the membrane pore will not enter this pore whereas a flexible, swollen coil in a good solvent is able to permeate across it.[7–9]

Polymer partitioning between solutions and micropores has been studied extensively both experimentally[2,45,108] and by computer simulations.[24,25,28,31,57,108] Most of these studies have dealt with the thermodynamic partitioning behaviour, which is determined by the properties of a fully confined polymer relative to those in the bulk polymer solution. When there is no attractive interaction between the polymer and the pore surface, the polymer chains are excluded from the pore according to their size relative to the pore size. In such a case, the partition coefficient K, defined as the polymer concentration in the pore relative to the polymer concentration in the bulk region, decreases as the molecular weight increases, which is the principle in GPC. It has been shown that when the pores at the interface are large compared to the polymer radius of gyration ($\lambda = R_g/R_p \ll 1$), the confinement energy and consequently the partition coefficient are not significantly affected by reducing the solvent quality.[25] At larger degrees of confinement ($\lambda \geq 1$), however, the confinement energy increases to very large values, resulting in negligible K values already before λ becomes unity.[13]

When the polymers have attractive interactions with the surface of the pore and this attraction exceeds a certain threshold (the critical adsorption point), the polymers will adsorb on the surface of the pore. The longer the chain, the stronger the adsorption will

be, therefore K will increase with the molecular weight. Reducing the solvent quality then results in increasing partition coefficients where K rises to values larger than unity.[23,24,43,44] For infinitely long random walk chains the partition coefficient $K = 1$ at the adsorption transition but is slightly smaller for self avoiding walks (good solvent conditions) depending on the chain length M and the degree of confinement λ.[43]

While many issues regarding the thermodynamic nature of polymer partitioning are well understood, much less attention has been devoted to polymer conformational changes and possible energetic (or entropic) barriers related to such changes upon penetrating pores smaller than the polymer size.

In this chapter we examine the conformational changes of collapsed polymer globules in poor solvent upon entering narrow cylindrical pores in adsorbing and non-adsorbing flat surfaces by means of Configurational Bias Monte Carlo simulations of a lattice chain model. In addition, detailed information on changes of the polymer's conformational entropy, energy, and free energy are presented. This chapter extends upon our recent work reported on the same topic, which dealt with self avoiding chains partially confined at the entrance of a cylindrical pore in a flat surface.[49,50]

The remainder of this chapter consists of a description of the simulation method, after which the results are presented. The results section is split into two parts. First, we discuss the effect of changing the solvent quality on polymer conformational and thermodynamical properties at a porous interface under conditions that monomer-wall interactions are repulsive. In the second part the same effects are discussed, but then monomer-wall interactions are attractive and stronger than the critical adsorption energy.

5.2 Simulation Details

The simulation details are similar to those described in our previous work.[49,50] A lattice Configurational Bias sampling method[39] is used to carry out the simulations, combined with the Bond Fluctuation polymer model.[16] All simulated polymers are 50 monomers (M) long, each monomer taking up 8 grid points (a box) on a 3D simulation grid. Apart from their excluded volume interactions, the thermal (attractive) interactions between two grid points belonging to different non-bonded monomers, ϵ_{pp}, are varied between 0.00kT (good solvent), 0.2577kT (Θ solvent) and 0.30kT (poor solvent). When one or more of the grid points of the monomer-box is in contact with the wall, the monomer experiences an attractive interaction energy of 0kT or 1.2kT. The solvent Θ-point was found by computing R_g^2/M of isolated chains for M =20, 50, 100, 150 and 200 and various ϵ_{pp} values and coincides with the ϵ_{pp} value where the curves intersect (not shown).

The critical adsorption point is determined using the method of Gong and Wang.[43] They used polymers end-grafted to a flat surface to calculate the polymer's excess chemical potential relative to its value when isolated in the bulk solvent and plotted this quantity as function of the monomer-wall interaction energy for various chain lengths. At the point where the graphs of the different chain lengths cross, the critical adsorption energy can be found. At this point the excess chemical potential becomes independent of the chain length (see also page 39).[43] We released the constraint of the end-graft and sampled conformations taking into account only the adsorbed chains in the calculation of the excess chemical potential. Polymer lengths of 30, 50, 70, and 100 monomers were used for this purpose. Figure 5.1a, b and c show the excess chemical potentials for polymers in a good solvent, a Θ-solvent, and a poor solvent ($\epsilon_{pp} = 0.30kT$) respectively. The critical adsorption point for a good solvent is situated at $\epsilon_{cr} = 0.96kT$. In Θ-solvents and in the poor solvent the critical adsorption points are $\epsilon_{cr} = 0.86kT$ and $\epsilon_{cr} = 0.77kT$ respectively.

The simulation box is set up by creating a flat surface with a straight cylindrical pore in the middle of the box. The length of the pore is large enough for the polymer to stretch

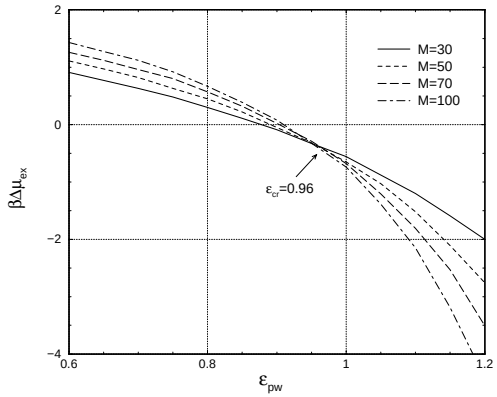

(a) $\epsilon_{cr} = 0.96kT$ at $\epsilon_{pp} = 0.0kT$

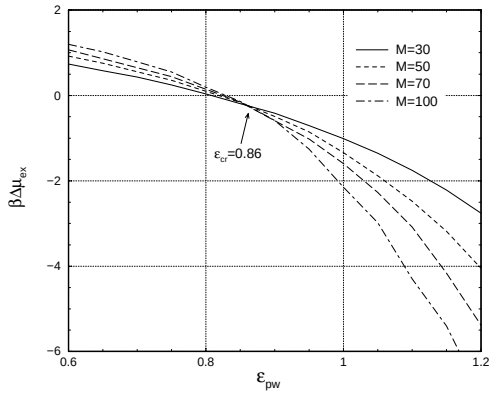

(b) $\epsilon_{cr} = 0.86kT$ at $\epsilon_{pp} = 0.2577kT$ (Θ-solvent)

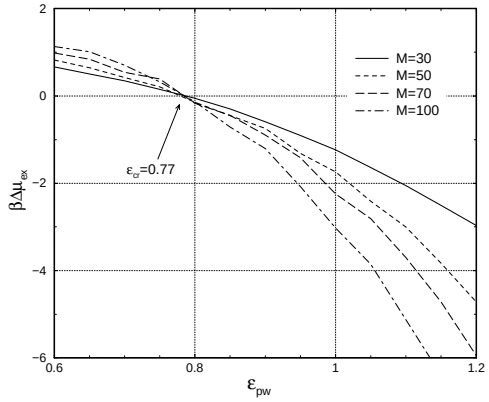

(c) $\epsilon_{cr} = 0.77kT$ at $\epsilon_{pp} = 0.30kT$

Figure 5.1: *Critical adsorption points in an athermal solvent ($\epsilon_{pp} = 0.0kT$), Θ-solvent ($\epsilon_{pp} = 0.2577kT$) and poor solvent ($\epsilon_{pp} = 0.30kT$)*

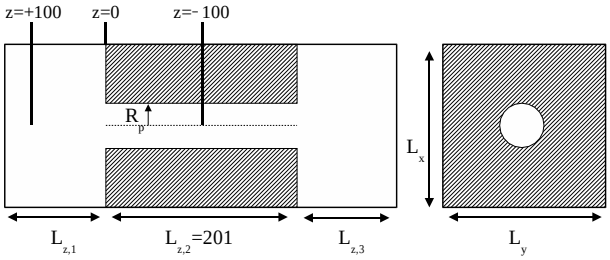

Figure 5.2: *Geometrical details of the simulation box. Cross sectional view (left) and top view (right).*

out completely without finding its chain ends at opposite pore mouths (Figure 5.2).[49] The degrees of confinement, $\lambda = R_g/R_p$ (R_p being the pore radius), studied in this chapter are $\lambda = 0.5$ and $\lambda = 1.5$. If changes in solvent quality were made (and thus R_g changes), the pore radius was adjusted to satisfy these confinement degrees. In athermal solvents $R_g = 11.3$, under Θ conditions the R_g equals 8.7, and in poor solvent ($\epsilon_{pp} = 0.30kT$) R_g equals 7.5.

Chain conformational properties were calculated as a function of the polymer centre of mass z-position $CM(z)$ (the direction along the pore axis) using the Rosenbluth weighting scheme:[39]

$$\langle \mathcal{A} \rangle_{\mathcal{R}} = \frac{\sum_{n=1}^{N} W(n)\mathcal{A}(n)}{\sum_{n=1}^{N} W(n)} \tag{5.1}$$

in which $\mathcal{A}$ is the configurational quantity of interest (e.g. the radius of gyration) and $W(n)$ denotes the Rosenbluth factor of conformation n. Chain conformations were generated segment by segment using a configurational bias favouring the energetic favourable monomer positions.[39] The z-position of the first chain segment was chosen randomly on the interval $[-100, 100]$ (Fig. 5.2). The x- and y-positions of the first monomer were taken at random within the available pore volume whenever $z < 0$ (inside the pore), whereas outside the pore they were randomly chosen within a radius of $2.5R_g$ away from the pore axis. This choice allows the chains to adsorb on the flat surface facing the bulk solvent phase. The conformations used for statistical averaging were always those that had their centre of

mass within a radius R_p from the pore axis. In this way we obtain the conformational and thermodynamic properties of chains in front of the pore entry while still accounting for adsorption that may occur on the flat surface perpendicular to the pore axis. All averaged quantities (eq. 5.1) were accumulated as a function of the chain centre of mass z-position ($z \in [-100, 100]$). In total, 10^8 conformations were used for the ensemble average.

The excess chemical potential of a chain as a function of its centre of mass position along the pore axis was calculated from the probability to successfully insert it in the system, which in the Rosenbluth sampling scheme equates to the average Rosenbluth factor $\langle W \rangle$ obtained by averaging over all generated conformations. The excess chemical potential is obtained from $\beta\mu_{ex} = -ln\langle W \rangle$.[39] This quantity was calculated as function of the chain centre of mass z-position by updating a histogram at the appropriate entry (the bin value representing the centre of mass z-component) with the chain Rosenbluth factor W.

5.3 Results and Discussion

5.3.1 Free Energy Profiles Below and Above the Adsorption Transition Versus Solvent Quality

A profile of the excess chemical potential as function of the centre of mass position is plotted in figure 5.3a for various solvent qualities at degrees of confinement $\lambda \approx 1.5$. The monomer interaction with the wall is repulsive ($\epsilon_{pw} = 0.0kT$). Negative values for the centre of mass indicate that the polymer centre is inside the pore, positive values indicate that the polymer centre is inside the solvent. Inside the pore the excess chemical potential increases with decreasing quality of the solvent (ϵ_{pp} increases). This means that, under non-adsorbing conditions, the partition coefficient $K = \exp(-\beta\Delta\mu_{ex})$ decreases with decreasing solvent quality. The interface at $z = 0$ affects the chain chemical potential up to distances of at least 2 (bulk solvent) radii of gyration (20 grid points) in the pore or in the bulk solvent phase. Within this interface region strong changes in the chain conformation occur as will

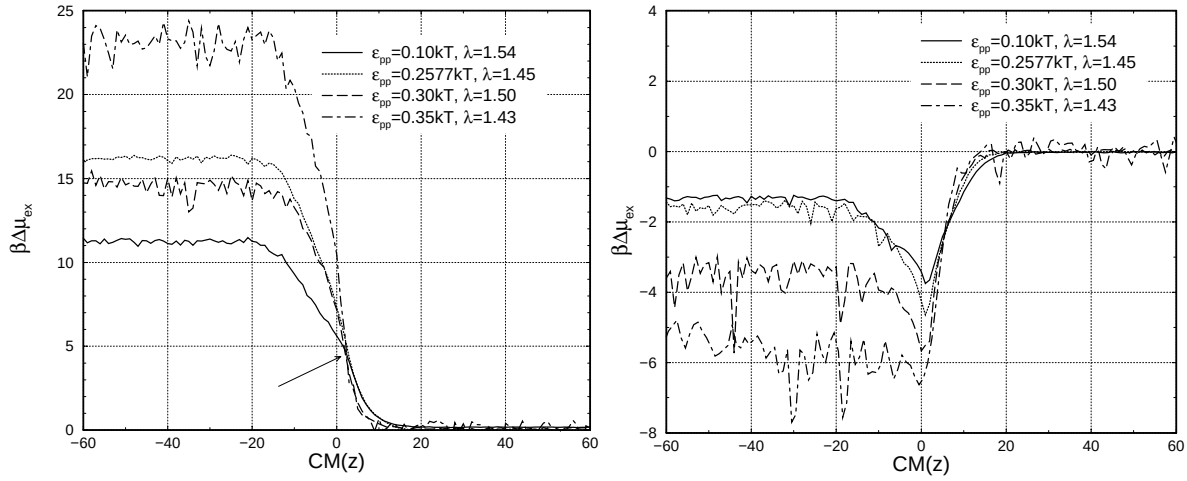

Figure 5.3: *$\beta\Delta\mu_{ex}$ profiles as function of the centre of mass $CM(z)$ position at monomer-wall interaction energy ϵ_{pw}=0.0kT (a) and $\epsilon_{pw} = 1.2kT$ (b). The degree of confinement is $\lambda \approx 1.5$ for various solvent qualities. Negative centre of mass values indicate that the polymer is inside the pore, at positive values the polymer is inside the solvent. The interface is positioned at $CM(z) = 0$.*

be discussed later on.

Figure 5.3b shows the same profiles, but now the interaction of the monomers with the walls is strongly attractive i.e. $\epsilon_{pw} = 1.2kT$, well above the critical adsorption point in all solvents. Inside the pore the order of the profiles is now reversed. The lower value of $\beta\Delta\mu_{ex}$ is obtained in a poor solvent, the higher value in a good solvent. Hence, at a fixed value of ϵ_{pw} above the adsorption transition, lowering the solvent quality leads to an increase of the partition coefficient. Note that decreasing the solvent quality causes a decrease of the critical adsorption energy ϵ_{cr} (Fig. 5.1). For $\epsilon_{pp} = 0.30kT$ the monomer-wall interaction energy ($\epsilon_{pw} = 1.2kT$) lies $0.45kT$ above ϵ_{cr}, for $\epsilon_{pp} = 0.0kT$ this value is $0.24kT$.

Increase of the partition coefficient achieved by reducing the solvent quality can be attributed to cooperative adsorption of monomer units on the pore wall.[83] Whereas steric

repulsions between monomers in a good solvent reduce the ability of a second monomer to adsorb close to the first, in a poor solvent mutual attractions between monomers promote the second monomer to adsorb close to the first.

Interestingly, free energy minima occur just in front of the pore entry at $CM(z) = 0$. While for $CM(z) < 0$ the adsorption energy favours a full chain confinement the entropic penalty associated with it causes the chain to preferably adsorb at the entry of the pore.[50]

Below we present conformational changes, conformational energies and entropies at the pore entrance in a poor solvent. Details on what happens in athermal solvents have been reported elsewhere.[49,50]

5.3.2 Partitioning in a Poor Solvent under Non-Adsorbing Conditions

Conformational Changes at the Pore Entry

In Fig. 5.4 snapshots are presented to illustrate the conformational changes occurring upon pore penetration ($\lambda = 1.5$). The accompanying changes in the radius of gyration components are shown in Fig. 5.5a. In bulk solvent (Fig. 5.4a) dense globules occur. In front of the pore entry (Fig. 5.4b) the globule slightly expands perpendicular to the pore axis to minimise the repulsion experienced from the surface. The polymer is slightly squeezed in the direction parallel to the pore axis and oriented into the perpendicular direction. The polymer has already penetrated the pore with one (Fig. 5.4c) or more (Fig. 5.4b) chain parts. Once the polymer penetrates the pore further (Fig. 5.4d) it loses its dense globular structure in order to make deformations possible to fit into the pore interior. As the chain penetrates the pore even further (Fig. 5.4e) the part of the chain inside the pore recollapses to experience the favourable intramolecular contacts again. In Fig. 5.5a this is revealed as a decrease of $R^2_{g,parallel}$ after passing through a maximum at

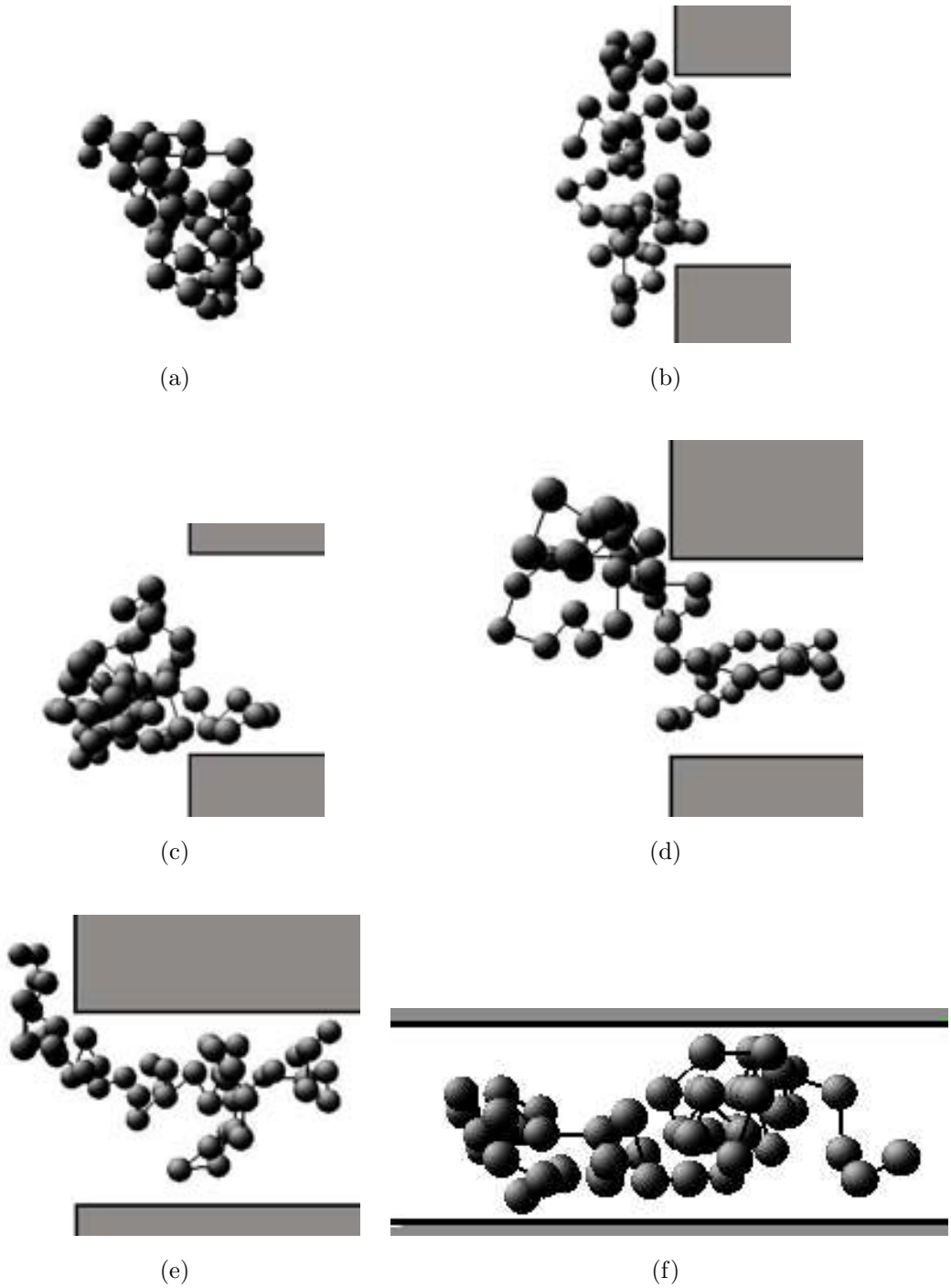

Figure 5.4: *Snapshots of polymer conformations under poor solvent conditions ($\epsilon_{pp} = 0.30kT$), degree of confinement $\lambda = 1.5$ and repulsive walls ($\epsilon_{pw} = 0.0kT$).*

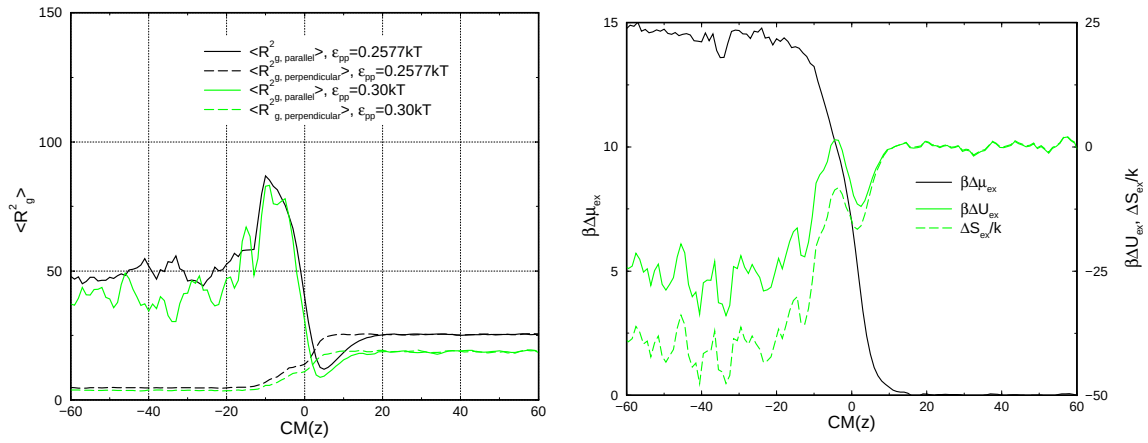

(a) (b)

Figure 5.5: *Radius of gyration components of polymers as function of the centre of mass at varying solvent qualities ϵ_{pp} (a) and their energetic properties in a poor solvent ($\epsilon_{pp} = 0.30kT$) (b), $\lambda = 1.5$ near repulsive walls ($\epsilon_{pw} = 0.0kT$).*

$CM(z) = -10$. Once the chain has fully penetrated the pore (Fig. 5.4f) the R_g-components no longer change.

Conformational Energy and Entropy

Figure 5.5b presents the chain excess chemical potential, $\beta\Delta\mu_{ex}$, and its entropic ($\Delta S_{ex}/k$) and energetic ($\beta\Delta U_{ex}$) components. When the chain CM approaches the pore entry, both the conformational entropy and intramolecular energy start to decrease at $CM(z) = 12$ (approximately 1.5 bulk radius of gyration in front of the pore entry). Note that in Fig. 5.5a the $R^2_{g,parallel}$ start to decrease as well. To avoid repulsions experienced from the flat surface the globule adopts a compressed conformation with its main axis oriented perpendicular to the pore axis. Due to this chain compaction, the number of intramolecular contacts between the monomers increases and $\beta\Delta U_{ex}$ decreases. The decrease of $\beta\Delta\mu_{ex}$ is compensated by the conformational entropy that decreases too, but stronger. As a net result, the chain

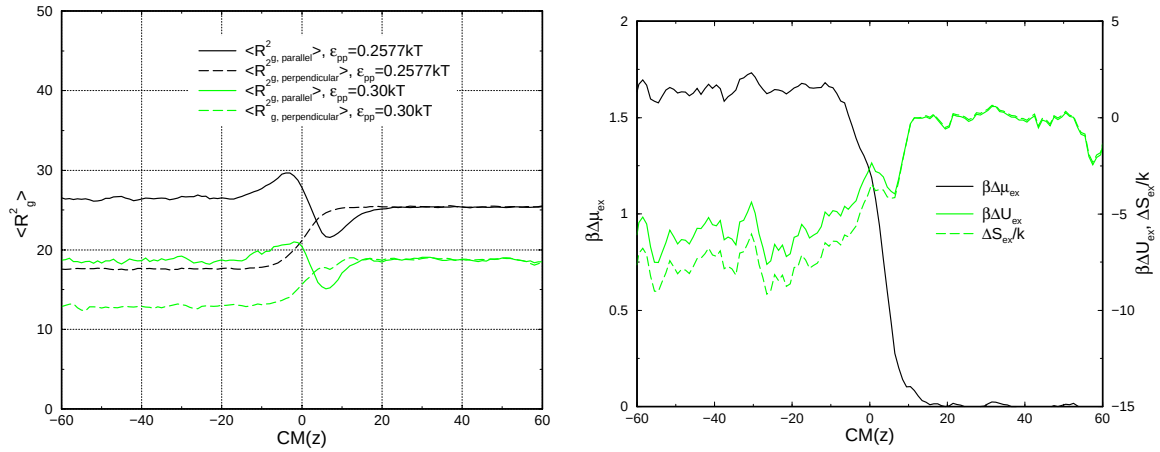

(a) (b)

Figure 5.6: *Radius of gyration components of polymers as function of the centre of mass position at varying solvent qualities ϵ_{pp} (a) and energetic properties in a poor solvent ($\epsilon_{pp} = 0.30kT$) (b), $\lambda = 0.5$ and repulsive walls ($\epsilon_{pw} = 0.0kT$).*

excess chemical potential, $\beta\Delta\mu_{ex} = \beta\Delta U_{ex} - \Delta S_{ex}/k$, shows no extremum at the pore entry and increases monotonically with decreasing $CM(z)$.

As soon as the chain centre of mass enters the pore, the conformational entropy and energy increase, reach a maximum, and next decrease toward a constant value. At the maximum, chain conformations resemble those depicted in Fig. 5.4e. At full chain confinement (Fig. 5.4f), both the energy and entropy have decreased below their respective values in the bulk solvent phase. The confinement value $\lambda = 1.5$ causes a compression of the globule leading to a reduction of its internal energy and conformational entropy.

Degrees of confinement smaller than unity, i.e. $\lambda = 0.5$, show different behaviour of the energetic and conformational properties. In Fig. 5.6b the maxima in $\beta\Delta U_{ex}$ and $\Delta S_{ex}/k$ that were present in Fig. 5.5b appear also here, but now these are clearly smaller and are shifted towards $CM(z)$ values at the pore entrance. Despite the pore radius being twice as large as the bulk radius of gyration, the energetic and entropic components decrease to

values well below the respective values in the bulk solvent indicating deformations taking place at the interface although to a much lesser extent than at $\lambda = 1.5$. The radius of gyration components shown in Fig. 5.6a no longer reveal strong anomalies: the weak minimum in front of the interface and the weak maximum inside the pore for the parallel R_g^2 component remains visible, both shifted towards slightly larger $CM(z)$ values.

5.3.3 Partitioning in Poor Solvent under Strong Adsorption Conditions

Conformational Changes at the Pore Entry

Whereas below the adsorption transition the pore penetration is much determined by the chain's attempt to avoid the surface, now adsorption effects strongly determine the observed mechanism. Figure 5.7 illustrates what happens in a poor solvent with a confinement degree $\lambda = 1.5$ and a monomer wall energy $\epsilon_{pw} = 1.2kT \gg \epsilon_{cr}$. Figure 5.8a shows the accompanying changes of $R^2_{g,perpendicular}$ and $R^2_{g,parallel}$. At distances within 1–3 bulk radii of gyration from the surface ($CM(z) < 20$) the dense globular structure is partly sacrificed in order to adsorb onto the surface (Fig. 5.7b). Although it involves disrupting attractive intramolecular monomer contacts there is a considerable payback in terms of the adsorption energy and conformational entropy as will be shown below. Fig. 5.8a shows that $R^2_{g,parallel}$ may increase by as much as 75% giving rise to a strong maximum in this quantity of approximately one bulk radius of gyration in front of the pore entrance. This feature occurs in an athermal solvent as well, however, opposite to what we find here for $\epsilon_{pp} = 0.30kT$, it reduces the conformational entropy.[50] When the polymer approaches the surface closer, $R^2_{g,parallel}$ drops below the bulk solvent value due to strong adsorption of the chain onto the surface (Fig. 5.7c and d).

The adsorbed chain either fully covers the pore entry while having small parts of the chain adsorbed in the pore ('drawing pins'.[50] Fig. 5.7c) or adsorbs on a smaller part of the outer surface while having a larger number of repeat units adsorbed on the pore

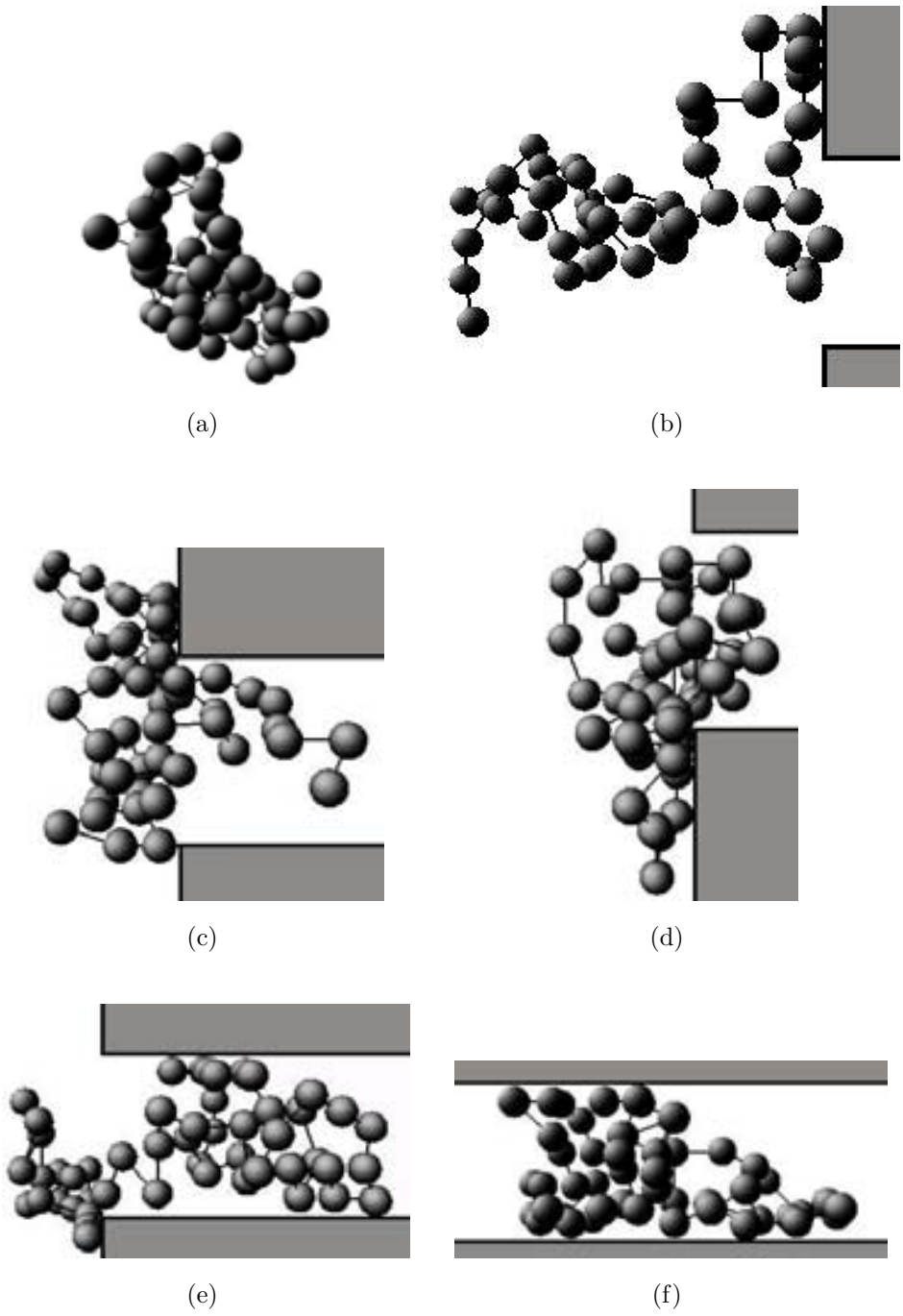

Figure 5.7: *Snapshots of polymer conformations under poor solvent conditions ($\epsilon_{pp} = 0.30kT$), degree of confinement $\lambda = 1.5$ and attractive walls with an interaction potential above the critical adsorption energy ($\epsilon_{pw} = 1.2kT$).*

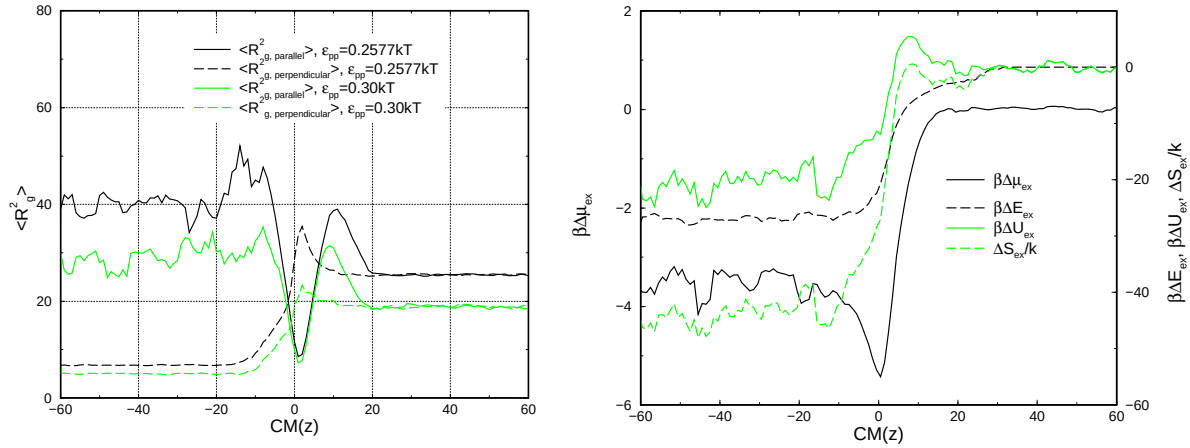

(a) (b)

Figure 5.8: *Polymer radius of gyration components as function of the centre of mass position at varying solvent qualities (ϵ_{pp}) (a) and energetic polymer properties in a poor solvent ($\epsilon_{pp} = 0.30kT$) (b), $\lambda = 1.5$ and with strongly attractive walls ($\epsilon_{pw} = 1.2kT$).*

wall. The chain eventually enters the pore (Fig. 5.7e) by desorbing monomers from the outer surface and adsorbing them inside. At this point, $R^2_{g,parallel}$ runs through a second maximum because the longest coil axis initially oriented perpendicular to the pore axis (Fig. 5.7c and d) needs to reorient. Moreover, the conformations in Figures 5.7c and 5.7d have the lowest free energy (see Fig. 5.3b and Fig. 5.8b), hence monomers try to remain at the interface while the chain centre of mass moves further into the pore (Fig. 5.7e). Only when $CM(z) < -20$ (almost 3 solvent bulk radii of gyration), $R^2_{g,parallel}$ becomes constant.

Conformational Energy and Entropy

Figure 5.8b shows the energy and entropy changes associated with the pore penetration process in Fig. 5.7. The energetic component of $\beta\Delta\mu_{ex}$ has been split into two contributions. The first, $\beta\Delta U_{ex}$, measures energy changes due to variation in the number of intramolecular monomer contacts. The second contribution, $\beta\Delta E_{ex}$, measures the energy of adsorption. At 1 bulk radius of gyration in front of the pore entrance, $\beta\Delta U_{ex}$ and $\Delta S_{ex}/k$

reach a maximum. At this distance, the chain tries to adsorb on to the surface (Fig. 5.7b) at the expense of disrupting the attractive monomer contacts within the globule. The increase of $\beta\Delta U_{ex}$ is compensated by a slightly larger negative contribution of $\beta\Delta E_{ex}$ while the conformational entropy assumes a value equal to the entropy of the globule in the bulk poor solvent. At CM distances closer to the surface, corresponding to the snapshots in Figures 5.7c and 5.7d, intramolecular contacts are restored and $\beta\Delta U_{ex}$ decreases. In addition, the conformational entropy decreases. The adsorption energy, $\beta\Delta E_{ex}$, now decreases faster because at these close distances between the surface and the chain centre of mass, monomers can more and more readily adsorb.

Note that the monomer-monomer energy ($\epsilon_{pp} = 0.30kT$) in the example of Fig. 5.7 matches closely with the monomer-wall energy $\epsilon_{pw} = 1.2kT$ (at maximum contact, two non-bounded monomers experience an attractive energy of $1.2kT$). Solvent quality (as determined by ϵ_{pp}) affects the energetic and entropic features correspondingly to the adsorption phenomenon in Fig. 5.7b. In Θ-solvent and athermal (good) solvents, chain adsorption is driven by the adsorption energy while a decrease of the conformational entropy, unlike in the situation here, opposes it.[50] The conformational changes in Θ and good solvents[50] are stronger as can be seen in Fig. 5.8a for $R^2_{g,parallel}$ in Θ-solvent.

At $CM(z) = 0$, the chain chemical potential, $\beta\Delta\mu_{ex}$, is at a minimum. Note that at this point $\beta\Delta E_{ex}$ and $\beta\Delta U_{ex}$ are not. The minimum in $\beta\Delta\mu_{ex}$ may thus be regarded as a compromise between the attempt of the polymer to minimise its energy while maintaining conformation flexibility (entropy). Because, in the pore interior $\beta\Delta\mu_{ex} < 0$, the partition coefficient is larger than unity ($K \approx 30$). This example therefore demonstrates the existence of an entropic barrier in front of a strongly adsorbing cylindrical confinement.

Figures 5.9a and 5.9b show the thermodynamic quantities and radii of gyration components versus the chain centre of mass position at smaller degrees of confinement ($\lambda = 0.5$). Noteworthy, all features present in Figure 5.8a and 5.8b ($\lambda = 1.5$) are retained. All char-

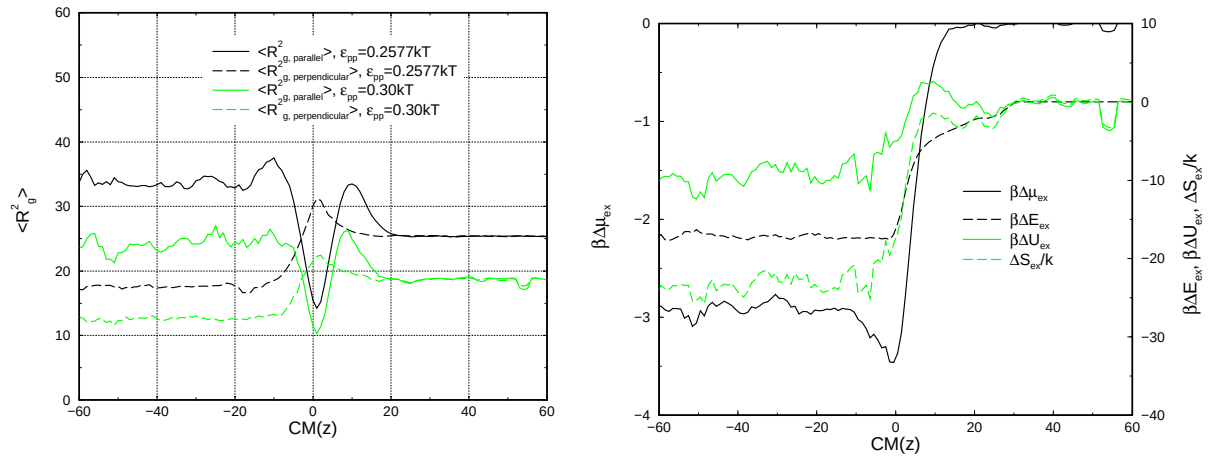

(a) (b)

Figure 5.9: *Polymer radius of gyration components at varying solvent qualities ϵ_{pp} (a) and energetic properties in a poor solvent ($\epsilon_{pp} = 0.30kT$) (b), $\lambda = 0.5$ and with strongly attractive walls ($\epsilon_{pw} = 1.2kT$).*

acteristic conformations shown in Figure 5.7 for $\lambda = 1.5$ occur at $\lambda = 0.5$ as well although deformation of the globule occurs to a lesser extent. A weak minimum of $\beta\Delta\mu_{ex}$ is still present at the pore entry despite the much smaller confinement degree.

Loops and trains

To gain some better insight in the nature of chain adsorption in solvents of different quality, we have examined the properties of adsorbed trains and the loops that connect them. The shape of the graphs for the number of trains n_t as function of the polymer centre of mass in poor solvent at $\lambda = 1.5$ is very similar to the situation for a good solvent (Figure 5.10). Upon approaching the surface the number of trains increases equally fast independent of the solvent quality until 2 grid points in front of the surface where n_t for $\epsilon_{pp} = 0.0kT$ has a light kink after which it starts to level off to a constant value ($n_t \approx 8$) at around $CM(z) = -20$ (inside the pore).

The number of trains for the poor solvent has a higher value inside the pore and reaches its constant value ($n_t \approx 10$) at $CM(z) = -15$, slightly closer to the interface. For $\epsilon_{pp} = 0.30kT$ and $\lambda = 0.5$ the behaviour at the interface is different. The graph shows a sharper kink than the other graphs due to weaker deformation of the chain upon entering the pore and does not change any further once inside the pore.

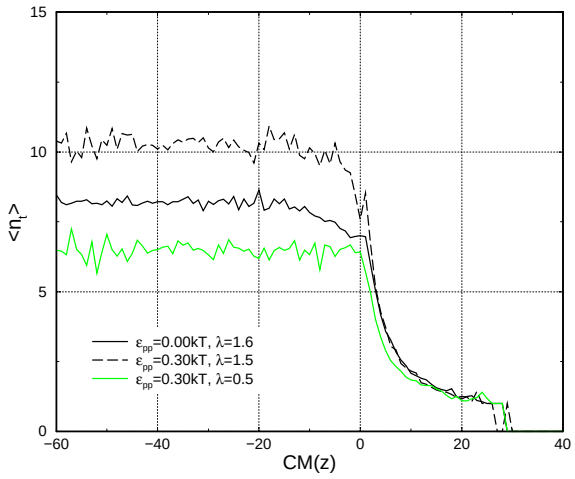

Figure 5.10: *Average number of trains per adsorbed polymer as function of centre of mass position in a poor ($\epsilon_{pp} = 0.30kT$) and a good solvent ($\epsilon_{pp} = 0.0kT$) for $\lambda = 1.5$ and 0.5 with strongly attractive walls ($\epsilon_{pw} = 1.2kT$).*

Fig. 5.11a shows the average train length of adsorbed polymers for $\lambda = 1.5$ in a good solvent and a poor solvent and for $\lambda = 0.5$ in poor solvent. Figure 5.11b shows the average loop length for the same situations. From about 1 bulk radius of gyration in front of the pore entry to far inside the pore the average train lengths remain constant. The lengths of the trains for both solvents are comparable where the trains for athermal chains are slightly larger. Lowering the degree of confinement in the poor solvent does not significantly affect the average train length. The number of trains shown in Figure 5.10 indicates that although the length of the trains is slightly shorter for the poor solvent, the number of trains is significantly larger resulting in a net larger amount of adsorbed monomers in the poor solvent due to the co-operative adsorption effect discussed above.

The loop lengths in Figure 5.11b show a large peak for both solvents at $\lambda = 1.5$ in front of the interface. This is due to polymers partly adsorbed on the outer surface at $z = 0$ and on the inside pore wall. These polymers will have large loops connecting trains inside the pore to the trains adsorbed on the surface. Polymers bridging across the pore entrance contribute significantly to the large loop length in front of the surface as well. At $\lambda = 0.5$,

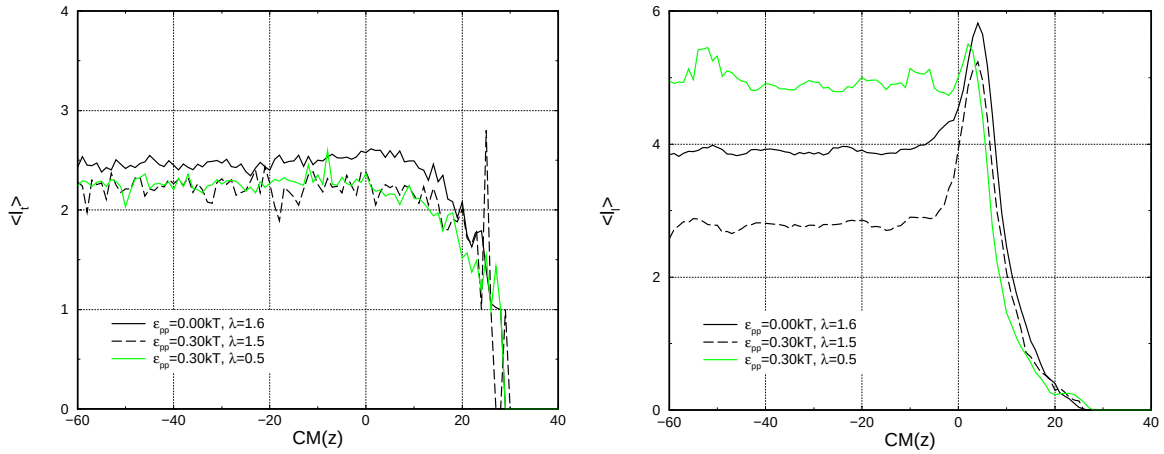

Figure 5.11: *Train lengths (a) and loop lengths (b) of adsorbed polymers as function of centre of mass position at poor ($\epsilon_{pp} = 0.30kT$) and good solvent conditions ($\epsilon_{pp} = 0.0kT$), $\lambda = 1.5$ and* 0.5 *with strongly attractive walls ($\epsilon_{pw} = 1.2kT$).*

the peak at the pore entrance is very weak as bridging across the pore entry becomes less probable.

Lowering the solvent quality gives rise to shorter loops inside the pore. The peak in the loop length in front of the surface is only slightly smaller than the peak for the good solvent. The geometry of the pore has a large effect on the height of the loop length peak in front of the surface.

5.4 Summary and Conclusions

Polymer penetration into narrow pores on a flat surface requires significant conformational changes at the interface. In this chapter we have examined how collapsed polymer chains (globules) in a poor solvent enter small pores on non-adsorbing and adsorbing surfaces. The degrees of confinement λ, defined as the unperturbed polymer radius of gyration relative to the pore radius, were chosen $\lambda = 1.5$ and $\lambda = 0.5$. Using the Rosenbluth

sampling method, computer simulations were performed with the Bond Fluctuation model to compute chain conformational properties, chain excess chemical potentials, as well as conformational entropies and energies as a function of the distance between the chain centre of mass and the pore entrance.

On non-adsorbing surfaces, polymer intrusion occurs through two major conformational changes. Within one bulk radius of gyration in front of the pore entrance the approaching globule is compressed in the direction normal to the surface. Once the chain centre of mass approaches the pore entrance the globule is distorted and elongated parallel to the pore axis at both values of λ. The R_g-component parallel to the pore axis runs through a maximum upon intrusion and levels off once the chain is completely confined. The over-extension upon intrusion causes a maximum in the chain conformational entropy and energy.

On adsorbing surfaces the intruding globule is not as significantly distorted along the direction of the pore axis. Instead, significant conformational changes occur prior to intrusion. At one bulk radius of gyration in front of the pore entrance the chain globular nature is lost due to the chain's attempt to adsorb. This causes chain elongation along the direction normal to the interface. Next, the chain adsorbs at the interface covering the pore entrance. This situation corresponds with a minimum of the chain excess chemical potential as a function of the chain centre of mass position along the pore axis. At this position the chain R_g-component parallel to the pore axis is at a minimum and chain segments only marginally explore the pore entry. The conformations here are very similar to the conformations found in a good solvent at attractive energies above the critical adsorption energy, although more tightly packed.[50] The polymer intrusion process proceeds by desorbing segments from the interface and adsorbing them on the inner pore surface causing the parallel R_g-component to increase. This process is favoured by the energetic part of the chain excess chemical potential but strongly opposed by the conformational entropy part for both degrees of confinement $\lambda = 1.5$ and $\lambda = 0.5$ and causes a free energy barrier for pore penetration.

CHAPTER

SIX

Evaluation and recomendations

6.1 Outlook on Larger Time and Length Scales

In this thesis the results of detailed Monte Carlo simulations are presented on very small length scales, giving insight into processes occurring at the bulk solvent/pore interface. Polymers are able to deform in order to enter narrow pores depending on e.g. the degree of confinement, adsorption characteristics, and solvent quality. Future work may be directed to bridge the gap towards macroscopic quantities, such as diffusive fluxes through porous networks (membranes). Ultimately, one hopes to gain insight and obtain predictions on macroscopic phenomena like concentration polarisation and fouling, as observed in membrane separation processes. Such a model can be very useful for membrane characterisation as well as for detailed understanding of concentration polarisation and fouling, altering membrane morphologies and surface properties. As presented in this thesis it is not a feasible option to obtain such information on the level of detail and complexity simply by extending the time and length scales at the current speed of computers. Other methods are needed for this which produce results on larger time and length scales.

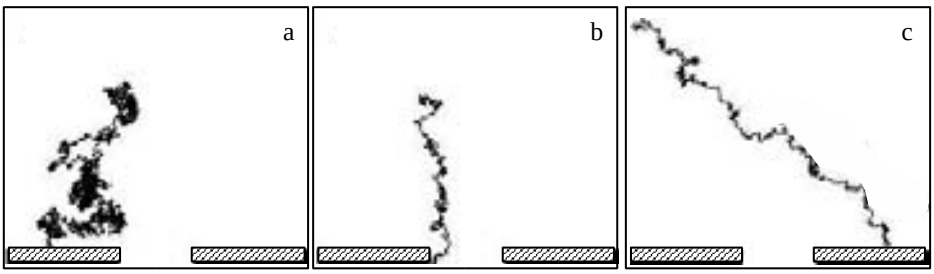

Figure 6.1: *Typical paths in a Particle Deposition experiment. a) Brownian motion, b) convection: dead-end mode, c) convection: cross-flow mode.*[107]

An example is a very simple, but effective, simulation method that involves successive particles depositing on a membrane. The particles move randomly in the simulation space with a bias towards the membrane. By changing the direction of the bias one changes the mode of convection which can be adjusted to situations resembling dead-end and cross-

flow filtration (Fig. 6.1).[107] The adjustable parameters in this model are, besides the flow conditions, the pore geometry and aggregation conditions (ability of the particle to stick to the surface or to other particles). After many particles have passed through the pore, adhere on the membrane or to each other, one is able to get a basic idea of how a cake layer builds up under these flow conditions (Fig. 6.2). The figure represents a cross-section of a circular pore and the lines represent the boundary of the cake layer. The accompanying numbers indicate the time (or number of particles simulated) belonging to these cake dimensions.

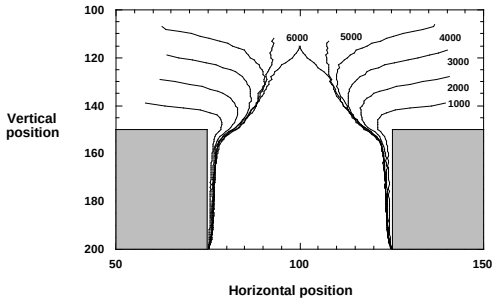

Figure 6.2: *Evolution of the cake layer. The cake layer narrows the pore and eventually the pore is completely blocked.*[107]

The model uses a crude way to describe the motion of a particle having a fixed probability from the particles to move in a certain direction and omitting much of the underlying physics described in this thesis. Both models describe phenomena on different time and length scales and have a different level of complexity. Fig. 6.3 aims to visualise the gap to be bridged, as well as the future challenges. In this figure we see two blocks indicating the regions where molecular simulations (e.g. Monte Carlo simulation and Molecular dynamics) and mesoscale simulations, like Particle deposition, can be applied. The specific region where the simulations are carried out in this thesis, is indicated by the black part of the molecular simulation region. The model used for those simulations can be expanded by defining monomers with different properties, thus increasing the complexity (arrow 1 in Figure 6.3), so that one is able to simulate heteropolymers or even more complex macromolecules. Section 6.3 suggests an approach to expand this model. To account for the macroscopic quantities and phenomena, i.e. diffusive fluxes and the build up of cake layers, one needs to simulate on larger time and length scales (arrow 2 in Fig. 6.3). Using molecular simulations involves large

amounts of computer time or a significant decrease of the model's complexity. However, by increasing the length and time scales or decreasing the complexity, one looses a lot of the information related to the underlying physics in the process. A method to decrease the complexity while maintaining a large part of the physics, is described below.

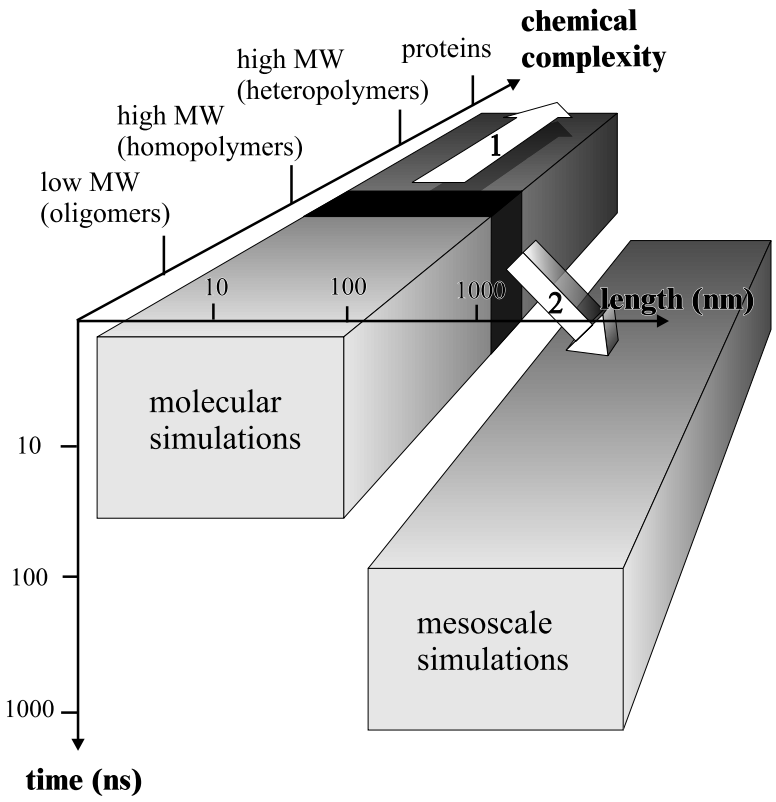

Figure 6.3: *Molecular simulations and mesoscale simulations, like Particle deposition, describe phenomena on different time and length scales. One can increase the model's complexity to describe e.g. heteropolymers (arrow 1) as described in section 6.3. Decreasing the complexity, coarse graining, and assigning a free energy to a centre of mass position, makes it possible to bridge the gap that separates the two simulation methods (Molecular simulations and the mesoscale simulations) as described in section 6.2 (arrow 2).*

6.2 Mesoscale simulations

The method can be based on the method used throughout this thesis. We presented free energy profiles when approaching pores along their central axis perpendicular to the membrane surface. Now the starting points of polymer growth are defined on a 3D lattice instead of along the pore axis or inside a narrow 'tunnel'. One keeps track of the free energy of every grown polymer by sorting it in a 3D histogram, based on the polymer centre of mass. Then one can sample the space above and inside the pore to make a 3D free energy landscape.

This will of course take up an enormous amount of CPU-time, in particular for complex pore geometries, but it reduces substantially for a cylindrical pore. Because the cylinder is symmetrical when rotated along the pore axis, one only needs to sample in one plane, as is shown in Figure 6.4a. The data thus gathered and averaged, result in one average free energy plane on which the reaction path can be identified by a path of minimum free energy leading from the solvent into the pore.

The free energy plane resulting from of the above simulations is transformed into a 3D free energy landscape by rotating it along the pore axis (Fig. 6.4b). Single particles as a coarse grained representation of a single polymer chain, can move over this energy landscape according to a probability calculated from the free energy of next neighbour positions. The particle position is equivalent with the centre of mass of the polymer chain used to generate the free energy landscape.

The method of simulation can be chosen from the broad range of mesoscale methods, like Brownian Dynamics, Dissipative Particle Dynamics, and various Monte Carlo methods. Interactions with other polymer particles can be included by simulating polymer chains of the desired type and in the desired concentration in a space without any interfering geometries. The long range interpolymer interaction potential can then be obtained from the resulting Radial Distribution Function.[59]

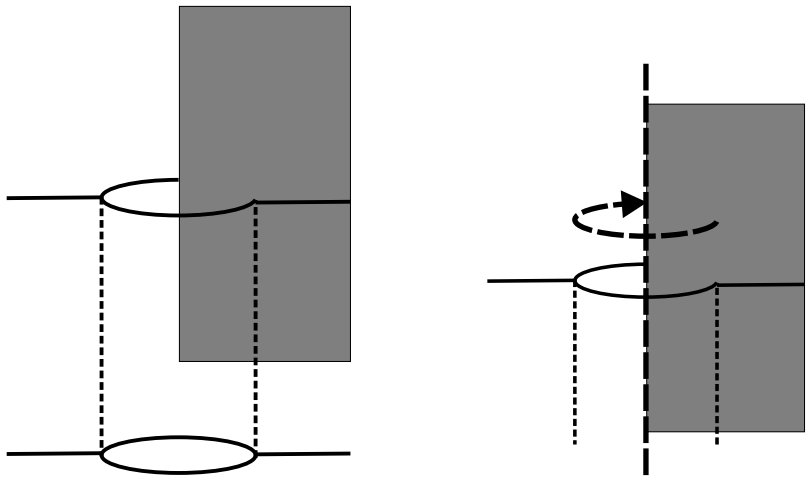

(a) (b)

Figure 6.4: *Sampling a 2D plane a) to obtain the free energy landscape at the pore mouth in 3D space by b) projecting the 2D energy plane to a 3D space by rotating the plane around the pore axis.*

Such simulations may give detailed information about the build up of the cake and gel layers, and the morphology by means of fractal dimensions or density landscapes. This data may be related to flux decrease and interaction potentials. Modifications of the pore structure, e.g. by making a system consisting of cages connected by narrow channels or irregular pores, can reveal additional information related to chromatography.

The application of this method looks very promising to obtain detailed information about fouling and concentration polarisation. However, conclusions should be drawn with caution when this method is used. Along the way of coarse graining we implicitly made some very crude assumptions. Firsty, the polymer particle concentration increases near the interface. This is expected and is exactly what one wants to study, but the energy landscape is based on the polymer-wall interactions of only one chain. More chains trying to enter the pore at the same time interfere with each other in a way not included in the energy landscape or the polymer-polymer interaction potential. Secondly, the same polymer-

polymer potential can also change, due to very high concentrations of polymers near the interface. Moreover, we considered for our calculations only diffusion. Any convective transport will make the situation even more complex.

The above simulation method can also be used to obtain dynamical data to compare with GPC experiments. Under GPC conditions the partition coefficient of macromolecules K_{GPC} depends on one dimensionless quantity: The degree of confinement ($\lambda = R_g/R_{pore}$). Both quantities can easily be obtained from dynamical simulations. In GPC mode the adsorption effects are negligible or small.[45] When varying adsorption characteristics, e.g. adjusting pH, the corresponding partition coefficient K differs from K_{GPC} and can be obtained from the retention volumes.[45] Using the simulation described in this thesis, it is also possible to derive partition coefficients ($K = \exp(-\beta\Delta\mu_{ex})$. However, one should be careful, as these partition coefficients are the result of simulations at infinitely dilute solutions, i.e. single chains, and the experiments are very sensitive to concentration changes.

6.3 Partially Confined Block Copolymers and Proteins

A large part of membrane ultrafiltration processes is used to separate and concentrate proteins. Separating proteins is a difficult task with a large chance on membrane fouling by the sometimes denatured product. It is clear that a detailed knowledge on processes involving proteins at the membrane interface is desirable.

A first step into this direction can be made by investigating the behaviour of block-copolymers at the membrane interface: Protein segments (amino acids) can roughly be divided up into hydrophilic and hydrophobic amino acids. Because proteins usually are dissolved in aqueous solutions, the hydrophobic segments are largely clustered in the *core* of the protein while the hydrophilic segments will be situated in a *shell* on the outside of

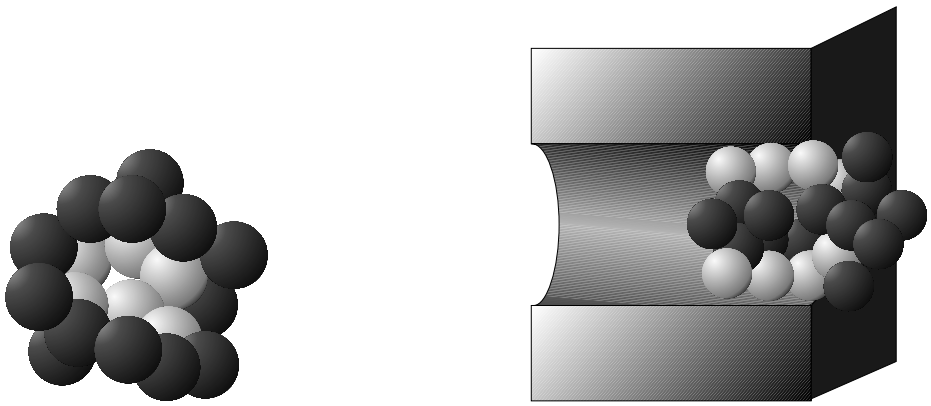

(a) Conformation in a aqueous solution.

(b) Conformation at a porous interface.

Figure 6.5: *Random copolymer conformations of the core-shell-type in an aqueous solution and at the porous interface. Black spheres represent hydrophilic segments. White spheres represent hydrophobic segments.*

the protein surrounding the hydrophobic globule to make it soluble in water. A simple and rough, but very suitable model to obtain information about the effect of these two groups at the membrane interface is to define these two types as blocks in a block copolymer.

In the previous chapters the monomers in linear homopolymers had an attractive interaction with the wall and a separate intramolecular interaction to account for the solvent quality. It is fairly easy to assign different interactions to individual monomers inside a polymer chain. In this way one is able to look at the behaviour of partially confined block copolymers or even protein-like structures with many different segments inside one chain.

Random copolymers, could reside in a solvent that acts as a good solvent for the A-type monomers and as a poor solvent for the B-type monomers. Then, the block copolymer segments can arrange in globules of B surrounded by an A-type shell (Fig. 6.5a).

The behaviour of such polymers at a porous interface will then differ substantially from the behaviour described in the previous chapters. The two types of segments will have very different interactions with the wall material causing deviation from the behaviour of the homopolymers at a porous interface. For instance, when this block copolymer is partially confined inside the pore and the core-monomers have attractive interactions with the wall material and the shell-monomers are repelled, the resulting situation may be visualised as shown in Fig. 6.5b. The polymer unfolds itself while entering the pore in order to let the B-type monomers (the core) experience favourable interactions with the wall and let the A-type monomers (the shell) avoid the wall; an inversion of conformation could then occur. Varying the interactions and the other parameters e.g. the degree of confinement λ, should reveal some unusual and exciting phenomena.

Although complete conformation inversion is not very likely to occur with real proteins because covalent and hydrogen bonds hold the structure together, partial inversion — like hydrophobic segments surfacing in the protein to make contact with a hydrophobic membrane— could occur. Such protein-surface interaction can result in conformational rearrangements, sometimes even in denaturation. Further detail on protein behaviour should include intramolecular bindings between the two types of segments in the block copolymer.

6.4 Translation to Real-Life Experiments

Until now this thesis dealt with model polymers and changes of various polymer properties near a porous interface. It remains the question how one can relate the theoretical results to real membrane systems used to separate macromolecules from a solution? The easiest way to answer this question is by considering the conclusions in respect to the experimentally accessible quantities of various solution/membrane systems such as the Θ-point of the solution in contact with the membrane and the degree of polymer confinement in micropores of the membrane. Also the adsorption regime in real systems can be put in

relation to the simulated systems as the critical absorption point for the polymer membrane systems; the critical absorption point for polymers can be found with elipsometry and reflectometry.[19,85,86,101] It is important, however, to bear in mind that the simulations carried out in this thesis are static simulations, resulting in equilibrium polymer conformations. Non-equilibrium events, like shear induced deformations, are not taken into account. Therefore, the conformational changes upon pore penetration reported in this thesis apply under those circumstances that only diffusive polymer motions in the absence of solvent flow occur. But, as we have seen in the previous chapters, polymer deformations at the interface under equilibrium conditions are very large already. Therefore, many of the phenomena described in this thesis will remain playing a significant role when solvent flow is introduced.

In chapter 3 it was found that in good solvents penetration of linear polymers into small pores involves a significant increase of the excess chemical potential, $\beta\mu_{ex}$, of the polymer. Recalling the partition coefficient K being equal to $K = \exp(-\beta\mu_{ex})$, indicates the likelihood of pore penetration. Taking $\lambda = 1.6$ as an example, we calculated a free energy difference of $11.5kT$ for repulsive walls ($\epsilon_{pw} = 0.0kT$). This results in a partition coefficient K of 10^{-5}. However, at equal pore size and polymer radius of gyration, the partition coefficient increases to 0.007.

Introducing weak/moderate monomer-wall attractions at $\epsilon_{pw} = 0.8kT$ ($\epsilon_{cr} = 0.96kT$) the partition coefficient becomes $K = 0.007$ at $\lambda = 1.6$. Chapter 3 shows that an asymmetric, 'over-stretched', conformation at repulsive monomer-wall interactions exists, also with weakly attractive interactions. Above the critical absorption energy the partition coefficient equals or is greater than unity as shown in chapter 4. Also an energy minimum was found at ϵ_{pw} above ϵ_{cr} at polymer centre of mass positions just in front of the interface. This means that also above the critical adsorption point there is a bottleneck for pore intrusion although the partition coefficient is greater than unity. Therefore, it is likely that polymer adsorption occurs at the pore entrance first, before the solid surface

is covered. This observation may have important implications for membrane ultrafiltration. Although solvent-flow may prevent pores from getting blocked due to this strong free energy of adsorption at the pore entrance, the observation shows that a detailed understanding of membrane fouling requires to take into account the nature of micropores at the surface. Polymer conformations resembling 'drawing pins', being partly adsorbed to the membrane surface and partly on the pore walls, are now dominant conformations replacing the 'over-stretched' polymer conformations at weakly absorptive and repulsive walls.

When polymers are dissolved in poor solvents, the polymer conformation in the bulk is more tightly packed than in good solvents. In poor solvents the solubility of the polymer is lower than in good solvents. At non-infinite diluted systems this will result in a high possibility on aggregation. Focussing on the behaviour of single chains in a poor solvent at a porous interface with repulsive walls, the free energy profiles in chapter 5 show the largest free energy (excess chemical potential) change of all studied so far, implying that the partition coefficient is the lowest: A polymer globule at a repulsive porous interface is not able to enter a small pore. Such a situation is ideal for concentrating a polymer solution. Also such polymers will probably aggregate because of the low solubility, making separation easier. Although cake layers could be formed, such fouling phenomena will be largely reversible due to the repulsive walls. When a polymer is dissolved in a poor solvent (above the Θ-energy) and is concentrated with a membrane having attractive interactions with the polymer, it will have a large chance on very severe fouling. The same chance on aggregation of polymer applies also here, but now polymers also adsorb strongly to the membrane. This results not only in a dense layer, strongly adsorbed to the membrane, but also in a build-up of a large cake layer that is difficult to remove. Now the larger pores are easily blocked by adsorbed polymers due to this combination of aggregation and strong adsorption. The method suggested in section 6.3 can result in additional valuable information on the cake layer build-up and the influence of concentration polarisation on the process.

CHAPTER

SEVEN

Summary

In many separation processes e.g. electrophoresis, chromatography, and membrane ultrafiltration, polymers being separated are able to deform in order to enter a narrow pore. This has implications for, for example, molecular weight cut off (MWCO) experiments where typically linear polymers like polydextran or PEG are used to measure the pore sizes of ultrafiltration membranes. The study reported in this thesis has, therefore, concentrated on the deformation of linear polymers at their entry into a pore. Pore entry was studied by means of Monte Carlo Configurational Bias simulations. Linear, flexible chains measuring 50 repeat units were used to obtain energetic and conformation related properties of partially penetrated polymers. Their values were compared to their unconfined and completely confined values.

When studying conformational properties of partially confined linear flexible polymers in narrow pores and in athermal conditions, polymers are found to deform upon entering the pore. The asphericity of the chain and the radius of gyration (R_g) component parallel to the pore axis as function of the polymers centre of mass position run through a maximium before all chain segments have entered the pore. This indicates, particularly in very narrow pores at $\lambda \equiv R_g/R_p \geq 1$, where R_g denotes the radius of gyration and R_p the pore radius, that the chain adopts an asymmetric, over-extended conformation. The part of the chain inside the pore is stretched along the pore axis while the part of the chain outside the pore remains coil like (Figure 3.2, page 52). When the chain centre of mass is located further inside the pore, the chain becomes less extended and adopts a conformation of a deformed coil. Weakly attractive interactions of the monomers between the outer surface and the pore wall affect the observed phenomena only to a minor extent.

However, strongly attractive monomer-wall interactions, still under athermal conditions, introduce chain conformations that are significantly different from conformations located at the interface of repulsive or weakly attractive porous materials with the bulk solvent. As the attractive monomer-wall potential approaches the critical absorption energy, the excess chemical potential profiles computed as a function of the centre of mass

of the chain develop an energy minimum outside the pore just in front of the pore entry. This location on the outer surface is favoured by the polymer over a location in the bulk solvent and the bulk pore, where polymers are preferably adsorbed onto the surface and partially on the pore walls. A sharp maximum in the average loop length indicates that the chain bridges the pore entry, which causes a conformation resembling a 'drawing-pin' (Figure 4.9, page 81). The parallel component of the radius of gyration experiences a minimum here and the perpendicular component a maximum. As the polymer's centre of mass approaches the surface from the bulk solvent side the excess chemical potential profile starts to decrease as the radius of gyration components parallel to the pore axis starts to increase. This is caused by chains attempting to bring as many monomers into contact with the surface by stretching out to the surface.

Decreasing the solvent quality causes polymers to collapse to a globular conformation inside the bulk solvent. When the porous material repels the monomers, at equal degrees of confinement and when the polymer chain is solved in a poor solvent, the partition coefficients are much lower compared to the situation where the polymers are solved in a good solvent at a porous interface with narrow pores. When above the critical absorption energy attractive potentials compensate for this effect: The partition coefficient is higher in a poor solvent than in a good solvent as a result of co-operative monomer absorption on the wall. As the polymer approaches the interface with repulsive walls containing a narrow pore ($\lambda > 1$) from the bulk solvent, the globule is slightly compressed when located just in front of the pore. Intramolecular interactions hold the globule together. Upon penetration of the pore the polymer extends into the direction parallel to the pore axis (Figure 5.4, page 95) much alike the situation described for polymers in good solvents near repulsive walls. Again this results in an asymmetric over-extended conformation although more tightly packed than for a good solvent. The conformation of a completely confined globule is squeezed in the dimensions perpendicular to the pore axis, while the polymer globules confined in larger pores only exhibit minor deformations and orientation effects. At attractive monomer-wall interactions, above the critical absorption energy, the

equilibrium conformations resemble those of coils in a good solvent at equivalent adsorption conditions (Figure 5.7, page 99). As in those cases the polymer stretches out towards the surface when the centre of mass of the polymer approaches the interface from the bulk solvent; at the pore entry there is a sharp energy well where drawing pin conformations can be found. Also the sharp peak in the length of the loop just in front of the interface can be found again indicating the parts of the polymers bridging the pore entry on the outer surface. Above the critical absorption energy the conformations in a poor solvent at a porous interface are very similar to those in good solvents although again more tightly packed.

Macroscopic and dynamic quantities at porous interfaces like shear, flux, as well as quantities related to membrane ultrafiltration like cake layer built up and concentration polarisation, have not been considered. The conclusions contained in this thesis could profitably be used for future research into these issues. The last chapter proposes a number of methods which are based on the results of this thesis and could be useful in this process.

CHAPTER

EIGHT

Samenvatting

Op de laatste bladzijden van dit proefschrift wordt het tijd om in begrijpelijk Nederlands samen te vatten wat ik allemaal heb gedaan in Enschede bij de vakgroep Membraantechnologie. Laat ik eerst beginnen met uit te leggen wat een membraan is en wat je ermee kunt doen.

Membranen zijn dunne plaatjes keramiek of dunne vellen plastic met kleine gaatjes die werken als een zeef, of filter. Ze houden grote deeltjes tegen en laten kleinere deeltjes door. Zo kun je bijvoorbeeld bacteriën, die maar een paar micrometer groot zijn, uit water halen. Het is zelfs mogelijk om een mengsel van nog kleinere deeltjes, zoals een mengsel van gassen, te scheiden. In de industrie worden membranen al veel toegepast en medische toepassingen, zoals nierdialyse, zijn niet meer weg te denken uit onze samenleving.

Voor dit proefschrift heb ik computer simulaties uitgevoerd van polymeren die een nauwe porie, kleiner dan het polymeer zelf, van zo'n membraan binnengaan. Polymeren zijn lange ketens van kleinere stukken molecuul (monomeren) achter elkaar die je het best kan voorstellen als een snoer met kralen. De monomeren in het polymeer kunnen vrij bewegen ten opzichte van hun buur, zolang ze maar niet te ver uit elkaar gaan. De verbinding tussen de monomeren is dus flexibel. De conclusies in dit proefschrift zijn getrokken aan de hand van berekende energieverschillen en grootteverschillen van gesimuleerde polymeren. Met deze resultaten wordt beter begrepen hoe nauwe poriën in een membraan verstopt kunnen geraken door grote polymeren tijdens het scheidingsproces.

In dit proefschrift is beschreven hoe flexibele, lineaire polymeren van vorm veranderen als ze van het oplosmiddel een nauwe porie in gaan. Een dergelijke polymeerketen is, opgelost in een zogenaamd goed oplosmiddel, een ongeordende kluwen, vergelijkbaar met een stuk touw dat je na lange tijd ergens achter in een kast terugvindt (Figuur 3.2A, pagina 52). Het zit helemaal door elkaar en hoe langer het stuk touw hoe meer kans op knopen. Zo ook met polymeren. Als een polymeerkluwen een nauwe porie ingaat die kleiner is dan de gemiddelde grootte van de kluwen, kan hij in elkaar gedrukt worden om toch naar binnen te

gaan. Als een deel de nauwe porie, waarvan de wand het polymeer afstoot (repulsief), naar binnen is gegaan zal dat deel in de porie enigszins gestrekt zijn. Het gedeelte buiten zit nog steeds in die kluwen (Figuur 3.2D-E, pagina 52). Een dergelijke vorm lijkt een beetje op een stronk 'broccoli': Het gedeelte in de porie ziet er uit als de dikke 'stengel' van de broccoli, het gedeelte buiten de porie dat nog in een kluwen zit zijn de 'bloemknoppen' (het eetbare deel).

Als nu de wand van het membraan en de wand van de porie het polymeer aantrekken gaat zo'n polymeer halverwege de porie er heel anders uitzien. Bij een sterke aantrekkingskracht gaat het polymeer zoveel mogelijk plat op de wand en aan de poriewand zitten. Een polymeer half in de porie en half er buiten heeft zijn monomeren buiten de porie zoveel mogelijk op het oppervlak van het membraan geplakt. Het deel binnen in de porie zit aan de poriewand geplakt. De vorm van het polymeer lijkt nu meer op een punaise. (Figuur 4.9, pagina 81). Deze punaise-vorm is energetisch bijzonder gunstig en zal veel voorkomen tijdens scheidingsprocessen wanneer het polymeer wordt aangetrokken door de wand.

Vervolgens gaan we weer naar de oude situatie terug: Het polymeer wordt niet aangetrokken door de wand. Deze keer gebruiken we een oplosmiddel waarin het polymeer slechter oplost. Hierdoor verandert de kluwenvorm in een dicht opeen gepakt bolletje. Omdat de monomeren van het polymeer zo dicht op elkaar gepakt zitten, is het ook veel moeilijker te vervormen om een nauwe porie binnen te gaan dan voor een kluwen. Als het dan toch een dergelijke porie binnen gaat, zal eerst het polymeerbolletje platgedrukt worden tegen de buitenwand, waarna de hele polymeerbol zich naar binnen wurmt (Figuur 5.4, pagina 95). Dit proces lijkt veel op wat er gebeurt met een polymeerkluwen in een goed oplosmiddel in de buurt van een repulsieve wand, maar de polymeervorm is nu dichter gepakt. Als zo'n bolletje wordt aangetrokken door de wand gebeurt in grote lijnen hetzelfde als met een kluwen die wordt aangetrokken door de wand in een goed oplosmiddel (Figuur 5.7, pagina 99).

CHAPTER

NINE

Dankwoord

Het is even wennen als je als zuiderling in Twente komt wonen, maar als je er eenmaal aan gewend bent heb je ook wat. Dit geldt zeker ook voor de vakgroep Membraantechnologie waar ik zo'n 5 jaar gewerkt heb aan mijn promotieonderzoek.

Gedurende deze tijd zijn er veel mensen geweest die bijgedragen hebben aan de tot stand koming van dit proefschrift. Als eerste zijn dat de twee professoren die deze vakgroep hebben geleid tijdens mijn promotieperiode. Heiner Strathmann, professor tijdens mijn beginperiode in de vakgroep, wil ik bedanken voor de gelegenheid die hij me gegeven heeft om in de vakgroep te komen werken. In de laatste fase van die periode was Matthias Wessling mijn professor en ik wil hem bedanken voor de originele ideeën en enthousiasme voor mijn onderzoek. 'Inspirator' Nico, regelmatig onze kamer binnenstormend met een oneindige stroom ideeën, wetenswaardigheden of gewoon voor een praatje wil ik in het bijzonder bedanken voor alles. Ook wil ik alle mensen in de vakgroep bedanken voor de goede tijd, speciaal al mijn kamergenoten en alle (ex-)leden van de 'mannenkabel' en verder ook de andere vakgroepkabels, de 'buren' Leon & Leon en de SGA-mannen.

Buiten de faculteit viel er ook veel te doen. Ik onmoette veel mensen in diverse 'clubjes' in Enschede die voor de juiste randvoorwaarden van mijn promotietijd zorgden: De Geusgangers (voornamelijk bevolkt door de 'mannenkabel'), het zwemclubje, de dixo en Gascongne. Verder de clubjes vrienden die ik uit Wageningen heb overgehouden: De Warhammergroep, de 'Droevendaalgroep' (onkruid vergaat niet), de Bioprocesclub, al mijn oudhuisgenoten en natuurlijk mag ik al die mensen niet vergeten die ik wel ben vergeten te noemen.

Diverse mensen hebben mij geholpen bij mijn proefschrift en ik wil die mensen bedanken die de moeite hebben genomen enkele stukken te lezen en er commentaar op te leveren: Bastiaan, Jonathan, Tom en Pa & Ma.

Uiteindelijk blijft mijn familie over die ik wil bedanken voor een van de belangrijkste

functies op de achtergrond: Pa, ma, Jan, Liesbeth en Bertien en niet te vergeten Dana. Altijd als er iets mis was (of juist niet) kon ik bij jullie terecht. Dat is best een prettig idee.

BIBLIOGRAPHY

[1] Adamski, R., and Anderson, J. Configurational effects on polystyrene rejection from microporous membranes. *J. Polym. Sci., Polym. Phys. Ed. 25* (1987), 765.

[2] A.M.Skvortsov, A.A.Gorbunov, D.Berek, and B.Trathnigg. Liquid chromatography of macromolecules at the critical adsorption point: behaviour of a polymer chain inside pores. *Polymer* (1998), 423.

[3] Aoyagi, T., Takimoto, J., and Doi, M. Molecular dynamics study of polymer melt confined between walls. *J. Chem. Phys. 115* (2001), 552.

[4] Arteca, G., Edvinsson, T., and Elvingson, C. Compaction of grafted wormlike chains under variable confinement. *Phys. Chem. Chem. Phys. 3* (2001), 3737.

[5] Arya, G., Maginn, E., and Chang, H. Effect of the surface energy barrier on sorbate diffusion in $alpo_4 - 5$. *J. Phys. Chem. B 105* (2001), 2725.

[6] Baker, R. *Membrane technology and applications.* McGraw-Hill, New York, 2000.

[7] Baker, R., and Strathmann, H. Ultafiltration of macromolecular solutions with high-flux membranes. *J. Appl. Pol. Sci. 14* (1970), 1197.

[8] Beerlage, M., Heijnen, M., Mulder, M., Smolders, C., and Strathmann, H. Non-aquous retention measurements: ultrafiltration behaviour of polystyrene solutions and colloidal silver particles. *J. Membr. Sci. 113* (1996), 259.

[9] Beerlage, M., Peeters, J., Nolten, J., Mulder, M., and Strathmann, H. Hindered diffusion of flexible polymers through polyimide ultrafiltration membranes. *Appl. Polymer Sci. 75* (2000), 1180.

[10] Bird, R., Armstong, R., and Hassager, O. *Dynamics of polymeric liquids, vol. 1*, 1st ed. Wiley, New York, 1977.

[11] Blanco, C., Saravanan, C., Allen, M., and Auerbach, S. Modeling benzene orientational randomization in na-y zeolites at finite loadings with kinetic monte carlo and master equation methods. *J. Chem. Phys. 113* (2000), 9778.

[12] Bleha, T., Cifra, P., and Karasz, F. The effects of concentration on partitioning of flexible chains into pores. *Polymer 31* (1990), 1321.

[13] Bleha, T., Mlýnek, J., and Berek, D. Concentration dependence of chain dimensions and its role in gel chromatography. *Polymer 21* (1980), 799.

[14] Boyd, R., Chance, R., and Strate, G. V. Effective dimensions of oligomers in size exclusion chromatography. a molecular dynamics simulation study. *Macromolecules 29* (1996), 1182.

[15] Brochard-Wyart, F. Polymer-chains under strong flows - stems and flowers. *Europhys. Lett. 30* (1995), 387.

[16] Carmesin, I., and Kremer, K. The bond fluctuation method: a new effective algorithm for the dynamics of polymers in all spatial dimensions. *Macromolecules 21* (1988), 2819.

[17] Casassa, E. Equilibrium distribution of flexible polymer chains between a macroscopic solution phase and small voids. *Polym. Lett. 5* (1967), 773.

[18] Casassa, E., and Tagami, Y. An equilbrium theory for exclusion chromatography of branched and linear polymer chains. *Macromolecules 2* (1969), 14.

[19] Caylor, C., and Law, B. The scaling behavior of critical adsorption in critical polymer solutions. *J. Chem. Phys. 104* (1996), 2070.

[20] Chandross, M., III, E. W., Grest, G., Martin, M., Thompson, A., and Roth, M. Dynamics of exchange at gas-zeolite interfaces i: pure component n-butane and isobutane. *J. Phys. Chem. B 105* (2001), 5700.

[21] Cifra, P., and Bleha, T. Anisotropy in dimensional and elastic parameters of confined macromolecules. *Macromol. Theory Simul. 8* (1999), 603.

[22] Cifra, P., and Bleha, T. Concentration dependence of the global and anisotropic dimensions of confined macromolecules. *Macromol. Theory Simul. 9* (2000), 555.

[23] Cifra, P., and Bleha, T. Steric exclusion/adsorption compensation in partitioning of polymers into micropores in good solvents. *Polymer 41* (2000), 1003.

[24] Cifra, P., and Bleha, T. Partition coefficients and the free energy of confinement from simulations of nonideal polymer systems. *Macromolecules 34* (2001), 605.

[25] Cifra, P., Bleha, T., and Romanov, A. Monte-carlo calculations of equilibrium partitioning of flexible chains into pores. *Polymer 29* (1988), 1664.

[26] Cifra, P., Bleha, T., Wang, Y., and Teraoka, I. Weak-to-strong penetration transition of macromolecules into a slit in theta solvent. *J. Chem. Phys. 113* (2000), 8313.

[27] Daoud, M., and de Gennes, P. Statistics of macromolecular solutions trapped in small pores. *J. Physique 38* (1977), 85.

[28] Davidson, M., Suter, U., and Deen, W. Equilibrium partitioning of flexible macromolecules between bulk solution and cylindrical pores. *Macromolecules 20* (1987), 1141.

[29] de Gennes, P. Coil-stretch transition of dilute flexible polymers under ultrahigh velocity gradients. *J. Chem. Phys. 60* (1974), 5030.

[30] de Gennes, P. *Scaling concepts in polymer physics*, 1st ed. Cornell University Press, 1979.

[31] Deen, W. Hindered transport of large molecules in liquid-filled pores. *AIChE J. 33* (1987), 1409.

[32] DiMarzio, E., and Rubin, R. Adsorption of a chain polymer between plates. *J. Chem. Phys. 55* (1971), 4318.

[33] Edwards, S. The size of a polymer molecule in a strong solution. *J. Phys. A: Math. Gen. 8* (1975), 1670.

[34] Eisenriegler, E., Kremer, K., and Binder, K. Adsorption of polymer chains at surfaces: scaling and monte carlo analysis. *J. Chem. Phys. 77* (1982), 6296.

[35] Fernandes, M., Huertas, M., Castanho, M., and de la Torre, J. G. Conformation and dynamic properties of a saturated hydrocarbon chain in a model membrane: a brownian dynamics simulation. *Biochim. Biophys. Acta 1463* (2000), 131.

[36] Ferry, J. Ultrafilter membranes and ultrafiltration. *Chem. Rev. 18* (1936), 373.

[37] Fleer, G., Stuart, M. C., Scheutjens, J., Cosgrove, T., and Vincent, B. *Polymers at interfaces*. Chapman and Hall, London, 1993.

[38] Frenkel, D., Mooij, G., and Smit, B. Novel scheme to study structural and thermal properties of continuously deformable molecules. *J. Phys.:Condens. Matter 4* (1992), 3053.

[39] Frenkel, D., and Smit, B. *Understanding molecular simulation: from algorithms to applications*, 2nd ed. Acedemic press inc., 2002.

[40] Giddings, J., Kucera, E., Russell, C., and Myers, M. Statistical theory for the equilibrium distribution of rigid molecules in inert porous networks. exclusion chromatography. *J. Phys. Chem. 72* (1968), 4397.

[41] Glandt, E. Distribution equilibrium between a bulk phase and small pores. *AIChE J. 27* (1981), 51.

[42] Glandt, E. Noncircular pores in model membranes: a calculation of the effect of pore geometry on the partition of a solute. *J. Membr. Sci. 8* (1981), 331.

[43] Gong, Y., and Wang, Y. Partitioning of polymers into pores near the critical adsorption point. *Macromolecules 35* (2002), 7492.

[44] Gorbunov, A., and Skvortsov, A. Statistical properties of confined macromolecules. *Adv. Colloid Interface Sci.* (1995), 31.

[45] Gorbunov, A., Solovyova, L. Y., and Skvortsov, A. General mechanism of the chromatography of macromolecules: Experimental test of the universal nature of adsorption effects. *Polymer 39* (1998), 697.

[46] Han, J., and Craighead, H. Separation of long dna molecules in a microfabricated entropic trap array. *Science 288* (2000), 1026.

[47] Han, J., Turner, S., and Craighead, H. Entropic trapping and escape of long dna molecules at submicron size constriction. *Phys. Rev. Lett. 83* (1999), 1688.

[48] Harris, J., and Rice, S. A lattice model of a supported monolayer of amphiphilic molecules: Monte carlo simulations. *J. Chem. Phys. 88* (1988), 1298.

[49] Hermsen, G., de Geeter, B., van der Vegt, N., and Wessling, M. Monte carlo simulation of partially confined flexible polymers. *Macromolecules 35* (2002), 5267. see also chapter 3 in this thesis.

[50] Hermsen, G., van der Vegt, N., and Wessling, M. Monte carlo simulations of polymer adsorption at the entrance of cylindrical pores in flat adsorbing surfaces. submitted to Soft Materials, see also chapter 4 in this thesis.

[51] III, E. W., and Grest, G. Interfaces between silicalite surfaces and liquid hexadecane: A molecular dynamics simulation. *J. Chem. Phys. 116* (2002), 6311.

[52] Jimenez, J., and Rajagopalan, R. Interaction between a grafted polymer chain and an afm tip: scaling laws, forces and evidence of conformational transition. *Langmuir 14* (1998), 2598.

[53] Kim, A., Bhattacharjee, S., and Elimelech, M. Shear-induced reoganization of deformable molecular assemblages: Monte carlo studies. *Langmuir 17* (2001), 552.

[54] Larson, R., and Magda, J. Coil-stretch transitions in mixed shear and extentional flows of dilute polymer solutions. *Polym. Prepr. 30* (1989), 93.

[55] Leermakers, F., and Gorbunov, A. Polymer-surface interactions in bridging escape and localization transitions. *Macromolecules 35* (2002), 8640.

[56] Leermakers, F., Male, J., and Skvortsov, A. Coil-to flower transition of a polymer chain pinned near a stepwise external potential: finite size effects. *Macromolecules 34* (2001), 8294.

[57] Lin, N., and Deen, W. Effects of long-ranged polymer-pore interactions on te partitioning of linear polymers. *Macromolecules 23* (1990), 2947.

[58] Link, A., and Springer, J. Light scattering from dilute polymer solutions in shear flow. *Macromolecules 26* (1993), 464.

[59] Louis, A., Bolhuis, P., Hansen, J., and Meijer, E. Can polymer coils be modelled as "soft colloids"? *Phys. Rev. Lett. 85* (2000), 2522.

[60] Maginn, E., Bell, A., and Theodorou, D. Sorption thermodynamics, siting and conformation of long n-alkanes in silicalite as predicted by cbmc integration. *J. Phys. Chem. 99* (1995), 2057.

[61] Mason, E., Wendt, R., and Bresler, E. Similarity relations (dimensional analysis) for membrane transport. *J. Membr. Sci. 6* (1980), 283.

[62] Menasveta, M., and Hoagland, D. Molecular weight dependence of the critical strain rate for flexible polymer solutions in elongational flow. *Macromolecules 25* (1992), 7060.

[63] Metropolis, N., Rosenbluth, A., Rosenbluth, M., Teller, A., and Teller, E. Equation of state calculations by fast computing machines. *J. Chem. Phys. 21* (1953), 1087.

[64] Milchev, A., Paul, W., and Binder, K. Polymer-chains confined into tubes with attractive walls - a monte carlo simulation. *Macromol. Theory Simul. 3* (1994), 305.

[65] Milchev, A., Yamakov, V., and Binder, K. Escape transition of a compressed polymer mushroom under good solvent conditions. *Europhys. Lett. 47* (1999), 675.

[66] Milchev, A., Yamakov, V., and Binder, K. Escape transition of a polymer chain: phenomenological theory and monte carlo simulations. *Phys. Chem. Chem. Phys. 1* (1999), 2083.

[67] Munch, W., Zestar, L., and Anderson, J. Rejection of polyelectrolytes from microporous membranes. *J. Membr. Sci. 5* (1979), 77.

[68] Muthukumar, M. Translocation of a confined polymer through a hole. *Phys. Rev. Lett. 86* (2001), 3188.

[69] Narh, K., Odell, J., and Keller, A. Temperature dependence of the conformational relaxation time of polymer molecules in elongational flow: invarialnce of the molecular weight exponent. *J. Polym. Sci., Polym. Phys. Ed. 30* (1992), 335.

[70] Nguyen, Q., and Néel, J. Characterization of ultrafiltration membranes. 4. influence of the deformation of macromolecular solutes on the transport through ultrafiltration membranes. *J. Membr. Sci. 14* (1983), 111.

[71] Nguyen, T., and Kausch, H. Chain extension and degradation in convergent flow. *Polymer 33* (1992), 2611.

[72] Olaj, O., Petrik, T., and Zifferer, G. Concentration dependence of static chain properties 2, off-lattice monte carlo simulations. *J. Chem. Phys. 107* (1997), 10214.

[73] Park, P., Chun, M., and Kim, J. Partitioning and conformational behaviour of polyelectrolytes confined in a cylindrical pore. *Macromolecules 33* (2000), 8850.

[74] Park, P., and Sung, W. Polymer release out of a spherical vesicle through a pore. *Phys. Rev. E 57* (1998), 730.

[75] Park, P., and Sung, W. Polymer translocation induced by adsorption. *J. Chem. Phys. 108* (1998), 3013.

[76] Park, P., and Sung, W. Dynamics of a polymer surmounting a potential barrier: the kramers problem for polymers. *J. Chem. Phys. 111* (1999), 5259.

[77] Perkins, T., Quake, S., Smith, D., and Chu, S. Relaxation of a single dna molecule observed by optical microscopy. *Science 264* (1994), 822.

[78] Perkins, T., Smith, D., Larson, R., and Chu, S. Stretching of a single tethered polymer in a uniform flow. *Science 268* (1995), 83.

[79] Pozrikidis, C. Effect of membrane bending stiffness on the deformation of capsules in simple shear flow. *J. Fluid Mech. 440* (2001), 269.

[80] Roe, R. Multilayer theory of adsorption from a polymer solution. *J. Chem. Phys. 60* (1974), 4192.

[81] Rosenbluth, M., and Rosenbluth, A. Monte carlo simulations of the average extension of molecular chains. *J. Chem. Phys. 23* (1955), 356.

[82] Runnebaum, R., and Maginn, E. Molecular dynamics simulations of alkanes in the zeolite silicalite: Evidence for resonant diffusion effects. *J. Phys. Chem. B 101* (1997), 6394.

[83] Scheutjens, J., and Fleer, G. Statistical theory of the adsorption of interacting chain molecules. 1. partition function, segment distribution, and adsorption isotherms. *J. Phys. Chem. 83* (1979), 1619.

[84] Scheutjens, J., and Fleer, G. Statistical theory of the adsorption of interacting chain molecules. 2. train, loop and tail size distribution. *J. Phys. Chem. 84* (1980), 178.

[85] Schlossman, M., Wu, X.-L., and Franck, C. Order-parameter profile at long distances in an adsorbed binary liquid mixture near criticality. *Phys. Rev. B 31* (1985), 1478.

[86] Schmidt, J. Universal adsorption at the vapor-liquid interface near the consolute point. *Phys. Rev. A 41* (1990), 885.

[87] Schmitz, H., and Müller-Plathe, F. Calculation of the lifetime of positronium in polymers via molecular dynamics simulations. *J. Chem. Phys. 112* (2000), 1040.

[88] Schüring, A., Auerbach, S., Fritzsche, S., and Haberlandt, R. On entropic barriers for diffusionin zeolites: A molecular dynamics study. *J. Chem. Phys. 116* (2002), 10890.

[89] Sevick, E., and Williams, D. A polymer end-tethered to a potential stripe: A simple example of an escape transition. *Macromolecules 32* (1999), 6841.

[90] Sheng, Y., and Lai, P. Nonequilibrium relaxation of a stretched polymer chain. *Phys. Rev. E 56* (1997), 1900.

[91] Sheng, Y., and Wang, M. Statics and dynamics of a single polymer chain confined in a tube. *J. Chem. Phys. 114* (2001), 4724.

[92] Shiokawa, K. End-to-end distance of a polymer confined between two plates. *Polymer J. 22* (1990), 925.

[93] Shiokawa, K. Chain dimensions of a polymer confined between two plates: a mean field theoretical approach. *Polymer J. 23* (1991), 885.

[94] Siepmann, J., and Frenkel, D. Configurational-bias monte carlo: a new sampling scheme for flexible chains. *Mol. Phys. 75* (1992), 59.

[95] Skvortsov, A., Klushin, L., van Male, J., and Leermakers, . F. First-order coil-to-flower transition of a polymer chain pinned near a stepwise external potential: numerical, analytical, and scaling analysis. *J. Chem. Phys. 115* (2001), 1586.

[96] Smit, B. Grand canonical monte carlo simulations of chain molecules: adsorption isotherms of alkanes in zeolites. *Mol. Phys. 85* (1995), 153.

[97] Smit, B., and Siepmann, J. Simulating the adsorption of alkanes and zeolites. *Science 264* (1994), 1118.

[98] Subramanian, G., Williams, D., and Pincus, P. Escape transitions and force laws for compressed polymer mushrooms. *Europhys. Lett. 29* (1995), 285.

[99] Subramanian, G., Williams, D., and Pincus, P. Interaction between finite-sized particles and end grafted polymers. *Macromolecules 29* (1996), 4045.

[100] Sung, W., and Park, P. Polymer translocation through a pore in a membrane. *Phys. Rev. Lett. 77* (1996), 783.

[101] Sussman, R., and Findenegg, G. Critical adsorption at the surface of a polymer solution. analysis of ellipsometric data on the depletion layer near the critical solution point. *Physica A 156* (1989), 114.

[102] Teraoka, I. Polymer solutions in confining geometries. *Prog. Polym. Sci. 21* (1996), 89.

[103] Tessier, F., Labrie, J., and Slater, G. Electrophoretic separation of long polyelectrolytes in submolecular-size constrictions: a monte carlo study. *Macromolecules 35* (2002), 4791.

[104] van Vliet, J., Luyten, M., and ten Brinke, G. Scaling behavior of dilute polymer solutions confined between parallel plates. *Macromolecules 25* (1992), 3802.

[105] Viovy, J. Electrophoresis of dna and other polyelectrolytes: physical mechanisms. *Rev. Mod. Phys. 72* (2000), 813.

[106] Walter, A., Rehage, H., and Leonard, H. Shear induced deformation of microcapsules: shape oscillations and membrane folding. *Colloids Surf. A 183* (2001), 123.

[107] Wessling, M. Two-dimensional stochastic modeling of membrane fouling. *Sep. Purif. Techn. 24* (2001), 375.

[108] White, J., and Deen, W. Equilibrium partitioning of flexible macromolecules in fibrous membranes and gels. *Macromolecules 33* (2000), 8504.

[109] Yashonath, S., and Santikary, P. Influence of non-geometrical factors on intracrystalline diffusion role of sorbate zeolite interactions. *Mol. Phys. 78* (1993), 1.

[110] Yashonath, S., and Santikary, P. Sorbate properties and cage-to-cage diffusion of argon in nacaa: a molecular dynamics study. *J. Phys. Chem. 97* (1993), 13778.

[111] Zhang, F. Molecular dynamics studies of chainlike molecules confined in a carbon nanotube. *J. Chem. Phys. 111* (1999), 9082.